THE EFFECTS OF FABRICATION PROCESSES ON THE MECHANICAL PROPERTIES OF WASTE PACKAGES—PROGRESS REPORT

Prepared for

U.S. Nuclear Regulatory Commission
Contract NRC–02–02–012

Prepared by

D.S. Dunn
Y.-M. Pan
D. Daruwalla
A. Csontos (NRC)

Center for Nuclear Waste Regulatory Analyses
San Antonio, Texas

August 2003

PREVIOUS REPORTS IN SERIES

Number	Name	Date Issued
CNWRA 91-004	A Review of Localized Corrosion of High-Level Nuclear Waste Container Materials—I	April 1991
CNWRA 91-008	Hydrogen Embrittlement of Candidate Container Materials	June 1991
CNWRA 92-021	A Review of Stress Corrosion Cracking of High-Level Nuclear Waste Container Materials—I	August 1992
CNWRA 93-003	Long-Term Stability of High-Level Nuclear Waste Container Materials: I—Thermal Stability of Alloy 825	February 1993
CNWRA 93-004	Experimental Investigations of Localized Corrosion of High-Level Nuclear Waste Container Materials	February 1993
CNWRA 93-014	A Review of the Potential for Microbially Influenced Corrosion of High-Level Nuclear Waste Containers	June 1993
CNWRA 94-010	A Review of Degradation Modes of Alternate Container Designs and Materials	April 1994
CNWRA 94-028	Environmental Effects on Stress Corrosion Cracking of Type 316L Stainless Steel and Alloy 825 As High-Level Nuclear Waste Container Materials	October 1994
CNWRA 95-010	Experimental Investigations of Failure Processes of High-Level Radioactive Waste Container Materials	May 1995
CNWRA 95-020	Expert-Panel Review of the Integrated Waste Package Experiments Research Project	September 1995
CNWRA 96-004	Thermal Stability and Mechanical Properties of High-Level Radioactive Waste Container Materials: Assessment of Carbon and Low-Alloy Steels	May 1996
CNWRA 97-010	An Analysis of Galvanic Coupling Effects on the Performance of High-Level Nuclear Waste Container Materials	August 1997
CNWRA 98-004	Effect of Galvanic Coupling Between Overpack Materials of High-Level Nuclear Waste Containers—Experimental and Modeling Results	March 1998

PREVIOUS REPORTS IN SERIES (continued)

Number	Name	Date Issued
CNWRA 98-008	Effects of Environmental Factors on Container Life	July 1998
CNWRA 99-003	Assessment of Performance Issues Related to Alternate Engineered Barrier System Materials and Design Options	September 1999
CNWRA 99-004	Effects of Environmental Factors on the Aqueous Corrosion of High-Level Radioactive Waste Containers—Experimental Results and Models	September 1999
CNWRA 2000-06 Revision 1	Assessment of Methodologies to Confirm Container Performance Model Predictions	January 2001
CNWRA 2001-003	Effect of Environment on the Corrosion of Waste Package and Drip Shield Materials	September 2001
CNWRA 2002-01	Effect of In-Package Chemistry on the Degradation of Vitrified High-Level Radioactive Waste and Spent Nuclear Fuel Cladding	October 2001
CNWRA 2002-02	Evaluation of Analogs for the Performance Assessment of High-level Waste Container Materials	March 2002
CNWRA 2003-01	Passive Dissolution of Container Materials—Modeling and Experiments	October 2002
CNWRA 2003-02	Stress Corrosion Cracking and Hydrogen Embrittlement of Container and Drip Shield Materials	October 2002
CNWRA 2003-05	Assessment of Mechanisms for Early Waste Package Failures	March 2003
In Review	Effect of Fabrication Processes on Materials Stability—Characterization and Corrosion	June 2003

ABSTRACT

Long lifetime of the waste package is identified by the U.S. Department of Energy (DOE) as a key system attribute for the performance of the proposed high-level waste repository at Yucca Mountain, Nevada. Sudden or sustained mechanical loading of the waste package may occur as a result of handling, emplacement operations, waste package drops, seismic events, rockfall, and drift degradation. The mechanical properties of the waste package materials are important because they may influence the mechanical disruption of the waste packages and, therefore, the lifetimes of the waste packages. Fabrication of the waste packages requires multiple processes that may alter the microstructure and affect the mechanical properties of the waste package materials. In support of the U.S. Nuclear Regulatory Commission (NRC) prelicensing activities on issues important to the preclosure safety analysis and postclosure performance of the proposed repository, the Center for Nuclear Waste Regulatory Analyses (CNWRA) is conducting an independent technical assessment of the effects of fabrication processes on the performance of the engineered barrier materials. This report presents results of the CNWRA experimental work on microstructural evaluation of Alloy 22, a review of the DOE evaluations on effects of fabrication processes on the mechanical properties of Alloy 22, and a review of the previous publications available in the open literature on fabrication effects for stainless steels and nickel-base alloys. Studies conducted with austenitic stainless steels suggest that mechanical properties and fracture toughness are influenced by the welding method, cold work, and composition of the base and filler metals. The CNWRA investigations indicate that fabrication processes alter the microstructure of Alloy 22 and lead to the formation of topologically close-packed phases. Studies conducted by DOE indicate that fabrication processes increase the yield strength, reduce the ductility, and affect adversely the Charpy impact toughness resistance of Alloy 22. Little data are available on the fracture toughness of corrosion resistant, nickel-base alloys. In the mill-annealed condition, the fracture toughness of Alloy 22 may be high; however, fabrication processes such as cold work, welding, and postweld heat treatments may decrease substantially the fracture toughness. The DOE investigations on the effects of fabrication processes on the mechanical properties are limited. Future work will need to address the effects of the entire fabrication sequence including forming operations, welding processes, and postweld heat treatments on the mechanical properties and fracture toughness of Type 316 nuclear grade stainless steel and Alloy 22. These concerns have been addressed in the DOE and NRC agreements, and DOE has provided a path forward for resolving, at the time of the license application, all the deficiencies and limitations identified in this report.

CONTENTS

CONTENTS (continued)

FIGURES

FIGURES (continued)

TABLES

ACKNOWLEDGMENTS

This report was prepared to document work performed by the Center for Nuclear Waste Regulatory Analyses (CNWRA) for the U.S. Nuclear Regulatory Commission (NRC) under Contract No. NRC–02–02–012. The activities reported here were performed on behalf of the NRC Office of Nuclear Material Safety and Safeguards, Division of Waste Management. This report is an independent product of the CNWRA and does not necessarily reflect the view or regulatory position of the NRC. The NRC staff views expressed herein are preliminary and do not constitute a final judgment or determination of the matters addressed or of the acceptability of a license application for a geologic repository at Yucca Mountain.

The authors gratefully acknowledge G.A. Cragnolino for technical review, the programmatic review of B. Sagar, and the editorial reviews of C. Cudd, B. Long and J. Pryor. Appreciation is due to J. Gonzalez for assistance in preparing this report.

QUALITY OF DATA: Sources of data are referenced in each chapter. CNWRA-generated laboratory data contained in this report meet quality assurance requirements described in the CNWRA Quality Assurance Manual. Data from other sources, however, are freely used. The respective sources of non-CNWRA data should be consulted for determining levels of quality assurance. Experimental data have been recorded in CNWRA scientific notebook number 498.

ANALYSES AND CODES: Thermo-Calc Version N was used for the phase stability and theoretical calculations presented in this report. This code is controlled according to requirements of CNWRA Technical Operating Procedure (TOP)–018. Detailed phase stability calculations can be found in CNWRA scientific notebook number 498.

REFERENCE:

Thermo-Calc Software AB. "Thermo-Calc Classic." Version N. Stockholm, Sweden: Thermo-Calc Software AB. 2001.

EXECUTIVE SUMMARY

Performance of the engineered barriers after waste emplacement is important to protect the public from any undue risk and keep exposures from normal and off-normal events to values as low as reasonably achievable as recognized by the U.S. Department of Energy (DOE) in its Repository Safety Strategy for the proposed Yucca Mountain repository. According to 10 CFR 63.112, a preclosure safety analysis that demonstrates the safety of the proposed design and operations in the geologic repository operations area with regard to the overall preclosure performance objectives must accompany a license application for construction authorization of a geologic repository. In addition, 10 CFR 63.21(c)(3) requires the safety analysis report to include a description and discussion of the design of the various components of the geologic repository operations area and the engineered barrier system including (i) dimensions, material properties, specifications, and analytical and design methods used, along with any applicable codes and standards; (ii) design criteria used and their relationships to the preclosure performance objectives specified in 63.111(b), 63.113(b), and 63.113(c); and (iii) the design bases and their relation to the design criteria. In the postclosure period, 10 CFR Part 63.311 requires the engineered barrier subsystem to be designed so that, working in combination with natural barriers, radiological exposures to the reasonably maximally exposed individual and release of radionuclides into the accessible environment are limited. For these reasons, DOE has identified the performance of the waste package as important for both the preclosure and the postclosure periods. In the preclosure period, the waste package is identified by DOE as a part of the structure, system, or components that prevents release of radionuclides for design basis events and beyond design basis events. In addition, DOE notes performance of the waste package is among the principal factors for the postclosure safety case.

In support of the U.S. Nuclear Regulatory Commission prelicensing activities on topics important to the preclosure safety analysis and postclosure performance of the proposed repository, the Center for Nuclear Waste Regulatory Analyses is conducting an independent technical assessment of the effects of fabrication processes on the mechanical properties of waste package materials. This report provides a review of the DOE assessment of the effects of fabrication processes on the mechanical properties of austenitic stainless steels and nickel base alloys.

Waste packages designed for the disposal of high-level waste in the proposed repository at Yucca Mountain include a Type 316 SS inner container to provide structural support for the waste package and an Alloy 22 outer container to provide corrosion resistance and containment in event the inner container fails. Fabrication of the disposal containers requires forming processes including rolling and machining operations. After waste loading, welding will be used to close the waste packages. Several postclosure weld stress mitigation methods are proposed by DOE including induction annealing, laser peening, and low-plasticity burnishing. The combination of cold work associated with the forming operations, and the welding and postweld stress mitigation methods may alter the microstructure and mechanical properties of the Type 316 nuclear grade stainless steel inner container and the Alloy 22 outer container. Characterization of the effects of fabrication processes on the microstructure and mechanical properties is necessary to assess performance of the waste packages.

The effects of fabrication processes on the microstructure of both Type 316 nuclear grade stainless steel and Alloy 22 are reviewed. The microstructure of both wrought materials is completely austenitic. Whereas welded Type 316 nuclear grade stainless steel has a duplex

structure consisting of austenite and ferrite phases, Alloy 22 solidifies as full austenitic welds. Based on the time-temperature-precipitation diagrams established for similar stainless steels, Type 316 nuclear grade stainless steel with a low carbon content is anticipated to hinder the formation of carbide precipitates. And, cold working prior to aging may accelerate the precipitation of both carbides and intermetallic phases. For welded material, although approximately 3–8 wt% ferrite is needed to prevent hot cracking, control of the ferrite content is critical for performance of the welds, primarily because of the transformation of ferrite to embrittled phases. The resultant weld microstructures, as influenced by the compositional variations and thermomechanical treatments, are shown to affect significantly the mechanical properties of the welds.

Alloy 22 undergoes phase transformations after thermal aging, including precipitation of secondary topologically close-packed phases and carbides long-range ordering. The time-temperature-precipitation diagrams for precipitation of topologically close-packed phases and long-range ordering in wrought Alloy 22 are established based on microstructural examination and theoretical calculations. Microstructural characterization of the welded Alloy 22 shows the formation of a dendritic structure and the presence of topologically close-packed phases in the interdendritic regions. Further aging and solution annealing treatments of the welded material promotes precipitation of the secondary phases. In addition, solution annealing of the welded materials is found to be unable to redissolve these precipitates into a solid solution because of the segregation of molybdenum in the interdendritic regions. Results from both experiments and theoretical calculations indicate that heat-to-heat variations in the base metal and element segregation in the welds may affect significantly the presence of topologically close-packed phases and, thus, the mechanical properties.

Austenitic stainless steels such as Type 316 nuclear grade stainless steel are characterized by low yield and tensile strengths, high ductility, and high fracture toughness. These alloys are resistant to failure by fracture and usually undergo significant plastic deformation prior to ductile failure. In the mill-annealed condition, the mechanical properties and, in particular, the fracture toughness of austenitic stainless steels can be reduced by the presence of impurities that form inclusions. Cold work and fabrication processes such as welding typically increase strength and reduce ductility and fracture toughness. Increases in strength and reduction of fracture toughness are dependent on the amount of cold work. In addition, fracture toughness is dependent on the type of welding method. Minimal reductions in fracture toughness are observed with cleaner welding processes such as gas tungsten-arc welding and gas metal-arc welding, which produce welds with low-inclusion contents. Submerged-arc welds and shielded metal-arc welds, which typically have higher inclusion contents, can have significantly reduced fracture toughness.

Corrosion resistant, nickel-base alloys such as Alloy 22 have mechanical properties similar to austenitic stainless steels; however, fracture toughness data for nickel base alloys are limited. Based on the relatively low yield and tensile strengths, high ductility, and high Charpy impact toughness, Alloy 22 in the mill-annealed condition is expected to have a high fracture toughness. The effects of cold work and fabrication processes on the mechanical properties of Alloy 22 are similar to austenitic stainless steels. Cold work increases the yield and tensile strengths of Alloy 22 and reduces ductility. Welded Alloy 22 also has a higher yield strength and reduced Charpy impact toughness compared with the mill-annealed material. The fracture toughness of welded Alloy 22 is estimated based on the Charpy V-notch impact toughness.

Decreased fracture toughness is estimated when welded Alloy 22 is aged at temperatures at which brittle intermetallic topologically close-packed phases are know to occur.

Although fabrication processes result in increased strength and reduced ductility and fracture toughness of nickel-base alloys and austenitic stainless steels, the alloys retain significant ductility. Failure assessment diagrams constructed for Type 316 SS and Alloy 22 show that, even when the effects of fabrication processes are considered, failure occurs by plastic collapse rather than by brittle fracture. Nevertheless, the combined effects of multiple fabrication steps necessary to construct waste packages should be considered in the evaluation of the mechanical properties of the waste package materials. According to agreements PRE.7.03, 7.04, and 7.05 and CLST.2.08, DOE agrees to conduct additional evaluations to reduce uncertainty and provide additional information on the effects of fabrication processes on the mechanical properties of the waste package materials.

1 INTRODUCTION

Performance of the engineered barriers during preclosure operations and after waste emplacement is important to protect the public from any undue risk, as recognized by the U.S. Department of Energy (DOE) in its Repository Safety Strategy for the proposed Yucca Mountain repository (CRWMS M&O, 2000a). As an independent regulatory agency, the U.S. Nuclear Regulatory Commission (NRC) has published licensing requirements for disposal of high-level wastes in the proposed repository. According to 10 CFR 63.112, a preclosure safety analysis must accompany a license application for construction authorization of a geologic repository. A preclosure safety analysis is required to demonstrate the safety of the proposed design and operations in the geologic repository operations area with regard to the overall preclosure performance objectives through a systematic examination of the site; the design; and the potential hazards, initiating events, and their resulting event sequences and potential radiological exposures to workers and the public. This analysis should include a general description of the structures, systems, components, equipment, and process activities at the geologic repository operations area. In addition, 10 CFR 63.21(c)(3) requires the safety analyses report filed with the license application must include a description and discussion of the design of the various components of the geologic repository operations area and the engineered barrier system including (i) dimensions, material properties, specifications, and analytical and design methods used, along with any applicable codes and standards; (ii) design criteria used and their relationships to the preclosure performance objectives specified in 63.111(b), 63.113(b), and 63.113(c); and (iii) the design bases and their relation to the design criteria. For the postclosure period, 10 CFR Part 63.311 requires the engineered barrier system to be designed so that, working in combination with natural barriers, radiological exposures to the reasonably maximally exposed individual and release of radionuclides into the accessible environment are limited.

In the preclosure period, the waste package is identified by DOE as a main part of the structure, system, or components that prevents release of radionuclides in the event of waste package drops, objects striking the waste package, waste package collisions, and fire or thermal hazards (CRWMS M&O, 2000a). In addition, DOE notes performance of the waste package, which is one of the two main components of the engineered barrier system, is among the principal factors for the postclosure safety case (CRWMS M&O, 2000a). The reference waste package design in the DOE site recommendation (CRWMS M&O, 2000b; DOE, 2002) consists of an outer container made of a highly corrosion resistant, nickel-chromium-molybdenum alloy, Alloy 22 (Ni-22Cr-13Mo-4Fe-3W), and an inner container made of Type 316 nuclear grade stainless steel (low C-high N-Fe-18Cr-12Ni-2.5Mo). Prior to repository closure, an inverted U-shaped drip shield, fabricated with Titanium Grade 7 (Ti-0.15Pd) and Titanium Grade 24 (Ti-6Al-4V-0.05Pd), will be extended over the length of the emplacement drifts to enclose the top and sides of the waste packages providing additional protection to the waste package from mechanical loads as a consequence of rockfall.

Components of the engineered barrier system must be designed to accommodate mechanical loads as a consequence of waste loading, transfer, and emplacement operations. The waste package may also be subjected to impacts as a result of drops. Engineered barrier system components, including the waste package, also may be mechanically loaded as a result of seismic activity, rockfall, and drift degradation. The responses of the waste package and the drip shield to loading will be dependent on the design and the mechanical properties of the engineered barrier system components. The ASME Boiler and Pressure Vessel Code (ASME

International, 1995a) provides requirements for the design, fabrication, and inspection of nuclear components to assure component integrity for the range of expected operating conditions. Although the applicability and use of the ASME Boiler and Pressure Vessel Code for the construction of the waste packages are not established, DOE indicates that waste packages will conform to the requirements of this code where practicable. Fabrication processes, including cold work during machining and forming, welding, and stress mitigation methods, such as induction annealing, laser peening, and low-plasticity burnishing, may alter the mechanical properties of the engineered barrier system components. This report focuses on the effects of fabrication processes on the mechanical properties of the materials proposed for the waste package.

1.1 Objective

In support of the NRC prelicensing activities on topics important to the preclosure safety analysis and postclosure performance of the proposed repository, the Center for Nuclear Waste Regulatory Analyses (CNWRA) is conducting an independent technical assessment of the effects of fabrication processes on the mechanical properties of the waste package materials. This report provides a review of the proposed DOE fabrication methods used to construct the disposal containers and seal the waste packages after waste loading operations and an evaluation of the effects of fabrication processes on the microstructure and mechanical properties of Alloy 22 and Type 316 nuclear grade stainless steel.

1.2 Scope and Organization of the Report

The effect of fabrication processes on the mechanical disruption of the Alloy 22 outer container is addressed in NRC (2001, 2002). Fabrication processes may alter the mechanical properties, the passive film stability, and the localized corrosion and stress corrosion cracking resistance of the Alloy 22 outer container, which could lead to early through-wall penetration or fracture of the waste package. NRC (2002) identifies several limitations and deficiencies in the DOE approach and in the technical bases provided for evaluation of the effects of fabrication processes on the performance of the Alloy 22 waste package outer barrier.

The DOE approach to evaluate the effects of fabrication processes on the mechanical properties of Alloy 22 is limited to the assessment of yield strength, ductility, and impact toughness (Charpy) based on the use of welded and thermally aged specimens. Effects of fabrication processes on the fracture toughness of Alloy 22 are not analyzed. In addition the DOE assessment is limited to a single welding method, and DOE has not considered the complete range of fabrication process necessary to construct and seal the Alloy 22 waste package outer container. At present, DOE has not performed an assessment of the effects of fabrication processes on the microstructural alteration and the mechanical properties of the Type 316 nuclear grade stainless steel inner container.

Fabrication and closure of the waste packages involves a range of forming and machining operations, welding, postweld heat treatments, and residual stress mitigation methods. Alloy 22 and other similar nickel-chromium-molybdenum alloys are known to exhibit phase instability at elevated temperatures. Formation of secondary phases as a consequence of welding, thermal exposure, or both may alter the mechanical properties of Alloy 22. The mechanical properties also may be influenced by the welding method and compositional variations of the base alloy and filler metals. The mechanical properties of Types 304 and 316 SS are known to be

dependent on the selection of the welding method and filler metal composition. It is anticipated the mechanical properties of the Type 316 nuclear grade stainless steel inner container also are dependent on the choice of the fabrication method and the base and filler metal composition. Degradation of mechanical properties as a consequence of fabrication and closure processes may lead to early failure of the waste packages. Therefore, the effects of fabrication processes on the mechanical properties of the waste package materials need to be assessed.

This report is organized into five chapters, with an introduction as Chapter 1. Waste package design and fabrication processes are discussed in Chapter 2. This chapter provides an overview of the fabrication sequence and a description of the welding and nondestructive examination methods. Chapter 3 addresses the effects of fabrication processes on the microstructure of Alloy 22 and Type 316 nuclear grade stainless steel. A review of the DOE approach and results for Alloy 22 are included along with results of the microstructural evaluation performed at CNWRA. Chapter 4 addresses the effects of fabrication processes on the mechanical properties of Type 316 SS and Alloy 22. A summary of conclusions and recommendations for future work needed to provide technical assistance to support the resolution of these closed-pending subissues prior to the license application is included in Chapter 5.

1.3 Relevant DOE and NRC Agreements

As noted, the effect of fabrication processes on the microstructure and mechanical properties of the waste package is considered in Subissue 2 of NRC (2001), and is incorporated in NRC (2002). Through the process of prelicensing consultation for issue resolution between DOE and NRC, these subissues are considered closed-pending. Agreements pertaining to stress corrosion cracking and environmentally assisted cracking of container and drip shield materials are listed in Table 1-1. According to the agreements for resolving all deficiencies and limitations identified in this report, DOE agrees to provide additional information prior to license application.

Table 1-1. DOE and NRC Agreements Related to This Report	
Agreement	**Agreement Statement**
PRE.7.03	Demonstrate that the allowed microstructural and compositional variations of Alloy 22 base metal and the allowed compositional variations in the weld filler metals used in the fabrication of the waste packages do not result in unacceptable waste package mechanical properties. DOE will provide justification that the ASME code case for Alloy 22 results in acceptable waste package mechanical properties considering allowed microstructural and compositional variations of Alloy 22 base metal and the allowed compositional variations in the weld filler metals used in the fabrication of the waste packages. DOE agrees to provide the information in FY03 and document the information in the waste package design.
PRE.07.04	Demonstrate that the non-destructive evaluation methods used to inspect the alloy 22 and 316 nuclear grade plate material and closure welds are sufficient and are capable of detecting all defects that may alter waste package mechanical properties. DOE will provide justification that the non-destructive evaluation methods used to inspect the alloy 22 and 316 nuclear grade plate material and welds are sufficient and are capable of detecting defects that may adversely affect waste package pre-closure structural performance. DOE agrees to provide the information in FY03 and document the information in the Waste Package Operations Fabrication Process Report.
PRE.07.05	Provide justification that the mechanical properties of the disposal container fabrication and waste package closure welds are adequately represented considering the (1) range of welding methods used to construct the disposal containers, (2) postweld annealing and stress mitigation processes, and (3) postweld repairs. DOE agrees to provide the information in FY03 and document the information in the Waste Package Operations Fabrication Process Report.

Table 1-1. DOE and NRC Agreements Related to This Report (continued)	
Agreement	**Agreement Statement**
CLST.2.08*	Provide documentation of the path forward items in the "Subissue 2: Effects of Phase Instability of Materials and Initial Defects on the Mechanical Failure and Lifetime of the Containers" presentation, slide 16 [future rockfall evaluations will address (1) effects of potential embrittlement of WP closure material after stress annealing due to aging, (2) effects of drip shield wall thinning due to corrosion; (3) effects of hydrogen embrittlement on titanium drip shield; and (4) effects of multiple rock blocks falling on WP and drip shield; future seismic evaluations will address the effects of static loads from fallen rock on drip shield during seismic events]. DOE stated that the rockfall calculations addressing potential embrittlement of the waste package closure weld and rock falls of multiple rock blocks will be included in the next revision of the AMR ANL–UDC–MD–000001, Design Analysis for UCF Waste Packages, to be completed prior to LA. Rock fall calculations addressing drip shield wall thinning due to corrosion, hydrogen embrittlement of titanium, and rock falls of multiple rock blocks will be included in the next revision of the AMR ANL–XCS–ME–000001, Design Analysis for the Ex-Container Components, to be completed prior to LA. Seismic calculations addressing the load of fallen rock on the drip shield will be included in the next revision of the AMR ANL–XCS–ME–000001, Design Analysis for the Ex-Container Components, to be completed prior to LA.

*Schlueter, J.R. "U.S. Nuclear Regulatory Commission/U.S. Department of Energy Technical Exchange and Management on Container Life and Source Term (September 12–13, 2000)." Letter (October 4) to S. Brocoum, DOE. Washington, DC: NRC. 2000.

2 WASTE PACKAGE DESIGN AND FABRICATION

The overall system design of the proposed repository at Yucca Mountain, Nevada, includes waste packages containing high-level waste horizontally emplaced in excavated drifts. The waste packages perform several functions during preclosure operations including containing the high-level waste, maintaining waste configuration to prevent criticality, allowing transfer and transportation of the waste to the emplacement drifts and, if necessary, retrieving the waste from the underground facility. Waste packages will be designed to fulfill the requirements of 10 CFR 63 Subpart K during operations and before final closure of the repository. Specifically, the U.S. Department of Energy (DOE) must ensure that no member of the public in the general environment receives more than an annual dose of 0.15 mSv [15 mrem]. In addition, the waste package design also supports attaining long-term repository objectives, including specific dose limits for the 10,000-year regulatory period defined in 10 CFR 63 Subpart L. DOE must demonstrate, using performance assessment, there is a reasonable expectation that for 10,000 years following disposal, the reasonably maximally exposed individual receives no more than an annual dose of 0.15 mSv [15 mrem] from releases from the undisturbed Yucca Mountain proposed disposal site.

2.1 Waste Package Design

Several broad classes of waste forms will be disposed in the proposed repository at Yucca Mountain, Nevada. These waste forms include commercial spent nuclear fuel, plutonium disposition waste, vitrified high-level reprocessed waste, and canistered DOE spent nuclear fuel (DOE, 2002). To accommodate these classes of waste forms, a suite of 10 waste packages is considered for the proposed license application (CRWMS M&O, 2000c). Of these, four representative waste packages will be more fully developed at the point of license application for construction authorization (Anderson, et al., 2003). A brief description of the proposed waste packages is provided in Table 2-1. The four selected designs are indicated with a double dagger. Although the features described previously are common to all these waste packages, the internal components of the waste packages vary to accommodate the different waste forms. The waste package for commercial fuel will have an internal basket design to support fuel assemblies. In other waste packages, the internal basket will have a different design, or the basket will be contained inside a canister. The predominant waste package design is the 21-pressurized water reactor commercial spent nuclear fuel assembly using neutron absorber plates. This design represents approximately 38 percent of the waste packages for the first repository's capacity of 70,000 metric tons [77,140 tons] of heavy metal waste (DOE, 2002).

All waste package designs consist of a pair of cylindrical containers fabricated from Alloy 22 and Type 316 nuclear grade stainless steel (Table 2-2) (CRWMS M&O, 2000c). The inner container will be constructed of Type 316 nuclear grade stainless steel and designed for structural support. The outer container will be constructed of Alloy 22 and designed for long-term corrosion resistance in the repository environment. Top and bottom lids made of Type 316 nuclear grade stainless steel complete the inner container. The Alloy 22 outer container will have one bottom lid and two top lids. The second Alloy 22 top lid will be used to provide further protection against stress corrosion cracking in the closure weld area (DOE, 2002). Two trunnion collars attached to the Alloy 22 outer container facilitate lifting and handling the waste package.

Table 2-1. Waste Package Design*	
Waste Package Design	**Description**
21 PWR† absorber plate‡	Capacity: 21 commercial pressurized water reactor assemblies and absorber plates for preventing criticality
21 PWR control rod	Capacity: 21 commercial pressurized water reactor assemblies with higher reactivity, requiring additional criticality control provided by placement of control rods in all assemblies
12 PWR long	Capacity: 12 commercial pressurized water reactor assemblies and absorber plates for preventing criticality; longer than fuel assemblies placed in 21 pressurized water reactor packages; because of the smaller capacity, an assembly also may be used for fuel with higher reactivity or thermal output
44 BWR§‡	Capacity: 44 commercial boiling water reactor assemblies and absorber plates for preventing criticality
24 BWR	Capacity: 24 commercial boiling water reactor assemblies and absorber plates for preventing criticality
5 defense high-level waste/DOE spent nuclear fuel short‡	Capacity: 5 short high-level waste canisters and 1 short DOE spent nuclear fuel canister. When high-level waste includes immobilized plutonium cans, no DOE spent nuclear fuel is placed in the center.‖
5 defense high-level waste/DOE spent nuclear fuel long	Capacity: 5 long high-level waste canisters and one long spent nuclear fuel canister‖
2 multicanister overpacks/ 2 defense high-level waste long	Capacity: 2 DOE multicanister overpacks and 2 long high-level waste canisters
Naval spent nuclear fuel short	Capacity: 1 short Naval spent nuclear fuel canister
Naval spent nuclear fuel long‡	Capacity: 1 long Naval spent nuclear fuel canister

*DOE. "Yucca Mountain Science and Engineering Report—Technical Information Supporting Site Recommendation Consideration." DOE/RW–0539–1. Rev. 1. Las Vegas, Nevada: DOE, Office of Civilian Radioactive Waste Management. 2002.
†PWR—pressurized water reactor
‡These four designs will be developed further at license application for construction authorization.
§BWR—boiling water reactor
‖DOE non-Naval spent nuclear fuel

Table 2-2. Chemical Composition*		
Element	**Composition of Alloy 22† (Weight Percent)**	**Composition of Type 316 Nuclear Grade Stainless Steel‡ (Weight Percent)**
Carbon (C)	0.015 (max)	0.020 (max)
Manganese (Mn)	0.50 (max)	2.00 (max)
Silicon (Si)	0.08 (max)	0.75 (max)
Chromium (Cr)	20.0 to 22.5	16.00 to 18.00
Molybdenum (Mo)	12.5 to 14.5	2.00 to 3.00
Cobalt (Co)	2.50 (max)	0.10 (max)
Tungsten (W)	2.5 to 3.5	—
Vanadium (V)	0.35 (max)	0.1 (max)
Iron (Fe)	2.0 to 6.0	Balance
Phosphorus (P)	0.02 (max)	0.030 (max)
Sulfur (S)	0.02 (max)	0.005 (max)
Nickel (Ni)	Balance	11.00 to 14.00
Copper (Cu)	—	0.50 (max)
Titanium (Ti)	—	0.05 (max)
Tantalum (Ta) and Niobium (Nb)	—	0.05 (max)
Nitrogen (N)	—	0.060 to 0.10
Boron (B)	—	0.002 (max)
Bismuth (Bi) + Tin (Sn) + Arsenic (As) + Lead (Pb) + Antimony (Sb) + Selenium (Se)	—	0.02 (max)
Aluminum (Al)	—	0.04 (max)

*DOE. "Yucca Mountain Science and Engineering Report—Technical Information Supporting Site Recommendation Consideration." DOE/RW–0539–1. Rev. 1. Las Vegas, Nevada: DOE, Office of Civilian Radioactive Waste Management. 2002.
†Source for Alloy 22: ASTM B 575-97, Standard Specification for Low-Carbon Nickel-Molybdenum-Chromium, Low-Carbon Nickel-Chromium-Molybdenum, Low-Carbon Nickel-Chromium-Molybdenum-Copper, and Low-Carbon Nickel-Chromium-Molybdenum-Tungsten Alloy Plate, Sheet, and Strip.
‡Sources for Type 316 nuclear grade stainless steel: for all elements except carbon and nitrogen, values presented are within the ranges and maximum limits provided by ASTM A276–91a, Standard Specification for Stainless and Heat-Resisting Steel Bars and Shapes. Values for carbon and nitrogen are given by Danko, J.C. "Corrosion in the Nuclear Power Industry." *Corrosion Metals Handbook.* 9th Edition. Vol. 13. Materials Park, Ohio: ASM International. p. 931. 1987.

2.2 Fabrication Methods for the Waste Package Components

Although all disposal containers will be fabricated in nearly identical fashion, their dimensions vary to accommodate the various waste forms. Because many disposal container designs are not fully developed, the commercial fuel disposal container, which is one of the waste package baseline designs, is presented in this section. All disposal containers are constructed of a Type 316 nuclear grade stainless steel inner cylinder and an Alloy 22 outer corrosion barrier (CRWMS M&O, 2001a; DOE, 2002). This combination of materials and design is selected for the long-term protection of the contained waste form.

The outer and inner disposal containers will be fabricated from mill-annealed plate that is rolled and welded to form cylinders. Two cylinders will be placed end-to-end and welded (circumferential weld) to form the body of the containers. Top and bottom lids will be cut and prepared from mill-annealed plate before being welded to the cylinders. Trunnion collar sleeves will be similarly cut and fabricated from plate material and welded to the outer surface of the Alloy 22 cylinder. A summary of the welds used in the fabrication of the waste package, together with important information on each weld such as the type of weld, welding and nondestructive examination methods used, and postweld treatment, is compiled in Tables 2-3 and 2-4. Welding processes used in the fabrication of the disposal containers will be limited to shielded metal-arc, gas tungsten-arc, submerged-arc, and gas metal-arc (CRWMS M&O, 2001a). The processes, procedures, or both are qualified for the material to be welded. The disposal container design for site recommendation was to be fabricated in accordance with the requirements of the 1995 ASME Boiler and Pressure Vessel Code Section III Division 1 Subsection NB (class 1 components) (ASME International, 1995a) to the maximum extent possible, however, the disposal container is not intended to be a nuclear or N-stamped vessel (CRWMS M&O, 2001a). Recently, the waste package design was changed to include a Type 316 nuclear grade stainless steel inner container constructed to the requirements of the 2001 (with 2002 addenda) ASME Boiler and Pressure Vessel Code Section III Division 1 Subsection NC (class 2 components) (ASME International, 2001a). The Alloy 22 outer container will not be an ASME stamped vessel.[1]

2.2.1 Fabrication of the Alloy 22 Outer Disposal Container

Significant changes to the design of the Alloy 22 outer container have been proposed since the site recommendation waste package design.[2] In the proposed design for license application, the outer closure lid design has been modified to eliminate the outer lid extension. Minor changes have also been made in the design of the bottom of the container. Figure 2-1 shows the main features of the design proposed for license application. At present, detailed information is not available on this modified design and the fabrication methods. The equipment and operational sequences described in this section, therefore, largely reflect the design described in Civilian Radioactive Waste Management and Operating Contractor (CRWMS M&O) (2001a).

---

[1]Brown, N.R. "Application of the ASME Code for Waste Package Fabrication." *Presentation at the NRC/DOE Technical Exchange on Waste Package Design, June 4, 2003.* Las Vegas, Nevada. 2003.

[2]Brown, N.R. "Background—Waste Package Design." *Presentation at the NRC/DOE Technical Exchange on Waste Package Design, June 4, 2003.* Las Vegas, Nevada. 2003.

Table 2-3. Welding Parameters Alloy 22 Outer Container					
Weld Location	**Weld Type**	**Welding Method**	**Nondestructive Examination Method**	**Postweld Treatment**	**Comments**
Cylinder, longitudinal weld	Full Penetration Longitudinal Weld	A, B, C, D*	Penetrant, radiographic, and ultrasonic examinations	Solution annealing	—
Cylinder, circumferential weld	Full Penetration Circumferential Weld	A, B, C, D	Penetrant, radiographic, and ultrasonic examinations	Solution annealing	—
Support ring	Fillet Weld?	—	—	Solution annealing	Changes in the design for license application; details not specified
Bottom lid	Full Penetration Circumferential Weld	B, D	Penetrant, radiographic, and ultrasonic examinations	Solution annealing	—
Top and bottom trunnion rings	—	—	—	—	Changes in the design for license application; details not specified
Top middle lid	Fillet weld	B	Method not specified	—	Changes in the design for license application; details not specified
Top closure lid	Full Penetration Circumferential Weld	B	Surface examination via alternating current field measurement (eddy current); ultrasonic examination	Laser peening or low-plasticity burnishing	Changes in the design for license application. Details not specified

*A—shielded metal-arc; B—gas tungsten-arc; C—submerged-arc; D—gas metal-arc

Table 2-4. Welding Parameters Type 316 Nuclear Grade Stainless Steel Inner Container				
Weld Location	**Weld Type**	**Welding Method**	**Nondestructive Examination Method**	**Postweld Treatment**
Cylinder, longitudinal weld	Full Penetration Longitudinal Weld	A,B,C,D*	Penetrant examination	None
Cylinder, circumferential weld	Full Penetration Circumferential Weld	A,B,C,D	Penetrant examination	None
Bottom lid	Full Penetration Circumferential Weld	B,C,D	Penetrant, radiographic, and ultrasonic examinations	None
Top lid	Spread Ring with Seal Weld	D	None	None
*A—shielded metal-arc; B—gas tungsten-arc; C—submerged-arc; D—gas metal-arc				

The main operations associated with the fabrication of the outer cylindrical wall of the disposal container include the following: after receipt inspection, the Alloy 22 plate will be cut and rolled to size. The long seam will be machined and prepared for welding, and welded using one of the four approved welding methods. In the site recommendation design, Alloy 22 outer container weld filler material is specified as ERNiCrMo-10 or a filler material used for welding alloys with the unified numbering system N06022 designation (CRWMS M&O, 2001a). The cylinder may need to be strutted or collapsible mandrels may be used to minimize weld distortion. The struts or mandrels will be removed and the weld seam is subject to penetrant, radiographic, and ultrasonic examinations. Finally, one end of the cylinder is prepared for circumferential seam welding which may require strutting of the cylinder. A second identical cylinder is fabricated using the second Alloy 22 plate, and the two cylinders will be joined end-to-end and circumferentially seam welded using one of the four approved methods. The seam will be prepared for nondestructive examination after removal of the struts, and nondestructive examination will be performed on the weld using penetrant, radiographic, and ultrasonic examinations. The cylinder will be inspected to verify dimensions including a minimum allowable plate thickness. The inside will be machined to allow for a loose fit {0–4 mm [0–0.157 in] radial gap} with the stainless steel cylinder (CRWMS M&O, 2001a).

A support ring is needed to hold the inner container after it is placed in the outer container. To fabricate the ring, a rectangular piece will be cut from the Alloy 22 plate and rolled into a ring shape (CRWMS M&O, 2001a). Weld preparations will be made, and the ring fitted at the bottom end of the cylinder and welded on the top side. The weld will be machined flush to enable the inner container to be set on the top of the ring (Figure 2-1). A penetrant examination will be performed on the machined surfaces (CRWMS M&O, 2001a).

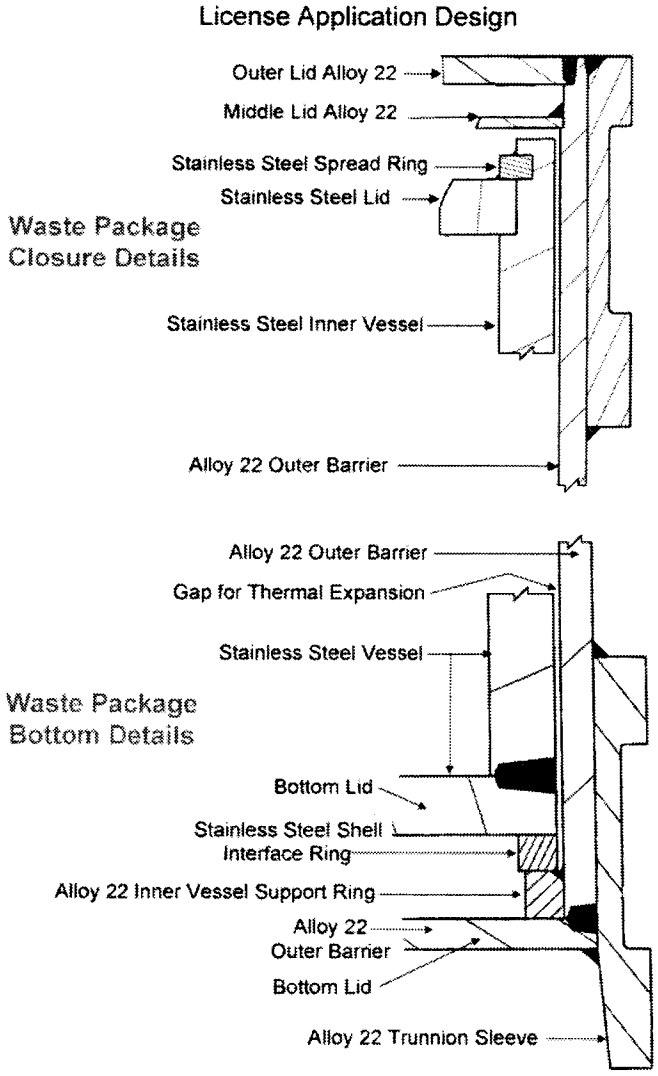

Figure 2-1. Schematic Illustration of Waste Package Design Details[3]

[3]Ibid.

The outer container will have one bottom lid and two top lids, each made of Alloy 22. Plates will be cut to the correct diameter and the edges cleaned to remove slag and scale before being machined to establish weld preparation. For the two top lids, a center lifting fixture will be fabricated and welded to the center of the lid (CRWMS M&O, 2001a).

To assemble the bottom lid, the Alloy 22 cylinder is set in the horizontal position, and the lid welded to the cylinder in this position using a gas metal-arc or a gas tungsten-arc method. The lid seam will be prepared for nondestructive examination, and inspected using penetrant, radiographic, and ultrasonic examinations (CRWMS M&O, 2001a). The inner Type 316 nuclear grade stainless steel and the outer Alloy 22 closure lids are not installed at the fabricator but will be shipped to the proposed repository site for installation after the disposal container is loaded.

The disposal container will have two trunnion collar sleeves made of Alloy 22—one for each end of the outer cylinder of the disposal container. The design of the sleeves has been changed to a one-piece design to improve operability.[4] The trunnion sleeves will be fitted to the disposal container by heating each sleeve to approximately 371 °C [700 °F], positioning it over the disposal container and allowing the sleeve to cool (CRWMS M&O, 2001a). Lessons learned from fiscal year 2000 closure weld mockup indicate the assembly sequence of the inner ring, bottom lid, and lower trunnion ring may be altered (CRWMS M&O, 2000d). Higher than expected distortion during the inner ring and bottom lid weldings may necessitate the assembly and partial welding of the lower trunnion ring prior to welding the inner ring and bottom lid. The trunnion ring provides reinforcement for the other welds and reduces distortion (CRWMS M&O, 2000d).

After fabrication, the Alloy 22 outer cylinder assembly (cylinder with support ring, bottom lid, and trunnion collars) will be solution annealed at approximately 1,125 °C [2,057 °F] to eliminate residual stresses created during the fabrication processes. The outer cylinder will be placed on a furnace car and heated to 1,150 °C [2,102 °F] in a furnace. The furnace car will be removed from the furnace and the outer cylinder quenched using water spray on the inside and outside surfaces of the cylinder to quickly reduce the temperature from 1,100 °C [2,012 °F] to below 800 °C [1,472 °F] in approximately 4 minutes. The cooling rate will be decreased to allow generation of compressive stresses on the outside (CRWMS M&O, 2001a).

2.2.2 Fabrication of the Type 316 Nuclear Grade Stainless Steel Inner Disposal Container

Fabrication methods to be used for the Type 316 nuclear grade stainless steel inner cylinder will be similar to those employed for the Alloy 22 outer cylinder. The Type 316 nuclear grade stainless steel plates will be cut, and machined to size and prepared for longitudinal welding. Each plate will be roll-formed to make a cylinder of the required diameter and welded longitudinally using one of the four acceptable methods including shielded metal-arc, submerged-arc, gas metal-arc, and gas tungsten-arc welding. Filler material for the Type 316 nuclear grade stainless steel inner container will be controlled so the delta ferrite content in the as-deposited weld-filler metal has a ferrite number between 5 and 15, determined by Magna-gage measurements (CRWMS M&O, 2001a). A penetrant examination is performed on the weld. The two half length cylinders thus formed are prepared for circumferential welding

[4] Ibid.

and welded end-to-end using one of the four approved methods. Penetrant examination inspection will be performed on the circumferential weld, and the cylinder machined externally to allow a loose fit inside the Alloy 22 outer cylinder of the disposal container. Loose fit is defined as 0–4-mm [0–0.157-in] radial gap between the cylinders. The minimum finished thickness and inner diameter of the cylinder must be maintained at the design value (CRWMS M&O, 2001a).

The top and bottom lids for the inner cylinder will be fabricated from Type 316 nuclear grade stainless steel plates. The edges will be cleaned to remove slag and scale, and the circular lids machined. The bottom lid will be assembled by setting the inner cylinder in the horizontal position and welding the lid to the cylinder in this position using a submerged-arc, shielded metal-arc, gas metal-arc, or gas tungsten-arc method. The lid seam will be prepared for nondestructive examination and inspected using penetrant, radiographic, and ultrasonic examinations (CRWMS M&O, 2001a).

2.2.3 Disposal Container Assembly

Following the completion of fabrication, nondestructive examination, solution annealing (Alloy 22 only), final machining, and dimensional inspection, the Type 316 nuclear grade stainless steel inner container will be placed inside the Alloy 22 outer container. To accommodate the installation, the outer surface of the Type 316 nuclear grade stainless steel container and inner surface of the Alloy 22 container will be machined to provide a radial gap of 0–4 mm [0–0.157 in] between cylinders on assembly. The disposal container will be assembled by heating the outer Alloy 22 container to approximately 371 °C [700 °F] before inserting the Type 316 nuclear grade stainless steel into the outer container and allowing the assembly to cool (CRWMS M&O, 2001a).

2.3 Waste Package Closure

The waste package has three closure lids—one for the inner Type 316 nuclear grade stainless steel container and two for the Alloy 22 outer container (Figure 2-1). These lids will be used to seal the waste form in the disposal container. For the proposed license application, significant changes are proposed to the design of the top and bottom lids. The full penetration lid weld of the top lid has been replaced with a spread ring and seal weld, and the plate thickness appears to have been decreased (Anderson, et al., 2003).

The closure operations will be performed in the closure cell facility and cover the remote placement, welding, inspection, and postweld stress relief of the closure lids. A detailed process sequence of the remote operations performed in the closure cell facility is given in CRWMS M&O (2001b).

2.3.1 Closure Cell Facility

The closure cell facility includes two gas metal-arc welding stations for the inner lid and six gas tungsten-arc welding stations for welding the two Alloy 22 outer shell closure lids. Postweld heat treatment stations were originally included in the closure cell facility to perform induction annealing of the outer Alloy 22 closure lid weld (CRWMS M&O, 2001b). Every station will be equipped with a closure gantry manipulator that delivers lids and end effectors from the maintenance bay via an air lock to the filled disposal container. There will be a clean control

room area for operators to oversee, track, and control remote disposal container closure operations.

The closure cell control system controls the remote operations in each closure cell in the facility. This system controls the closure gantry manipulator and end effectors while also controlling the data-acquisition subsystem, machine vision/image processing system, welding power supply, and various valves and regulators. The closure cell control system also communicates with the human machine interface that provides real-time status and operating conditions, alerts, and a data entry/control means to the operator. A central disposal container tracking system will be used to provide central coordination and control for all cells and for the storage of data pertaining to each disposal container.

2.3.2 Remote Operations Associated with the Three Closure Lids

Closure operations for the inner Type 316 nuclear grade stainless steel closure lid will be performed in one of two gas metal-arc welding inner lid weld stations located in the closure cell facility. The main steps in the sequence of remote operations include the following.

- A visual inspection, using a remote pan and tilt high-radiation camera with lights, is performed of the weld preps for the inner Type 316 nuclear grade stainless steel closure lid and the two Alloy 22 outer closure lids and of the top of the spent nuclear fuel/high-level waste (CRWMS M&O, 2001b). Digital image processing and machine vision techniques will be used. Process parameter anomalies generate a flag in the data stream and alert the operator.

- A confirmatory check of the weld preparations will be performed using a tactile coordinate measuring machine. This machine employs a linear voltage displacement transducer probe mounted on a rotational axis. The machine will be used to determine cylindricity of the disposal container by locating the disposal container center relative to the closure gantry manipulator coordinate system (CRWMS M&O, 2001b).

- An inner lid fixture will be used next to simultaneously deliver the inner lid and the four shear ring segments to the disposal container. After the lid is positioned on the disposal container, the four segments will be inserted with the help of pneumatic linear slides, and the shear ring segments will be tack welded. A six-axis gas metal-arc welding robotic arm welder will be used (CRWMS M&O, 2001b).

- The inner lid fixture will be removed and the inner ring seal welded using the gas metal-arc welding robotic arm welder. The gas metal-arc welding robotic arm used for this operation will have a rotational range greater than 360 degrees and the ability to perform a full circumferential weld (CRWMS M&O, 2001b).

- Real-time weld inspection will be performed using digital image processing and machine vision techniques. All critical welding parameters such as filler metal usage, weld current, voltage, wire speed, gas flow, and robotic arm coordinates will be recorded in process. The closure cell control system notifies the operator immediately of parameter anomalies, and a flag will be placed in the data stream. If possible, weld repair is performed in the inner lid weld station. If extensive machining of the weld is necessary,

the disposal container will be moved to the inner lid repair station, also located in the closure cell facility (CRWMS M&O, 2001b).

After welding, a vacuum check will be performed to verify the integrity of the inner lid shear ring seal weld. The inner shell will be filled with helium to a pressure of approximately 1 atmosphere. The purge port will be welded shut using the gas metal-arc welding robotic arm welder, and a final seal integrity test will be conducted. Nondestructive examination of the seal weld will be limited to visual examination. The sealed Type 316 nuclear grade stainless steel inner disposal container will be transported out of the inner weld station (CRWMS M&O, 2001b).

The Alloy 22 outer cylinder of the disposal container will have a middle closure lid and a thicker outer closure lid, both constructed of Alloy 22 (see Figure 2-1). The welding of the lids will be performed in one of the six gas tungsten-arc welding weld stations in the closure cell facility.

The sequence of remote operations performed and equipment used will be similar to that used for the inner lid. Visual inspection of the middle and outer lid weld preparations will be performed using the same visual inspection and end effector systems described previously. The tactile coordinate measuring machine will be then used to determine the cylindricity and location of the disposal container center relative to the closure gantry manipulator coordinate system.

The middle closure lid fixture used contains the middle closure lid and a gas tungsten-arc welding orbital welder equipped with a cross seam axis, automatic arc voltage control axis, and dual axis wire manipulator. The fixture will have one rotational axis with a gas tungsten-arc welding torch mounted at a 45-degree angle to an adjustable indexed arm (CRWMS M&O, 2001b). Unlike the gas metal-arc welding robotic arm, the end effector requires water cooling of the welding torch. All critical welding parameters such as filler metal usage, weld current, voltage, wire speed, gas flow, and robotic arm coordinates will be recorded during the welding process. The closure cell control system notifies the operator immediately of parameter anomalies, and a flag will be placed in the data stream. A nondestructive examination will be performed on the fillet weld[5] of the middle lid; however, the method and procedure are still being developed.

After the middle closure lid is installed and inspected, the disposal container will be fitted with the outer closure lid at the same gas tungsten-arc welding weld station. Visual inspection and scan of the outer lid weld preparation will be performed using the same equipment described in the preceding sections. The outer closure lid fixture used contains the outer closure lid and a nuclear grade gas tungsten-arc welding orbital welder equipped with the same components as the middle lid orbital welder. The fixture will have one rotational axis with a gas tungsten-arc welding torch mounted at a 90-degree angle to an adjustable indexed arm. The end effector requires water cooling of the welding torch. When the outer lid is positioned on the disposal container, an argon purge will be performed to displace air within the disposal container with argon.

---

[5]Cogar, J.A. "Overview of the Design." *Presentation to the Nickel Development Institute, October 16, 2002.* Las Vegas, Nevada. 2002.

The orbital welder will be used to first tack weld and then weld the lid on to the disposal container. All critical welding parameters such as filler metal usage, weld current, voltage, wire speed, gas flow, and robotic arm coordinates will be recorded in process. The closure cell control system notifies the operator immediately of parameter anomalies, and a flag will be placed in the data stream.

A nondestructive examination on the lid weld will be performed using a special end effector capable of performing both a surface examination and a volumetric inspection (CRWMS M&O, 2001b). Alternating current field measurement will be used for the surface examination while ultrasonic testing with couplant will be used for the volumetric inspection. The present design (CRWMS M&O, 2001b) calls for two passes (rotations) to perform the inspection. On the first pass (rotation), the inspection scans the weld using the alternating current field measurement probe (eddy current). An ultrasonic examination inspection will be performed on the second scan. Any repairs needed will be performed before the disposal container is transferred to the postweld heat treatment station for annealing.

A visual inspection and tactile coordinate measuring machine routine will be performed at the postweld heat treatment station to verify the disposal container has not been damaged during transfer and to determine the location of the center of the disposal container relative to the closure gantry manipulator coordinate system. The disposal container will be annealed using laser peening or low-plasticity burnishing. A general description of these processes is provided in later sections. A final set of nondestructive examinations will be performed using the two methods described in the preceding paragraph. The nondestructive examination includes the surface and volumetric inspections of the postannealed closure weld.

2.3.3 Postweld Stress Mitigation

Postweld stress mitigation is proposed for the Alloy 22 closure lid welds to eliminate residual stresses that may promote stress corrosion cracking. The postweld stress mitigation methods presently being investigated include induction annealing, laser peening, and low-plasticity (or controlled plasticity) burnishing. All proposed processes are designed to impart compressive residual stresses to the closure weld region. Complete details of the process parameters, as well as depth and stress distribution profiles, are not determined.

For the site recommendation waste package design, local induction annealing is proposed for the extended Alloy 22 outer closure lid as a method to eliminate residual tensile stresses in the Alloy 22 outer closure weld. The proposed induction annealing process heats the end of the Alloy 22 disposal container with the completed closure weld to a temperature of 1,150 °C [2,102 °F] . Forced air or water will be used to rapidly reduce the temperature of the closure weld region (CRWMS M&O, 2001b). Specifications for cooling times and temperature distributions are not reported. Laser peening is proposed for the inner Alloy 22 closure lid weld. Because this remote operation must take place in the closure cell facility, a laser peening end effector (laser mounted on an adjustable indexed arm) is likely to be used. A cross seam and vertical axis may be employed to adjust the laser position as it rotates over the weld. The process is likely to require constant water spraying to help direct and propagate the heat-sustained shock waves into the metal interior. The end effector, therefore, needs to incorporate a recirculation system to minimize water usage in the cell. Because the power requirements of such a system are expected to be high (~20 MW), a mirror transmission technique is likely to become necessary. DOE plans to investigate a fiber optic system developed by Toshiba for

in-situ laser peening of welds in stainless steel core shrouds of nuclear power plants (CRWMS M&O, 2001b).

Recent changes to the waste package design eliminated the extended Alloy 22 outer closure lid design intended to serve as a heat sink during the proposed induction annealing processes. The most recent proposed waste package design calls for a flat closure lid with either laser peening or low-plasticity burnishing used as a postweld stress mitigation method (Anderson, et al., 2003). It is assumed a similar method will be employed in the case of the Alloy 22 outer lid closure weld previously described in CRWMS M&O (2001b).

Low-plasticity burnishing is proposed as an alternate method to impart compressive residual stresses to the Alloy 22 outer container closure welds (Anderson, et al., 2003). Gordon[6] reported compressive stresses to depths of 8 mm [0.31 in] for 100 mm [1.25 in] with a maximum residual stress of 1,350 MPa [195 ksi] at a depth of 0.2 mm [0.008 in] using high-pressure, low-plasticity burnishing with an applied load of 5,400 kg [12,000 lbs]. For depths of 1–8 mm [0.039–0.315 in], the compressive residual stress is 480–170 MPa [70–25 ksi]. The amount of cold work or changes to the microstructure are not reported, however, compressive stresses to depths 1.2–1.5 mm [0.047–0.059 in] with less than 10-percent cold work throughout the depth of the near surface region are reported for Alloy 718 (Migala and Jacobs, 2002; Prevey, et al., 2000).

[6]Gordon, G. "Stress Corrosion Cracking and Stress Mitigation." *Presentation at the 5th Nickel Development Institute Workshop on the Fabrication and Welding of Nickel Alloys and Other Materials for Radioactive Waste Containers, October 16–17, 2002.* Las Vegas, Nevada. 2002.

3 EFFECTS OF FABRICATION PROCESSES ON THE MICROSTRUCTURE OF TYPE 316 NUCLEAR GRADE STAINLESS STEEL AND ALLOY 22

In this chapter, the effects of fabrication processes on the microstructure of both Alloy 22 and Type 316 nuclear grade stainless steel are discussed. Microstructural changes in Alloy 22 resulting from fabrication processes have been reviewed and evaluated in a recent Center for Nuclear Waste Regulatory Analyses report (Dunn, et al., 2003). The section on Alloy 22 provides a summary of the microstructure that may influence the mechanical properties of the alloy in both the wrought and welded conditions. The section on Type 316 nuclear grade stainless steel reviews the effects of thermomechanical treatments (i.e., aging, solution annealing, cold work, and welding) on the microstructure in both the wrought and welded conditions based on the information reported in the literature. The influence of compositional variations on both the precipitation and solidification behavior is also discussed.

3.1 Microstructure of Type 316 Nuclear Grade Stainless Steel

The microstructure and material properties of Type 316 nuclear grade stainless steels are strongly dependent on its chemical composition and thermomechanical history. The composition of the alloy is provided in Table 2-2. The microstructure of Type 316 nuclear grade stainless steel is completely austenitic in the wrought condition, whereas welded material has a duplex structure consisting of austenite and ferrite phases. Further thermal exposure during waste package fabrication and storage can promote the formation of second phase precipitates that may be detrimental to the mechanical properties and the corrosion resistance of the alloy. The microstructure of the wrought and the welded Type 316 nuclear grade stainless steel, as influenced by compositional variation and thermomechanical treatment, is discussed in the following sections.

3.1.1 Wrought Material

The precipitation behavior of wrought Type 316 SS has been reviewed by Lai (1983). The major factors that may influence the characteristics of precipitation include alloy composition, temperature, time, and thermomechanical treatments. Weiss and Stickler (1972) show that aging of Type 316 and 316L SS in the temperature range of approximately 400–900 °C [752–1,652 °F] results in the precipitation of carbides ($M_{23}C_6$ and M_6C) and the intermetallic phases (σ, χ, and η). Electrolytic phase extraction in a hydrochloric acid-methanol mixture and subsequent chemical analysis by energy-dispersive x-ray spectroscopy in a scanning electron microscope reveals the $M_{23}C_6$-type carbide contained mostly chromium and some molybdenum and nickel with a composition formula of $(Cr_{16}Fe_5Mo_2)C_6$. For the chemical composition of the intermetallic phases, the σ- and χ-phases are enriched in chromium and molybdenum, whereas the η-phase is enriched in molybdenum. Lai (1983) notes other minor phases such as ferrite, R-phase, and ϵ-martensite also have been observed.

Weiss and Stickler (1972) also report the time-temperature regions for the stability of the various precipitate phases in Types 316 and 316L SS based on the results of optical and electron microscopic analyses. Figure 3-1 shows the time-temperature-precipitation diagrams (also known as the C-curves) of Type 316L SS after solution-annealing treatments at 1,090 °C [1,994 °F] and 1,260 °C [2,300 °F] for 1.5 hours, followed by water quenching. As shown in Figure 3-1, the stability regions of the various precipitates are partially overlapping, suggesting a complex

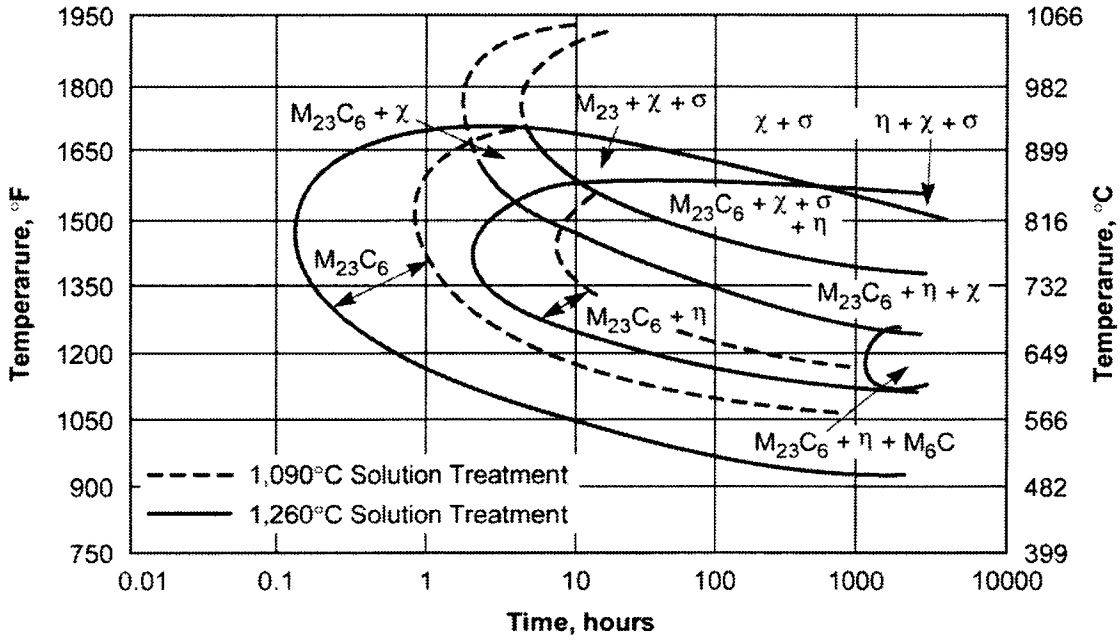

Figure 3-1. Time-Temperature-Precipitation Diagram for Wrought Type 316L SS Solution-Treated at 1,090 °C [1,994 °F] and 1,260 °C [2,300 °F] (Weiss and Stickler, 1972)

sequence in the precipitation reactions in Type 316 SS. Nevertheless, $M_{23}C_6$ is found to be the first precipitate phase to form at grain boundaries, and increasing aging temperature results in coarser carbide particles at grain boundaries with reduced intragranular precipitation. Higher solution-annealing treatment is also observed to shift the C-curve for the precipitation of $M_{23}C_6$ carbide to shorter times and slightly lower temperatures, but no significant effect is seen on the precipitation kinetics of the intermetallic phases. The observed effect of solution-annealing temperature on aging is attributed to large grain sizes and high quench-in vacancy concentrations after solution annealing at higher temperatures. In addition, the presence of a higher carbon content in Type 316 SS, in comparison with that in Type 316L SS (0.066 versus 0.023 wt%), accelerates the formation of $M_{23}C_6$ carbide, while the formation of the intermetallic phases is retarded. These sensitization to intergranular corrosion of stainless steels has been known to occur in specific environments as a result of the precipitation of chromium-rich carbides and the formation of a chromium-depleted area adjacent to the grain boundary (Hall and Briant, 1984). It is important to note that Type 316 nuclear grade stainless steel is characterized by a maximum carbon content of 0.020 wt%, as listed in Table 2-2. This low carbon content is anticipated to further hinder the formation of carbide precipitates further and thus improve sensitization resistance.

The effect of cold working prior to aging on the precipitation behavior of Type 316L SS has been studied by Weiss and Stickler (1972). Figure 3-2 shows the time-temperature-precipitation diagram of Type 316L SS with 20-percent cold work. A comparison of Figures 3-1 and 3-2 indicates that cold working accelerated the precipitation of carbides and intermetallic phases by shifting the C-curves to shorter times. The nose temperature of the C-curves for $M_{23}C_6$ dropped approximately 40 °C [104 °F] with the addition of 20-percent cold work. The cold-worked

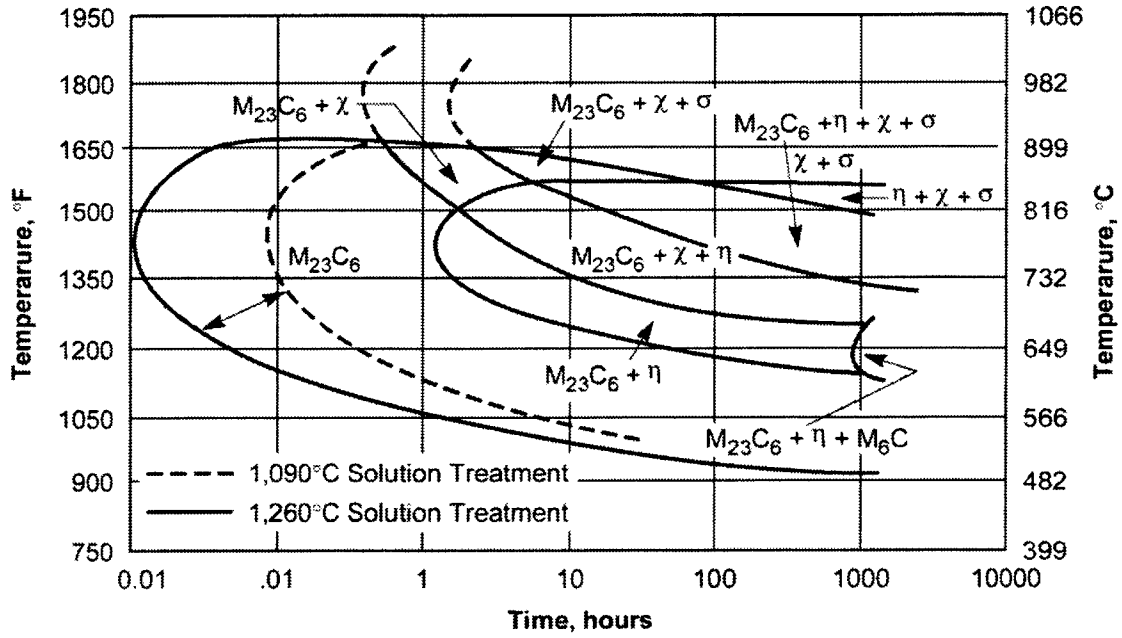

Figure 3-2. Time-Temperature-Precipitation Diagram for Type 316L SS Solution-Annealed at 1,090 °C [1,994 °F] and 1,260 °C [2,300 °F] with 20-Percent Cold Work

microstructure of Type 316L SS exhibits the network of dislocations and stacking faults, resulting in increased rates of nucleation and growth of the precipitates as a consequence of enhanced diffusion in the highly dislocated matrix. Advani, et al. (1991) also finds that cold working (plastic strain) prior to aging increases the kinetics of precipitation in Type 316 SS, consistent with the observations of Weiss and Stickler (1972). Advani, et al. (1991) calculates the activation energy for chromium diffusion as a function of prior cold work on the basis of the sensitization kinetics. The activation energy for unstrained Type 316 SS is 76 kcal mol^{-1} [318 kJ mol^{-1}] and decreases to 62 kcal mol^{-1} [259 kJ mol^{-1}] for the 16-percent strained material. The accelerated precipitation in the cold-worked alloy is attributed to the changes in diffusion kinetics by reducing the preexponential term and the activation energy.

3.1.2 Welded Material

Fabrication of Type 316 nuclear grade stainless steel inner containers by welding is a design requirement. The microstructure of austenitic stainless steel welds typically contains a variety of complex austenite-ferrite structures as a result of the solidification behavior and subsequent solid-state transformations. The solidification processes, solid-state transformations, and the resultant microstructures in austenitic welded metals have been reviewed by Brooks and Thompson (1991). It is well known that, in welding austenitic alloys such as Type 316L SS, a certain amount of ferrite is needed in the weld fusion zone to prevent hot cracking. Control of the ferrite content, however, is critical for the performance of the welds because ferrite can transform to a variety of carbides and intermetallic phases on subsequent exposure to service temperatures and postweld heat treatments. In addition, segregation of alloying elements such as chromium and molybdenum to the ferrite during solidification of the austenitic welded metal may promote hot cracking and adversely affect the mechanical properties because of the

precipitation of carbides and intermetallic phases. Hence, the solidification microstructure, the effect of aging on the microstructure, and the influence of alloy composition are considered of primary importance in controlling the mechanical properties of the welded material.

Prediction of ferrite content in austenitic weld metals based on empirical diagrams, such as the Schaeffler and DeLong diagrams, has been reviewed by Olson (1985). The Schaeffler diagram was originally developed for predicting the microstructure in dissimilar steel joints based on chromium and nickel equivalents. The use of chromium equivalent allows correction of the effects of ferrite stabilizing elements (i.e., chromium, molybdenum, silicon, and niobium), whereas nickel equivalent accounts for the effects of austenite stabilizing elements (i.e., nickel, manganese, and carbon). The calculation of chromium and nickel equivalents (Cr_{eq} and Ni_{eq}) in the Schaeffler diagram on a weight percent basis is defined as Eqs. (3-1) and (3-2)

$$Cr_{eq} = Cr + Mo + 1.5Si + 0.5Nb \quad (3\text{-}1)$$

$$Ni_{eq} = Ni + 0.5Mn + 30C \quad (3\text{-}2)$$

The DeLong diagram is a modification of the Schaeffler diagram for predicting ferrite content, taking into account the austenitising effect of nitrogen and the effect of welding conditions. The nickel equivalent, also on a weight percent basis, is expressed as Eq. (3-3)

$$Ni_{eq} = Ni + 0.5Mn + 30C + 30N \quad (3\text{-}3)$$

The DeLong diagram for predicting ferrite content of shielded metal-arc welds in austenitic stainless steels is given in Figure 3-3. Lines of constant ferrite number, as well as magnetically measured volume percent ferrite, are provided in the diagram. The scale for ferrite number, calibrated by measurements of standard ferrite specimens using a magnetic device, has been adopted by the International Welding Institute for measurement of ferrite content. As shown in Figure 3-3, the ferrite number is numerically equal to volume percent ferrite for 6 percent or less ferrite. Also shown in Figure 3-3 is the allowable composition range for Type 316 nuclear grade stainless steel based on the alloy composition provided in Table 2-2. On the basis of this diagram, the as-welded ferrite content in the Type 316 nuclear grade stainless steel welds with heat-to-heat variations in alloy composition can be evaluated. It has been shown that 3–8 wt% ferrite is expected in the austenitic stainless steel welds, which is required to reduce the susceptibility of hot cracking (Olson, 1985).

The microstructure of solidified austenitic stainless steels is generally characterized by the ferrite morphology. Brooks and Thompson (1991) review the effect of the primary solidification mode on the resultant weld microstructure of austenitic stainless steels. In general, there are two primary solidification modes, depending on the alloying compositions: primary austenite solidification and primary ferrite solidification. Brooks and Thompson (1991) summarize the as-welded microstructures resulting from solidification and transformation of austenitic stainless steels into four types of ferrite microstructures based on the distribution and morphology of the retained ferrite, namely, eutectic ferrite, skeletal ferrite, lathy ferrite, and Widmanstatten austenite. Olson (1985) notes the amount, morphology, and distribution of ferrite required to produce optimal weld strength are service-temperature dependent. Ferrite has a ductile-to-brittle transition temperature that lowers the fracture toughness of the welds at low service temperatures, whereas ferrite transforms to the embrittled σ-phase at high service

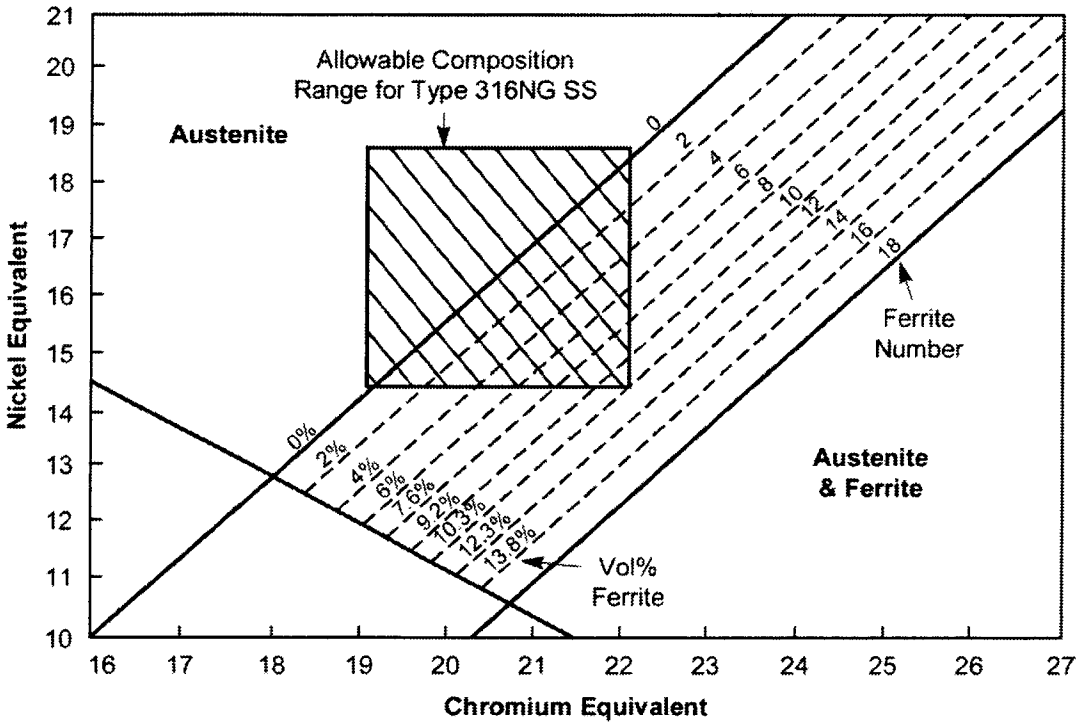

Figure 3-3. DeLong Diagram for Predicting Ferrite Content of Shielded Metal-Arc Welds in Austenitic Stainless Steels (Brooks and Thompson, 1991)

temperatures. It has been reported that for welded Type 316 SS, 5 vol% ferrite provides a noncontinuous network and optimum high-temperature creep strength.

Welding processes also have been known to alter the welded microstructures due to the changes in solidification behavior as a consequence of the heat input and the thermal history of the weldment. Brooks and Thompson (1991) review the effect of cooling rate on weld microstructures and note the high cooling rates during high-energy density welding, such as electron beam and laser welding, result in a refined microstructure and a change in solidification mode in austenitic stainless steel welds. Mills (1988a) studies the effect of weld processes on the fracture toughness of austenitic stainless steel welds, including shielded metal-arc, submerged-arc, and gas tungsten-arc processes. Formation of manganese silicide inclusions is found to be detrimental to ductile fracture behavior as a consequence of silicon pickup from the flux during welding. Gas tungsten-arc welds that contain no silicide particles yield the highest fracture resistance. Although cold working was found to increase the precipitation kinetics in wrought Type 316 SS, the combined effects of welding and cold working on the precipitation behavior of Type 316 SS have not been reported.

The phase transformations of the ferrite phase and the factors controlling the mechanical properties of austenitic weld metals have been reviewed by Smith and Farrar (1993). The review shows the resultant precipitate type and morphology have a significant effect on the mechanical properties. Therefore, it is important to determine the amount, type, and morphology of precipitates and how they vary with time and temperature during aging. It has been reported in numerous studies on the effect of aging of austenitic-welded metals that aging

at 500–900 °C [932–1,652 °F] results in the progressive dissolution of ferrite and the precipitation of carbides and intermetallic phases. Figure 3-4 shows the time-temperature-precipitation diagram of Type 316 SS (Fe-19Cr-12Ni-3Mo in weight percent) in wrought and welded conditions. As shown in Figure 3-4, precipitation of $M_{23}C_6$ carbide, and particularly intermetallic phases in the welded material, is much faster than in the wrought material. The accelerated precipitation kinetics are attributed to segregation of chromium and molybdenum during solidification and an increase in diffusivity as a result of higher dislocation density in the welded material.

The alloy chemistry also has profound effects on the formation of the carbide and intermetallic phases in the welds. Studies by various investigators on Type 316 SS welds show that higher levels of carbon content suppress the formation of intermetallic phases, whereas higher levels of molybdenum and silicon content increase the propensity for intermetallic formation (Smith and Farrar, 1993). In addition, microsegregation of chromium and molybdenum in the a-swelded state accelerate the kinetics of the phase transformations by a factor of 2 to 3. Gill, et al. (1989) examine the microstructures evolved and consequent changes in the tensile properties on aging of Type 316L SS weld at 500–700 °C [932–1,292 °F] for up to 5,000 hours. The amount and morphology of σ-phase that depend on the relative kinetics of various transformations are found to be the key factors in determining the tensile strength of aged welds.

3.2 Microstructure of Alloy 22

Changes in material microstructure and microchemistry resulting from fabrication processes are considered possible degradation mechanisms that may impair corrosion resistance and mechanical properties of the Alloy 22 waste package outer barrier (NRC, 2002; Payer, et al., 2002). The composition of Alloy 22 is provided in Table 2-2. The microstructure of Alloy 22 in the wrought condition is a single-phase, face-centered cubic solid solution. Unlike Type 316 nuclear grade stainless steel, Alloy 22 solidifies as fully austenitic welds. Segregation of chromium and molybdenum, however, occurs in the solidified Alloy 22 weld fusion zone. In addition, Alloy 22 can undergo solid-state transformations as a consequence of thermal

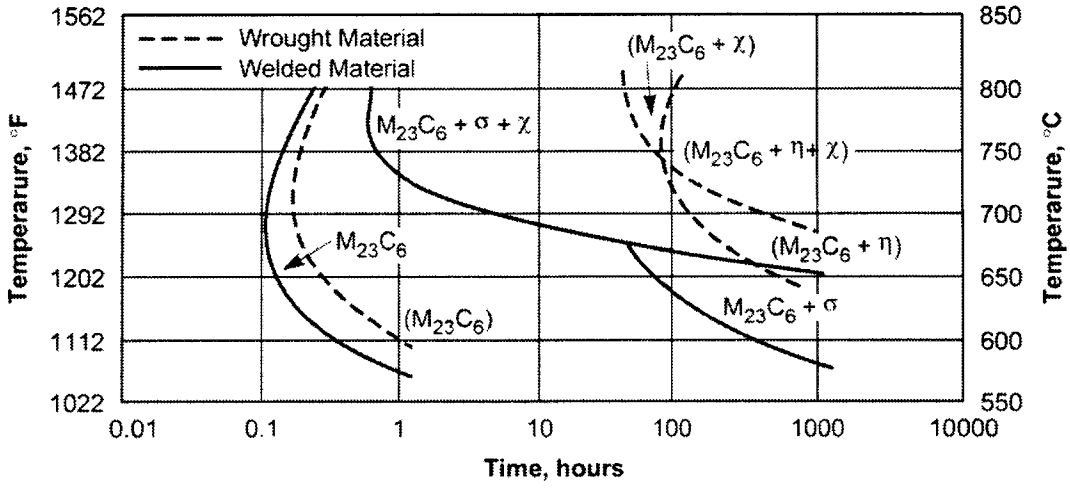

Figure 3-4. Time-Temperature-Precipitation Diagram for Wrought and Welded Type 316 SS (Smith and Farrar, 1993)

exposure in the wrought and welded conditions. The microstructures of the wrought and the welded Alloy 22, as influenced by compositional variation and thermomechanical treatment, are discussed in the following sections.

3.2.1 Wrought Material

The phase stability of mill-annealed Alloy 22 has been studied by aging samples in the temperature range 260–800 °C [500–1,472 °F] for time periods up to 40,000 hours (CRWMS M&O, 2000e). Several phases are observed to form in Alloy 22 after thermal aging, including topologically close-packed phases (σ, P, and μ), carbides, and $Ni_2(Cr, Mo)$ long-range ordering. The observations of second-phase formations in the thermally aged Alloy 22 are summarized in a time-temperature-precipitation diagram in Figure 3-5 where the type of precipitation is not presented. As shown in Figure 3-5, Alloy 22, when subjected to thermal aging, undergoes two types of phase transformation, depending on the temperature range: precipitation of topologically close-packed phases at temperatures greater than approximately 600 °C [1,112 °F] and long-range ordering at temperatures less than approximately 600 °C [1,112 °F]. Precipitation of topologically close-packed phases in Alloy 22 is observed to first start preferentially at grain boundaries and later within the grains. Three stages of precipitation are determined through scanning electron microscopy examination: partial grain-boundary coverage, full grain-boundary coverage, and bulk precipitation. Figure 3-5 also shows that long-range ordering is observed to start after 1,000 hours of aging at temperatures of 538 and 593 °C [1,000 and 1,099 °F]. Long-range ordering is also observed in the samples aged at 427 °C [800 °F] for 30,000 and 40,000 hours.

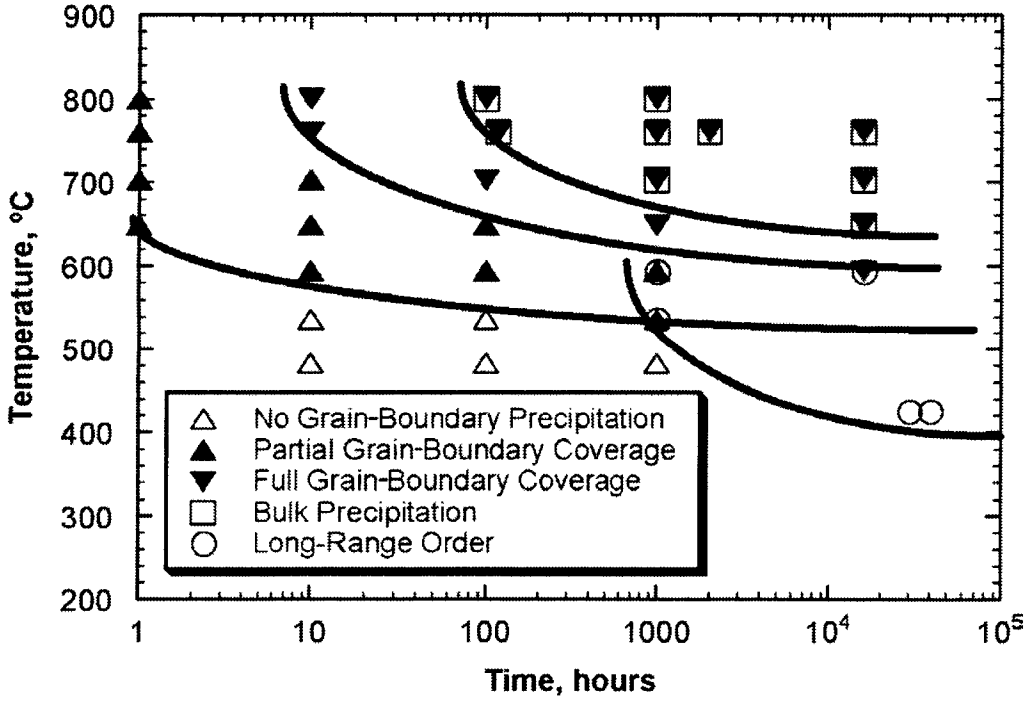

Figure 3-5. Time-Temperature-Precipitation Diagram for Wrought Alloy 22 (CRWMS M&O, 2000e)

NOTE: Temperature provided in °C; for temperature conversion, use °F = 9/5 °C + 32.

Heubner, et al. (1989) establish the time-temperature-precipitation diagram of Alloy 22 solution annealed at 1,160 °C [2,120 °F] in Figure 3-6 based on microstructural examination using optical microscopy. It is apparent in Figure 3-6 that precipitation starts at grain boundaries after aging at 750 °C [1,382 °F] for 15 minutes. Shorter aging times for formation of precipitates at grain boundaries 800–900 °C [1,472–1,652 °F] can be anticipated. The time-temperature-precipitation diagrams for the precipitation of topologically close-packed phases and long-range ordering in Alloy 22 are also calculated using the Thermo-Calc and DICTRA software packages (CRWMS M&O, 2001c). The DICTRA application linked with Thermo-Calc is used to simulate the diffusion-controlled phase transformations for both the ordered Ni_2Cr phase and the topologically close-packed P-phase. The predicted time-temperature-precipitation diagrams for bulk precipitation are shown in Figure 3-7, together with experimental results indicated by the data points. In the case of the ordered Ni_2Cr phase, 10-percent transformation of the ordered phase in a binary nickel-chromium matrix is calculated for constant temperature conditions. The predictions are consistent with the results extracted from the work of Karmazin (1982). For the isothermal transformation of P-phase, a ternary nickel-chromium-molybdenum alloy was considered with a composition of 55.7Ni-21.1Cr-13.5Mo in weight percent with the transformation rate ranging from 1 to 20 percent. The time-temperature-precipitation diagrams in Figure 3-7, however, are predicted for precipitation of P-phase controlled by bulk diffusion, and the calculated times are longer than the experimental results in the case in which only grain-boundary precipitation is observed. In addition, the calculated time-temperature-precipitation diagrams are observed to shift the C-curves for the precipitation of topologically close-packed phases to lower temperatures in comparison with the work of Heubner, et al. (1989) shown in Figure 3-6. In Figures 3-5 and 3-7, no data are presented for times shorter than 1 hour.

The microstructure of mill-annealed Alloy 22 after aging at 870 °C [1,598 °F] for times ranging 5 to 30 minutes has been reported (Pan, et al., 2003; Dunn, et al., 2003). Optical microscopic examination of the polished Alloy 22 specimens reveal that, while the grain boundaries of the mill-annealed and the 5-minute-aged specimens appeared clean, partial grain-boundary precipitation coverage is observed in the 30-minute-aged specimen. Further grain-boundary microstructure characterization of the thermally aged Alloy 22 by transmission electron microscopy indicates that an aging time of 5 minutes produced thin-film type grain-boundary precipitates having a thickness of approximately 10 nm [3.9×10^{-7} in], which is beyond the resolution of the optical microscope. The size of the precipitates increases substantially after aging for 30 minutes. No grain-boundary precipitate is observed in the mill-annealed specimen. The chemical compositions of the grain-boundary precipitates and the regions adjacent to the precipitates measured in the thin-foil specimens by energy-dispersive x-ray spectroscopy spot analysis show the measured concentrations of molybdenum and tungsten in the precipitates are much higher than the bulk content of these elements. In addition, the composition at the regions adjacent to the precipitates is similar to the bulk composition of Alloy 22 with a slightly lower molybdenum content. Concentration profiles of nickel, chromium, molybdenum, iron, and tungsten obtained across precipitate-matrix interfaces and along grain boundaries between precipitates show a smooth transition from the matrix to the precipitate in all cases. These results indicate that no significant depletion of chromium and molybdenum is detected in the matrix adjacent to the precipitates nor in the grain-boundary regions between precipitates.

Chromium depletion in sensitized stainless steels is widely accepted to be prompted by the precipitation and growth of chromium-rich carbides at grain boundaries because of the fast diffusion of carbon, compared with chromium, to the grain boundaries (Bruemmer, 1990). In

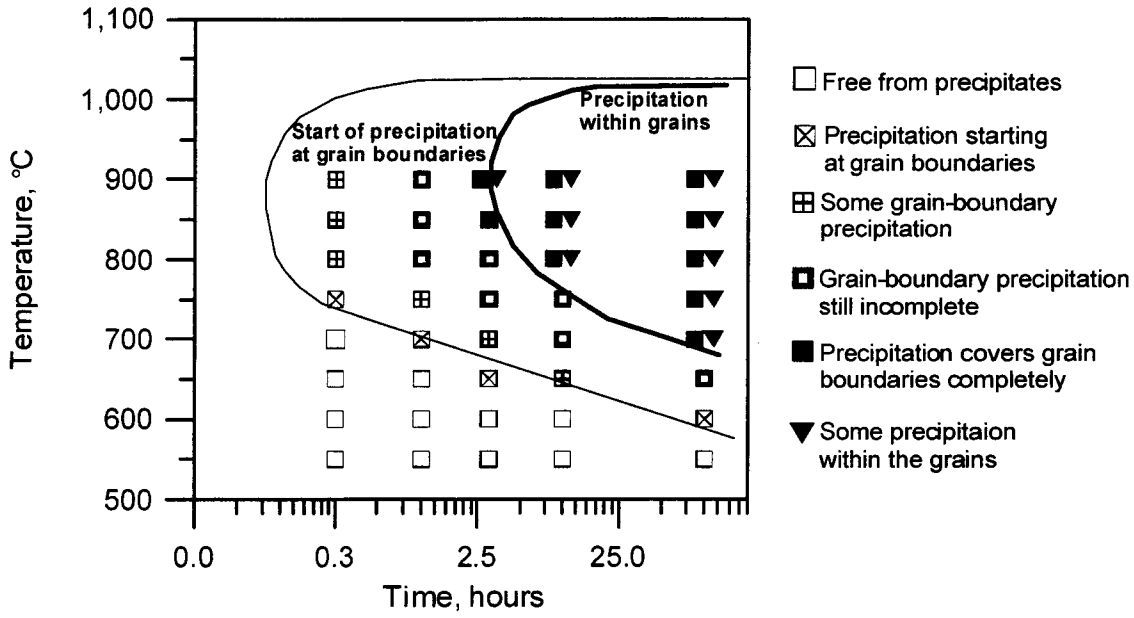

Figure 3-6. Time-Temperature-Precipitation Diagram for Wrought Alloy 22 (Huebner, 1989)

NOTE: Temperature provided in °C, for temperature conversion use, °F = 9/5 °C + 32.

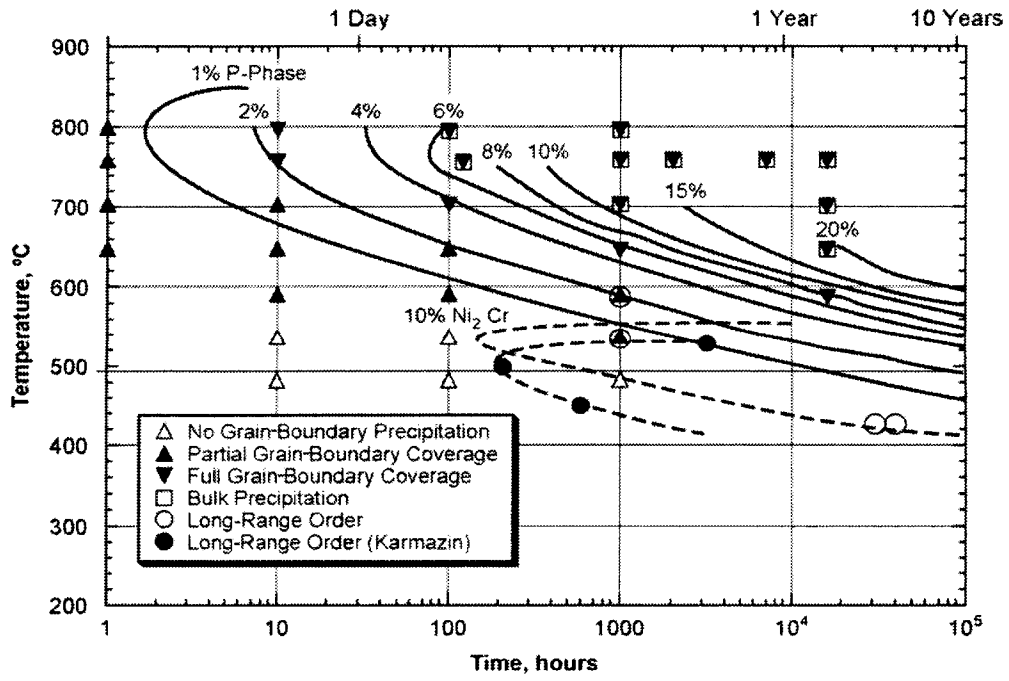

Figure 3-7. Predicted Time-Temperature-Transformation Diagrams for Ni_2Cr and P-Phase (DOE, 2002)

NOTE: Temperature provided in °C, for temperature conversion use, °F = 9/5 °C + 32.

contrast with the kinetics of carbide precipitation that is determined by carbon diffusion, precipitation of the topologically close-packed phases is anticipated to be governed by substitutional element diffusion. The major elements in forming the topologically close-packed phases, such as molybdenum, nickel, and chromium, are expected to have comparable bulk diffusivities. For this reason, development of a sharp depletion of chromium or molybdenum, if any depletion zone is present, should not be expected.

The phase-transformation theory of nucleation and growth is employed in an attempt to derive precipitation kinetics for extrapolation of the short-term, high-temperature data to repository-relevant temperatures (CRWMS M&O, 2000e). Figure 3-8 shows the log(time) versus reciprocal temperature plots for the various precipitation stages of topologically close-packed phases in thermally aged Alloy 22 base metal. Note the time errors are because of the uncertainty associated with the widely spaced aging time periods. From the slopes of the lines in Figure 3-8, an average activation energy for the precipitation of topologically close-packed phases can be determined to be near 280 kJ mol^{-1} [66.9 kcal mol^{-1}]. Using this activation energy value, the lines associated with grain-boundary coverage and bulk precipitation can be extrapolated to 10,000 years. Both grain-boundary coverage and bulk precipitation of topologically close-packed phases are predicted not to occur in 10,000 years at 300 °C [572 °F]. Using the minimum-allowed slope from the time-error bars, however, bulk precipitation of topologically close-packed phases is not expected, but grain-boundary precipitation may occur.

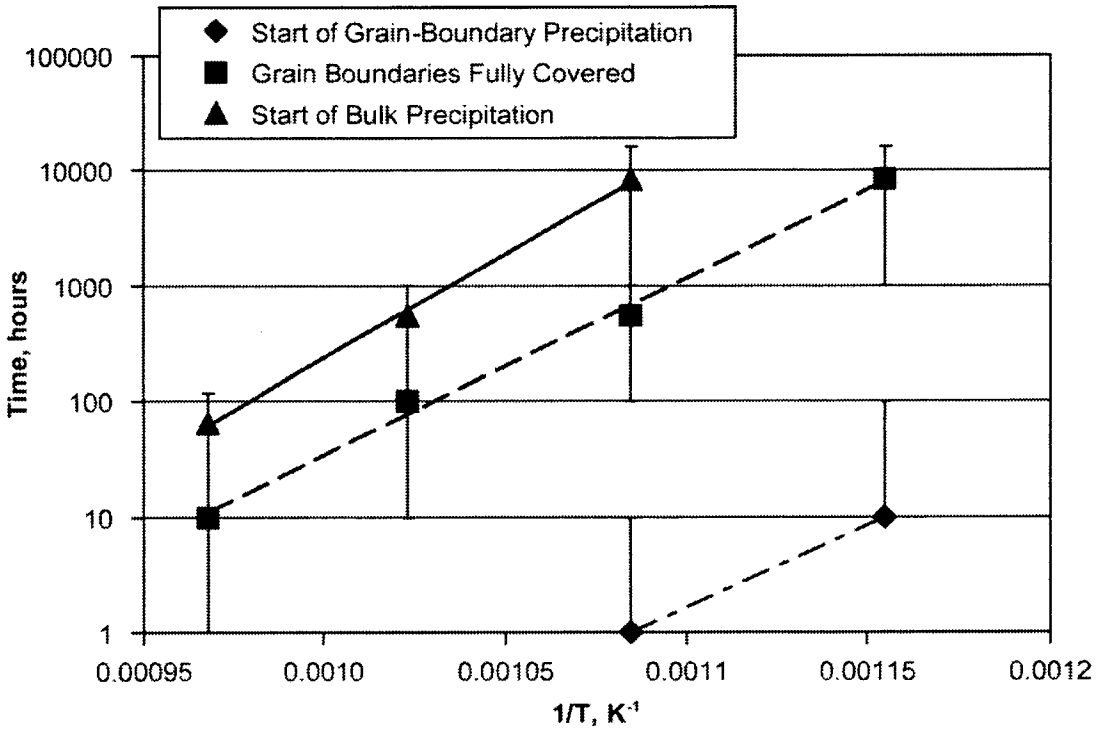

Figure 3-8. Log(Time) Versus Reciprocal Temperature Plots for Various Precipitation Stages of Topologically Close-Packed Phases in Alloy 22 Base Metal (CRWMS M&O, 2000e)

A similar extrapolation of the short-term data for long-range ordering in Alloy 22 base metal was reported (CRWMS M&O, 2000e). The kinetics of long-range ordering in Alloy 22 is estimated using the shortest times at which long-range ordering is observed. From the limited experimental data, two points corresponding to aging at 538 °C [1,000 °F] for 1,000 hours and 427 °C [800 °F] for 30,000 hours are plotted. A curve fit to these data yields Eq. (3-4)

$$t = 5 \cdot 10^{-7} \exp\ (17395 / T) \tag{3-4}$$

where

T — aging temperature (Kelvin)
t — time (hours)

Extrapolation of this curve indicated that, at 300 °C [572 °F], long-range ordering may occur in Alloy 22 base metal in 872 years.

A revised curve fit, based on two new data points corresponding to aging at 538 °C [1,000 °F] for 100 hours and 427 °C [800 °F] for 20,000 hours where long-range ordering was observed in Alloy 22 base metal, is expressed as Eq. (3-5) (CRWMS M&O, 2001c)

$$t = 3 \cdot 10^{-13} \exp\ (27098 / T) \tag{3-5}$$

It should be noted that from Eqs. (3-4) and (3-5), the activation energy for the formation of long-range ordering can be calculated. The calculated activation energy varies from 144 kJ/mol [34.4 kcal/mol] to 225 kJ/mol [53.8 kcal/mol]. Extrapolation of the revised curve shows the occurrence of long-range ordering in Alloy 22 base metal is not expected in 10,000 years at 300 °C [572 °F]. Because nucleation and growth of the topologically close-packed phases and long-range ordering may be kinetically sluggish, a large uncertainty is associated with the extrapolation of short-term, high-temperature data to repository-relevant temperatures and times.

The upper stability temperature of topologically close-packed phases (also known as solvus temperature) in wrought Alloy 22, as influenced by alloy compositional variation, is evaluated using thermodynamic calculations (Dunn, et al., 2003). Evaluation of the effect of compositional variation on the solvus temperature of P-phase is accomplished by varying the composition between the specified limits for each element, as listed in Table 2-2. The baseline Alloy 22 composition is assumed to be 21.2Cr-13.5Mo-4Fe-3W-2Co-0.08Si-0.01C-balance nickel in weight percent. The estimated P-phase solvus temperatures, as each element is varied between its maximum and minimum limits, are shown in Figure 3-9. The thermodynamic calculation using the baseline composition gives a solvus temperature for P-phase of 1,074 °C [1,965 °F]. Molybdenum, as the major topologically close-packed phase forming element, exhibits the greatest effect on the upper stability temperature of the P-phase. Other P-phase forming elements (i.e., chromium and tungsten) also have a profound effect. The potent influence of iron must be attributed to the largest variation between its maximum and minimum limits. Hence, heat-to-heat variations in the Alloy 22 composition may influence the formation and dissolution of topologically close-packed phases.

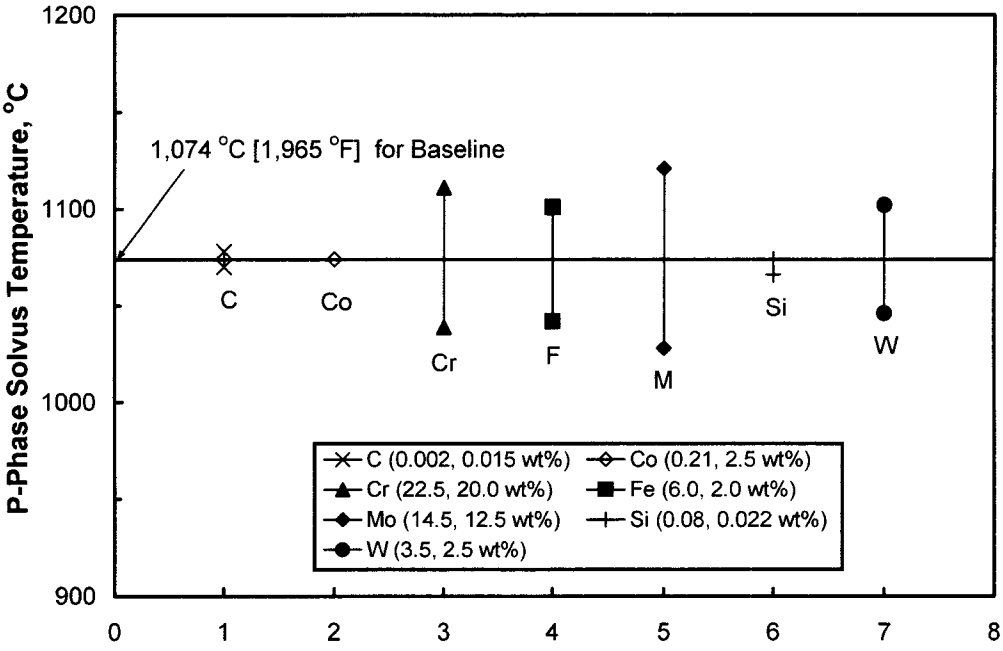

Figure 3-9. Variation in Calculated P-Phase Solvus Temperature by Varying Each Element in Alloy 22 within Its Composition Limits (Dunn, et al., 2003)

NOTE: Temperature provided in °C, for temperature conversion use, °F = 9/5 °C + 32.

3.2.2 Welded Material

The phase stability of Alloy 22 gas tungsten-arc welds, emphasizing the formation of the topologically close-packed phases (CRWMS M&O, 2001c). The amount and size of precipitates in the welds are noted to vary with position in the welds. Because of the inhomogeneous distribution of the precipitates, the amount of precipitates in the as-welded condition was measured to be 2.9 and 2.5 vol% from multiple measurements for several positions at 200× and 400× magnification. Microstructural characterization of the welds in the as-welded condition shows the formation of a dendritic structure and the presence of topologically close-packed phases in the interdendritic regions (CRWMS M&O, 2000e). Chemical analysis of the precipitates in the welds by energy-dispersive x-ray spectroscopy indicates the precipitates in the interdendritic regions are molybdenum rich, whereas, few particles in the dendrite cores appear to be carbides.[1] Additionally, microprobe concentration profiles show segregation of molybdenum and chromium to a lesser extent in the interdendritic regions.

Summers, et al. (2002) report precipitate volume fraction measurements in Alloy 22 welds. Aging of the welded materials is conducted at temperatures between 593 and 760 °C

[1]Summers, T. "Potential Degradation Modes—Metallurgical Issues." *Presentation to the DOE Waste Package Materials Performance Peer Review Panel, September 25, 2001.* Las Vegas, Nevada. 2001.

[1,099 and 1,400 °F] for time periods up to 1,000 hours. Figure 3-10 shows the volume fraction of topologically close-packed phases in the welded samples measured from optical micrographs using imaging analysis software as a function of aging time and temperature. From these volume fraction data of topologically close-packed phases in the Alloy 22 welds, precipitation kinetics for topologically close-packed phases are evaluated on the basis of the plots in log(time) versus reciprocal temperature. The activation energy calculated from the slopes of the plots for both 5- and 10-vol% topologically close-packed phases precipitation is approximately 210 kJ mol^{-1} [50.2 kcal mol^{-1}]. Using this activation energy value, extrapolation to 10,000 years indicated that both predicted temperatures are above 300 °C [572 °F]. It is noted the activation energy for precipitation of topologically close-packed phases in welded Alloy 22 is lower than the value of 280 kJ mol^{-1} [66.9 kcal mol^{-1}] for wrought material, as previously discussed. These kinetics data suggest that welding treatment increases the precipitation kinetics in Alloy 22.

Dunn, et al. (2003) also report the microstructure of gas tungsten-arc welded Alloy 22. Formation of a dendritic structure and precipitation of secondary phases are evident in the fusion zone of the welded material. An average value of 0.42 vol% of precipitates is measured in the as-welded condition. It is noted, however, that the microstructure adjacent to the fusion zone is not significantly altered, and a heat-affected zone is not clearly evident in the welded material. Local compositions of the dendrite cores and the interdendritic regions are determined using energy-dispersive x-ray spectroscopy analysis. Table 3-1 shows the mean and standard deviation chemical composition values of the dendrite cores and the interdendritic regions measured by spot analysis in the Alloy 22 welded specimen in the as-welded condition. It is

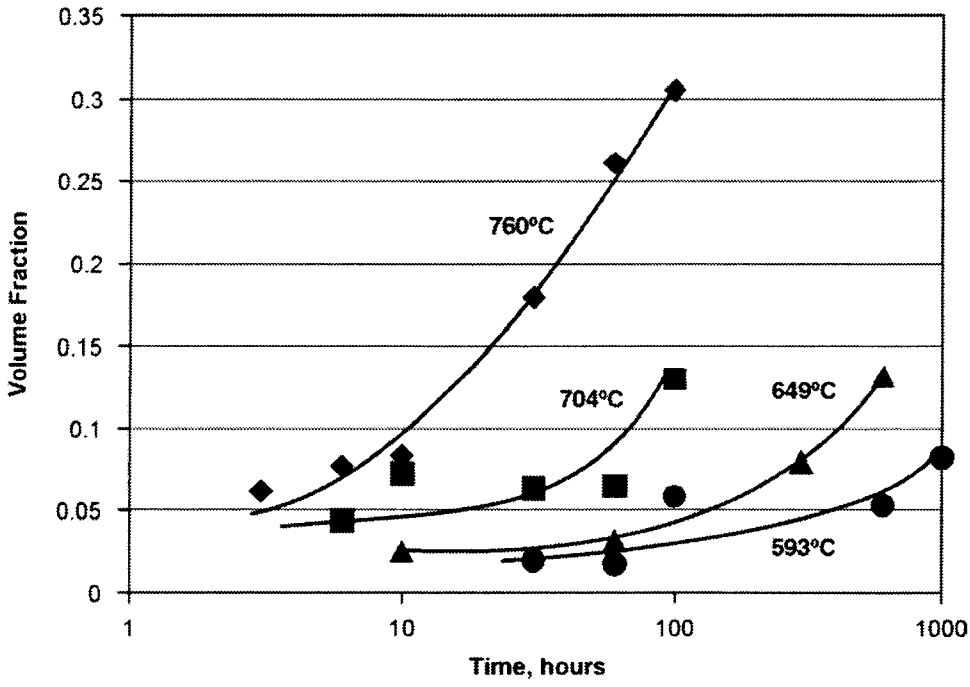

Figure 3-10. Volume Fraction of Precipitates in Alloy 22 Welds As a Function of Time for Various Temperatures (Summers, et al., 2002)

NOTE: Temperature provided in °C, for temperature conversion use, °F = 9/5 °C + 32.

Table 3-1. Measured Chemical Compositions and Calculated P-Phase Solvus Temperatures in the Weld Fusion Zone*						
	Chemical Content (Weight Percent)					
Location	Nickel	Chromium	Molybdenum	Iron	Tungsten	P-Phase Solvus Temperature
Dendrite Core	59.8 ± 1.3	21.8 ± 0.4	13.0 ± 1.1	2.75 ± 0.11	2.60 ± 0.09	1,024 °C [1,875 °F]
Interdendritic Region	54.4 ± 1.6	22.6 ± 0.2	18.0 ± 1.6	2.48 ± 0.07	2.48 ± 0.06	1,271 °C [2,320 °F]
Alloy 22 Base Metal	60.64	20.44	12.80	2.63	3.08	1,026 °C [1,879 °F]
Alloy 622 Filler	59.89	20.41	13.99	2.46	2.96	1,066 °C [1,951 °F]

*Dunn, D.S., D. Daruwalla, and Y.-M. Pan. "Effect of Fabrication Processes on Material Stability—Characterization and Corrosion." San Antonio, Texas: CNWRA. 2003.

apparent in Table 3-1 that molybdenum tends to segregate to the interdendritic regions as a consequence of nonequilibrium solidification because of its higher melting point in comparison with the other major alloying elements (i.e., nickel and chromium). The measured molybdenum concentration is much higher than the bulk molybdenum content in the Alloy 22 base metal and the Alloy 622 filler metal, as listed in Table 3-1. Cieslak, et al. (1986) analyze the welding microstructure and microchemistry of gas tungsten-arc welds of Alloy 22. The concentration profiles are obtained transverse to the dendritic growth direction using electron microprobe analysis. It is also observed that the dendrite core is enriched in nickel and depleted in molybdenum relative to the interdendritic region.

Aging and solution-annealing treatments of the welded material are studied to evaluate the precipitation stability in the weld (Dunn, et al., 2003). Although the aging treatments are conducted at 760 °C [1,400 °F] for 6 and 60 hours and at 870 °C [1,598 °F] for periods ranging from 5 minutes to 4 hours, the solution annealing is performed at 1,125 °C [2,057 °F] for periods ranging from 15 to 60 minutes and at 1,200; 1,250; and 1,300 °C [2,192; 2,282; and 2,372 °F] for 15 minutes. It is shown the amount of precipitates increases with increasing aging time at the aging temperature of 870 °C [1,598 °F], whereas a decrease is observed for the aging temperature of 760 °C [1,400 °F]. With aging at 870 °C [1,598 °F], the size of the precipitates increases with increasing aging time. In contrast, the precipitate morphology after a 60-hour treatment at 760 °C [1,400 °F] becomes coarse, but the number of precipitates decreases significantly. The low volume fraction of precipitates measured for the welded sample aged at 760 °C [1,400 °F] for 60 hours can be attributed to a substantial grain growth in the fusion zone as a result of a prolonged aging. Also it is noted, the precipitate volume percent values measured for the 760 °C [1,400 °F] aged Alloy 22 welded specimens are much lower than the values reported by Summers, et al. (2002). Given that different Alloy 22 welds are used in these analyses, the observed discrepancies could be attributed to the effects of different welding process parameters on the resultant weld microstructure.

Regarding the effect of solution annealing, residual precipitates are observed for all solution annealing times at 1,125 °C [2,057 °F]. There are approximately 1.8 vol% precipitates after a 15-minute heat treatment at 1,125 °C [2,057 °F], a value higher than that in the as-welded condition. A long hold time up to 60 minutes does not significantly change the microstructure. Solution annealing at 1,125; 1,200; and 1,250 °C [2,057; 2,192; and 2,282 °F] results in homogenization of the fusion zone in comparison with that in the as-welded condition, and the extent of homogenization increases with increasing temperature. In contrast, after solution annealing at 1,300 °C [2,372 °F] for 15 minutes, the dendrite structure in the fusion zone is completely dissolved, and abnormal grain growth is observed with the majority of the precipitates located inside the grains. In all cases, the amount of precipitates per unit area seems to slightly decrease as the solution-annealing temperature increases. Nevertheless, the high volume fraction of precipitates in the solution annealed Alloy 22 welds indicates the solution annealing conditions employed, instead of forming a solid solution, promote precipitation of secondary phases.

Dunn, et al. (2003) evaluate the effect of alloying element segregation on the upper stability temperature of the P-phase in the Alloy 22 weld. The calculated solvus temperatures for the P-phase are listed in Table 3-1, based on the measured compositions in the Alloy 22 weld (Table 3-1). The thermodynamic calculation predicts a solvus temperature for the P-phase of 1,271 °C [2,320 °F] in the interdendritic regions, suggesting the P-phase is stable at temperatures up to 1,271 °C [2,320 °F]. Similar calculations are conducted using the compositions measured in the weld fusion zone by Cieslak, et al. (1986). The composition estimated from the microprobe profiles is approximately 62.2Ni-19.6Cr-10.9Mo-3.13Fe-2.75W in weight percent inside the dendrite core, and approximately 52.4Ni-21.1Cr-18.8Mo-2.90Fe-3.43W in the interdendritic region. From these values, the solvus temperatures for the P-phase in the dendrite core and the interdendritic region are calculated to be 872 and 1,319 °C [1,602 and 2,406 °F]. These results imply that current solution annealing of the Alloy 22 weld is inadequate to form a single-phase solid solution by dissolving the topologically close-packed precipitates.

4 MECHANICAL PROPERTIES OF ALLOY 22 AND TYPE 316 STAINLESS STEEL

Mechanical properties of the container materials are important for the structural integrity of the waste package. The candidate waste package materials, Type 316 nuclear grade stainless steel and Alloy 22, are known to be low-strength and highly ductile materials in the mill-annealed condition. Significant strain hardening is observed in both alloys. The high ductility and resistance to brittle fracture usually result in failure only after significant plastic deformation. The mechanical properties of the waste package container materials will likely be influenced by metallurgical factors including orientation with respect to processing for wrought materials, compositional variations and inclusions, and phase instability. Processes such as cold forming and machining operations can impart cold work to the materials and significantly alter mechanical properties. Welding and postweld heat treatments can also alter mechanical properties through a variety of physical metallurgy processes including alloy element segregation and precipitation of secondary phases.

4.1 Mechanical Properties of Importance for the Waste Package Container Materials

As previously indicated, the container materials for the waste packages are known to be low-strength, high-ductility alloys resistant to brittle fracture mechanisms. Important mechanical properties for the waste package container materials are listed in Table 4-1, along with a brief description of the property and appropriate test standards (ASTM International, 2002a–e). The strength of engineering alloys is typically measured using a combination of the yield strength and the ultimate tensile strength. The average of these two parameters is called the flow stress, which is used in the calculation of fracture toughness parameters. Ductility is a measure of plastic deformation that occurs prior to failure and is typically measured using tensile test specimens as the reduction in area of a tensile specimen or the measured elongation prior to failure. Impact toughness is a measure of the resistance of the material to fracture under impact loading. Impact tests are usually performed using the Charpy (simple-beam) or the Izod (cantilever-beam) method. Charpy impact tests, which are most common for the alloys of interest, measure the energy required to break a test specimen using a moving mass. For some alloys, the impact toughness can be related to other measures of fracture toughness using established empirical relationships.

Several parameters for fracture toughness are included in Table 4-1. The plane-strain fracture toughness, K_{Ic}, is a measure of the resistance of a material to cracking in the opening mode I under plane-strain conditions in an inert environment in the presence of a sharp crack (ASTM International, 2002d). Cracks can propagate at velocities comparable to the sound velocity if the stress intensity, K_I, at a flaw is greater than the K_{Ic}. The tests are performed under tensile constraint such that the stress near the crack tip approaches tritensile plane-strain conditions and the crack tip plastic region is small compared to the crack size and specimen dimensions. A variety of specimen geometries can be used, and the selection of the test specimen is dependent on the product form and specimen size constraints. For low-strength, high-ductility materials, it is generally difficult to obtain valid measurements of K_{Ic}.

Table 4-1. Relevant Mechanical Properties for Waste Package Container Materials			
Parameter	**Symbol**	**Units SI [English]**	**Standard Test Methods**
Yield Strength	σ_{YS}	MPa [ksi]	ASTM A 370* ASTM E 8†
Tensile Strength	σ_{UTS}	MPa [ksi]	ASTM A 370 ASTM E 8
Flow Strength	σ_f	MPa [ksi]	ASTM A 370 ASTM E 8
Reduction in Area (Ductility)	%RA	percent	ASTM A 370 ASTM E 8
Charpy V-notch toughness	CVN	J [ft·lb]	ASTM A 370 ASTM E23‡
Ductile-brittle transition temperature	DBTT	°C [°F]	ASTM A370 ASTM E23
Plane-Strain Fracture Toughness	K_{Ic}	$MPa \cdot m^{1/2}$ [$ksi \cdot in^{1/2}$]	ASTM E399§
Fracture toughness (without significant crack extension)	J_c	kJ/m^2 [$ft \cdot lb/in^2$]	ASTM E1820‖
Fracture toughness for the onset of stable crack extension	J_{Ic}	kJ/m^2 [$ft \cdot lb/in^2$]	ASTM E1820
Crack growth resistance	dJ/da	MPa [ksi]	ASTM E1820
Tearing modulus	T	unitless	ASTM E1820

*ASTM International. "Standard Test Methods and Definitions for Mechanical Testing of Steel Products." *A 370-02: Annual Book of Standards. Vol. 3.01: Metals—Mechanical Testing; Elevated and Low-Temperature Tests; Metallography.* West Conshohocken, Pennsylvania: ASTM International. 2002.
†ASTM International. "Standard Test Methods for Tension Testing of Metallic Materials." E 8-01: *Annual Book of Standards. Vol. 3.01: Metals—Mechanical Testing; Elevated and Low-Temperature Tests; Metallography.* West Conshohocken, Pennsylvania: ASTM International. 2002.
‡ASTM International. "Standard Test Methods for Notched Bar Impact Testing of Metallic Material." E 23-02: *Annual Book of Standards. Vol. 3.01: Metals—Mechanical Testing; Elevated and Low-Temperature Tests; Metallography.* West Conshohocken, Pennsylvania: ASTM International. 2002.
§ASTM International. "Standard Test Method for Plane-Strain Fracture Toughness of Metallic Materials." E 399-90: *Annual Book of Standards. Vol. 3.01: Metals—Mechanical Testing; Elevated and Low-Temperature Tests; Metallography.* West Conshohocken, Pennsylvania: ASTM International. 2002.
‖ASTM International. "Standard Test Method for Measurement of Fracture Toughness." E 1820-01: *Annual Book of Standards. Vol. 3.01: Metals—Mechanical Testing; Elevated and Low-Temperature Tests; Metallography.* West Conshohocken, Pennsylvania: ASTM International. 2002.

The fracture toughness may also be determined using the J-integral characterization (ASTM International, 2002e; Mills, 1995). The types of test specimens are similar to those used in the determination of K_{Ic}. Size requirements specified in the ASTM International standard (ASTM International, 2002e) are generally not applicable to stainless steels and corrosion resistant nickel-chromium-molybdenum alloys as a result of the high-toughness, ductility, and strain-hardening capability. Alternative analysis methods to obtain fracture toughness using the J-integral characterization have been described by Mills (1995). Several characterization parameters can be obtained using this test method. The parameters of interest for fracture toughness include the fracture toughness without significant crack extension, J_c the fracture toughness for the onset of stable crack extension, J_{Ic}, and the crack growth resistance, dJ/da. The tearing modulus can be determined from the crack growth resistance, elastic modulus, and the flow stress according to Eq. (4-1)

$$T = \frac{dJ}{da}\frac{E}{\sigma_f^2} \tag{4-1}$$

where

E — elastic modulus {MPa [ksi]}
σ_f — flow stress {MPa [ksi]}

The tearing modulus is essentially a dimensionless form of the crack growth resistance.

In general, engineered structures are designed to yield before failure. To avoid yield, the structures are designed to sustain stresses well below the yield strength, usually 60 to 70 percent of the yield strength at room temperature. Although brittle failure of engineered structures is usually undesirable, there are many noteworthy examples of unexpected brittle failures (Kanninen and Popelar, 1985). Brittle failures can occur as a result of a variety of mechanisms. The fracture toughness parameters in Table 4-1 are defined in an inert environment (i.e., laboratory air). Fracture toughness can be significantly altered by material–environment interactions. Examples of material–environment interactions that lead to brittle failures include stress corrosion cracking and hydrogen embrittlement. Such interactions, although relevant to the disposal of high-level waste, are beyond the scope of this report and are addressed in previous Center for Nuclear Waste Analyses (CNWRA) reports. Fabrication processes such as cold working, welding, and postweld heat treatments can also alter mechanical properties of engineering materials. Such processes can reduce the fracture toughness and lead to brittle failure.

Conditions for safe operation of an engineered structure can be determined using a failure-assessment diagram (Anderson, 1995). The failure-assessment diagram, which can be used to determine failure by both fracture and plastic collapse, considers the strength and fracture toughness of the material, structural dimensions, and flaw size. Conditions for safe operation are defined by Eq. (4-2)

$$K_r = S_r\left[\frac{8}{\pi^2}\ln\sec\left(\frac{\pi}{2}S_r\right)\right]^{-1/2} \tag{4-2}$$

Sr — the stress ratio defined by Eq. (4-3)

$$S_r = \frac{\sigma}{\sigma_c} \tag{4-3}$$

where

σ — applied stress
σ_c — plastic collapse stress defined by Eq. (4-4)

$$\sigma_c = \sigma_f A \tag{4-4}$$

where

A — area of the structure under load; does not include area of flaws

The term K_r is a ratio of K_I to K_{Ic} shown in Eq. (4-5).

$$K_r = \frac{K_I}{K_{I_c}} \tag{4-5}$$

The calculation of stress intensity is dependent on the geometry of the structural component and the nature of the applied load (Anderson, 1995).

A key parameter to the development of failure assessment diagrams is the fracture toughness that can be difficult to measure for many alloys. As an alternative to actual fracture toughness measurements, the fracture toughness can be estimated using several methods. For plane-strain conditions, the fracture toughness, K_{Jc}, can be calculated from J_{Ic} using Eq. (4-6) (Begley and Landes, 1971).

$$K_{Jc} = \left[\frac{J_{Ic}E}{1-\mu^2}\right]^{1/2} \tag{4-6}$$

where

E — elastic modulus or plane-stress conditions

K_{Jc} can be determined from J_{Ic} using Eq. (4-7) (Anderson, 1995).

$$K_{Jc} = \left[J_{Ic}E\right]^{1/2} \tag{4-7}$$

The fracture toughness of ferritic pressure vessel steels with yield strengths of more than 690 MPa [100 ksi] can be related to the Charpy impact energy through the empirical relationship shown as Eq. (4-8) reported by Barsom and Rolfe (1970) and Rolfe and Novak (1970).

$$\left(\frac{K_{Ic}}{\sigma_{YS}}\right)^2 = 5.0\left(\frac{CVN}{\sigma_{YS}} - 0.05\right) \qquad (4\text{-}8)$$

Iwadate, et al. (1977) has shown that Eq. (4-8) can be used to estimate the K_{Ic} from Charpy V-notch impact energy data for $2^1/_4$ Cr-1 Mo pressure vessel steels with yield strengths in the range 405–620 MPa [59–90 ksi].

An example of a failure-assessment diagram is shown in Figure 4-1. The diagram was calculated assuming a material with a yield strength of 440 MPa [63 ksi] and a tensile strength of 786 MPa [114 ksi]. The fracture toughness is varied from 10 to 250 MPa $m^{1/2}$ [9 to 227 ksi $in^{1/2}$]. The geometry of the specimen shown in Figure 4-2 was assumed to be a center cracked panel with W = 0.10 m [0.33 ft] and a = 0.50 cm [0.20 in]. The specimen is remotely loaded in tension. When $K_r \leq 0.6$ and $S_r \approx 1$, or $K_r/S_r \leq 0.6$, it can be reasonably assumed that failure of the structure occurs by plastic collapse rather than fracture. From the failure-assessment diagram in Figure 4-1, it is apparent that reducing the fracture toughness to values less than 100 MPa $m^{1/2}$ [91 ksi $in^{1/2}$] causes the failure mode to change from plastic collapse to a mixed failure mode. Further reductions in the fracture toughness result in failure dominated by fracture.

4.2 Effect of Fabrication Processes on the Mechanical Properties of Type 316 SS

The mechanical properties of the Type 316 nuclear grade stainless steel inner container may be altered by fabrication processes necessary to construct and close the waste packages. The information included in this section is compiled from data for austenitic stainless steels such as Types 304, 304L, 316, 316L, and several weld-filler metals readily available from the literature. Although information specific for Type 316 nuclear grade stainless steel is rare, the mechanical properties of Type 316 nuclear grade stainless steel is likely to be similar to the mechanical properties of Type 304 and 316 austenitic stainless steels.

The chemical compositions of selected austenitic stainless steels are included in Table 4-2. Minimum mechanical properties measured at room temperature including the yield strength, tensile strength, and elongation are provided in Table 4-3 (ASME International, 2001b; ASM International, 1992). The low-carbon grades (i.e., 304L and 316L) have slightly lower yield and tensile strength compared to the standard grade. The addition of nitrogen to low-carbon stainless steels restores the yield and tensile strength. Type 316 nuclear grade stainless steel, which has lower carbon and nitrogen compared with Type 316LN, has properties similar to Types 316L and 316LN. Actual mechanical properties are typically greater than those listed in Table 4-3. All grades listed in Tables 4-2 and 4-3 have good ductility. The various stainless steel grades were developed to improve corrosion resistance, weldability, and stress corrosion cracking resistance. Decreasing the carbon content decreases sensitization that can occur in the heat-affected zone of welds; however, decreasing the carbon content reduces the yield and tensile strength. The addition of nitrogen to increase the strength of the low-carbon grades can result in an increased susceptibility to transgranular stress corrosion cracking. Type 316

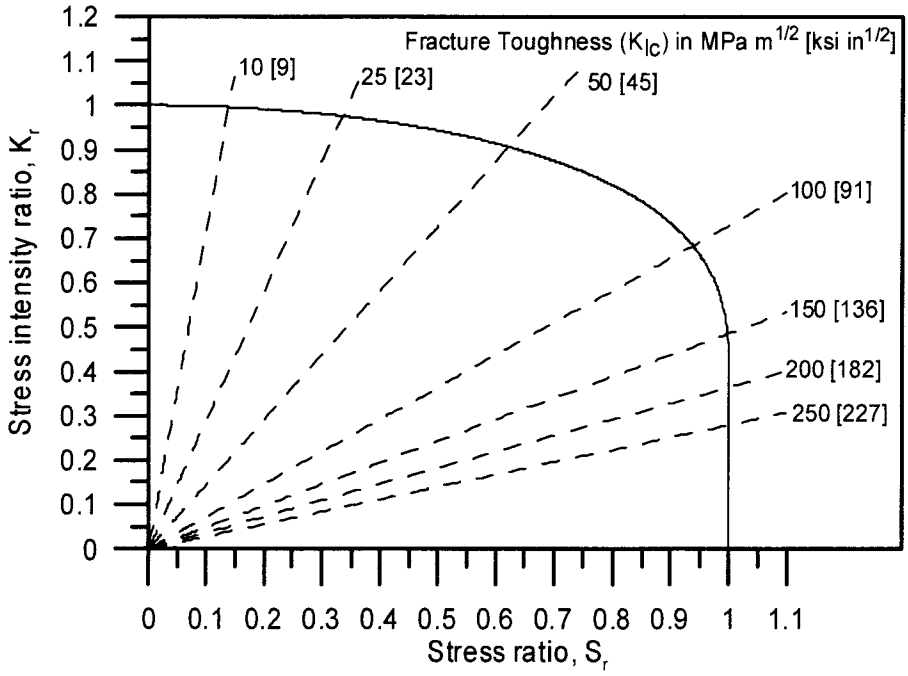

Figure 4-1. Example Failure Assessment Diagram Using Plane-Strain Fracture Toughness

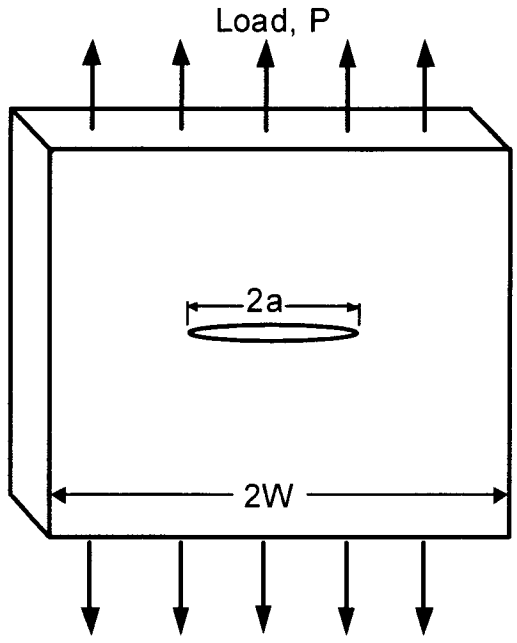

Figure 4-2. Schematic of Through Thickness Crack in Plate Remotely Loaded in Tension

Table 4-2. Chemical Composition of Selected Austenitic Stainless Steels*†									
Grade	Fe‡	Cr	Ni	Mo	N	C (max)	P (max)	S (max)	Si (max)
304	Balance	18.00–20.00	8.00–10.50	—	—	0.08	0.045	0.030	0.75
304L	Balance	18.00–20.00	8.00–12.00	—	—	0.030	0.045	0.030	0.75
304LN	Balance	18.00–20.00	8.00–10.50	—	0.10–0.15	0.030	0.045	0.030	0.75
316	Balance	16.00–18.00	10.00–14.00	2.00–3.00	—	0.08	0.045	0.030	0.75
316L	Balance	16.00–18.00	10.00–14.00	2.00–3.00	—	0.030	0.045	0.030	0.75
316LN	Balance	16.00–18.00	10.00–14.00	2.00–3.00	0.10–0.30	0.030	0.045	0.030	0.75

*ASME International. "SA–240 Specification for Heat Resisting Chromium and Chromium Nickel Stainless Steel Plate, Sheet, and Strip for Pressure Vessels." New York City, New York: ASME International. 2001.
†ASM International. *Metals Reference Book.* M. Bauccio, ed. 3rd Edition. Metals Park, Ohio: ASM International. 1992.
‡Notes: Fe—iron; Cr—chromium; Ni—nickel; Mo—molybdenum; N—nitrogen; C—carbon; P—phosphorus; S—sulfur; Si—silicon

Table 4-3. Minimum Mechanical Properties of Selected Austenitic Stainless Steels at 25 °C [77 °F]*†			
Grade	Yield Strength MPa [ksi]	Tensile Strength MPa [ksi]	Elongation (Percent)
304	205 [30]	515 [75]	40.0
304L	170 [25]	485 [70]	40.0
304LN	205 [30]	515 [75]	40.0
316	205 [30]	515 [75]	40.0
316L	170 [25]	485 [70]	40.0
316LN	205 [30]	515 [75]	40.0

*ASME International. "SA–240 Specification for Heat Resisting Chromium and Chromium Nickel Stainless Steel Plate, Sheet, and Strip for Pressure Vessels." New York City, New York: ASME International. 2001.
†ASM International. *Metals Reference Book.* M. Bauccio, ed. 3rd Edition. Metals Park, Ohio: ASM International. 1992.

nuclear grade stainless steel was developed to avoid stress corrosion cracking observed with welded Type 304 SS in boiling water reactors.

4.2.1 Mechanical Properties of Wrought Type 316 SS

The minimum yield and tensile strengths for Type 316L stainless steel are shown in Figure 4-3 (ASME International, 1995b). Both yield and tensile strengths decrease with temperature. The ASME International maximum allowable stress is typically $66^2/_3$ percent of the yield strength. For Type 316L and other alloys with low yield strengths, the maximum allowable stress is greater than $66^2/_3$ percent of the yield strength. The higher allowable stress may not be appropriate for applications over extended periods or where permanent strain is not permitted. Typical values for the yield strength, tensile strength, and elongation for annealed Type 316L SS sheet as a function of temperature are shown in Figure 4-4 (Allegheny Ludlum, 1999). The yield strength is approximately 300 MPa [43.5 ksi] at 20 °C [68 °F] and decreases to near 220 MPa [32 ksi] at 204 °C [400 °F]. Similarly, the tensile strength decreases from approximately 600 MPa [87 ksi] at 20 °C [68 °F] to approximately 475 MPa [69 ksi] at 204 °C [400 °F]. In addition to reductions in the yield and tensile strength, the ductility of Type 316L also decreases with increasing temperature. At 20 °C [68 °F], typical elongations measured on 51-mm [2-in] sections are approximately 55 percent. This value decreases to 37 percent at

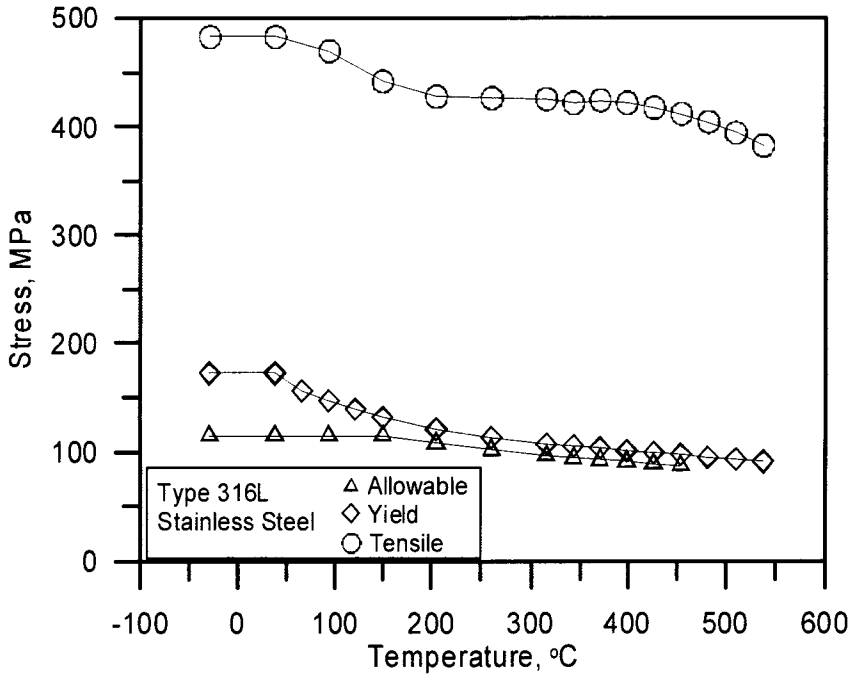

Figure 4-3. Minimum Yield Strength, Tensile Strength, and Maximum Allowable Stress for Type 316L SS (ASME International, 1995b)

NOTE: Temperature provided in °C; for conversion to °F, use °F = 9/5 °C + 32. Stress provided in MPa; for conversion to ksi, use ksi = MPa/6.895.

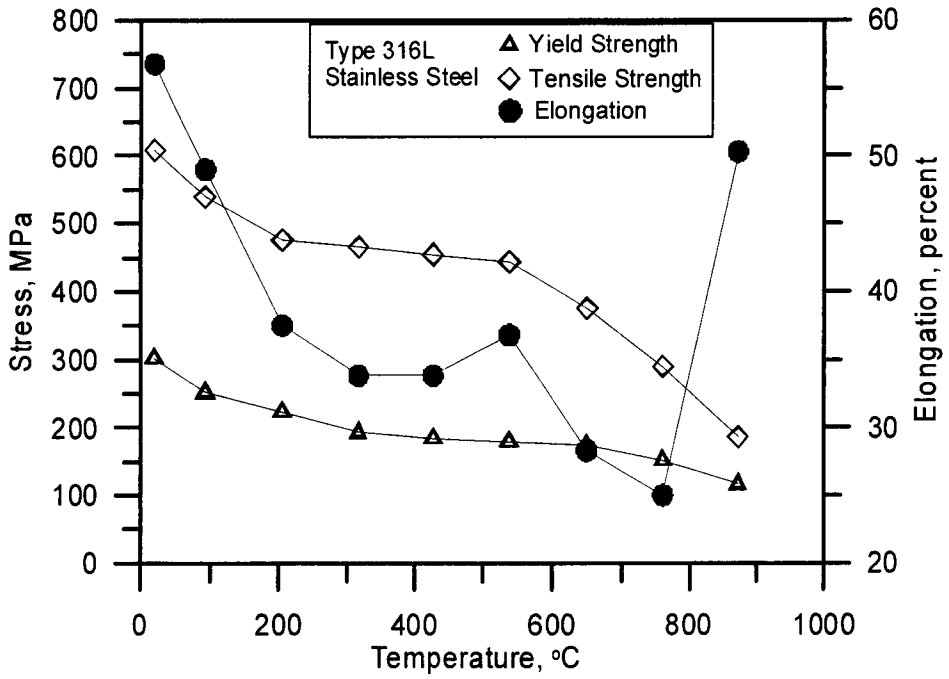

Figure 4-4. Typical Yield Strength, Tensile Strength, and Ductility of Type 316L SS (Allegheny Ludlum, 1999)

NOTE: Temperature provided in °C; for conversion to °F, use °F = 9/5 °C + 32. Stress provided in MPa; for conversion to ksi, use ksi = MPa/6.895.

204 °C [400 °F]. Figure 4-5 shows typical values of yield strength, tensile strength, and elongation for Type 316L SS at 20 °C [68 °F] as a function of cold work. Strain hardening as a result of cold work significantly increases the yield and tensile strength and decreases the ductility of the alloy. The typical yield strength of 300 MPa [43.5 ksi] in the annealed condition increases to 535 MPa [77.5 ksi] with 10-percent cold work. Although the ductility decreases with cold work, the alloy is still quite ductile with cold work reductions to less than 20 percent.

Inclusions, which are typically a result of impurities in the melt, can reduce the ductility of austenitic stainless steels. Table 4-4 lists the mechanical properties of two heats of Type 316L SS with different inclusion contents (Balladon, et al., 1983). All tests were performed at 20 °C [68 °F] with the material in the solution-annealed condition {1,070 °C [1,958 °F] for 30 minutes and water quenched}. The chemical compositions of the Type 316L heats are very similar, with the primary difference resulting from the deoxidation techniques that yield different inclusion contents. The inclusion content of Heat B is much greater than Heat A, and the inclusions tend to be aligned along the rolling direction. From the data shown in Table 4-2, it is apparent that the yield strength and the tensile strength are not strongly affected by specimen orientation or inclusion content. On the other hand, the clustering of inclusions along the rolling direction has a detrimental effect on ductility in the short transverse-longitudinal (S-L) orientation. For Heat A, the total elongation is greater than 70 percent for all specimen orientations. With the increased inclusion content of Heat B, the ductility in the short transverse-longitudinal (S-L) orientation is reduced to 15 percent.

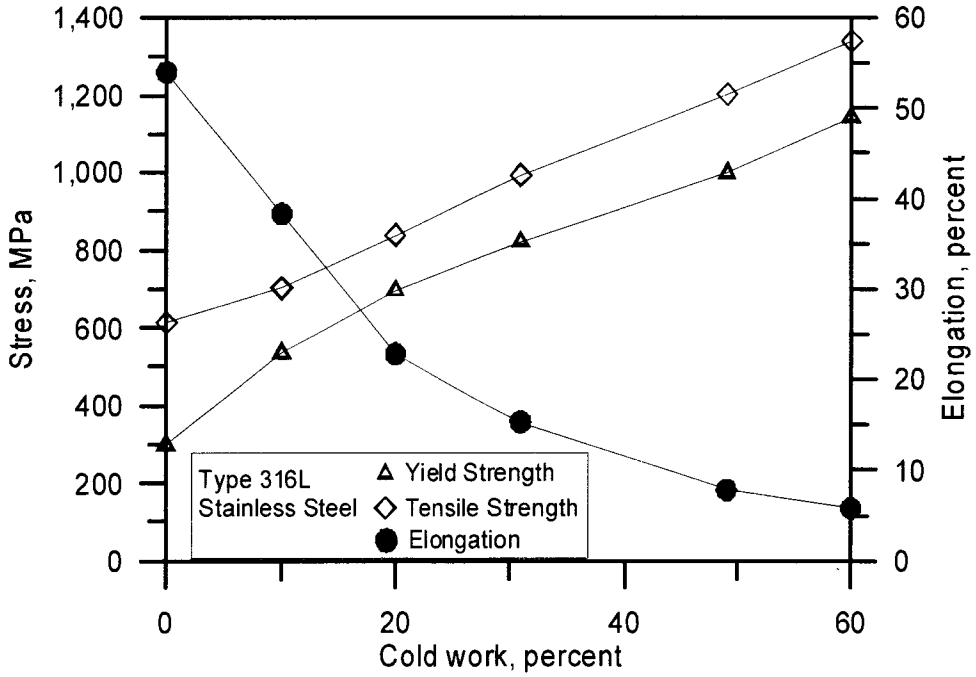

Figure 4-5. Yield Strength, Tensile Strengths, and Ductility of Type 316L SS at 20 °C [68 °F] As a Function of Cold Work (Allegheny Ludlum, 1999)

NOTE: Stress provided in MPa; for conversion to ksi, use ksi = MPa/6.895.

Table 4-4. Effect of Inclusions and Specimen Orientation on Yield Strength, Tensile Strength, and Ductility*

Orientation†	Type 316L Heat A Inclusion Number: 41			Type 316L Heat B Inclusion Number: 85		
	Yield Strength MPa [ksi]	Tensile Strength MPa [ksi]	Elongation Percent	Yield Strength MPa [ksi]	Tensile Strength MPa [ksi]	Elongation Percent
S-L	293 [42.5]	571 [82.8]	73	281 [40.8]	445 [64.5]	15
T-L	303 [43.9]	597 [86.6]	73	279 [40.5]	558 [80.9]	74
L-T	310 [44.9]	591 [85.7]	76	279 [40.5]	561 [81.4]	78

*Balladon, P., J. Heritier, and P. Rabbe. "Influence of Microstructure on the Ductile Rupture Mechanisms of a 316L Steel at Room and Elevated Temperatures." *Fracture Mechanics: Fourteenth Symposium-Volume II: Testing and Applications.* ASTM STP 791. J.C. Lewis and G. Sines, eds. West Conshohocken, Pennsylvania: ASTM International. pp. II-496 through II-513. 1983.

†Notes: S-L — short transverse-longitudinal
T-L — long transverse-longitudinal
L-T — longitudinal-long transverse

The fracture toughness of stainless steels has been reviewed by Mills (1995, 1997). The fracture toughness of Types 304 and 316 SS is generally high but has large variations (Mills, 1988b). A summary of the fracture toughness of Types 304 and 316 SS is shown in Table 4-5. The J_c and dJ/da values are reported by Mills (1995, 1997), and the values of the tearing modulus are calculated using the yield and tensile strengths in Figure 4-4. The mean value of J_c decreases from 672 kJ/m^2 [321 ft lb/in^2] to 421 kJ/m^2 [201 ft lb/in^2] when the temperature is increased. Similarly, the lower bound values of the J_c also decrease. Although the value of J_c decreases with temperature, the fracture toughness of Types 304 and 316 SS is still quite high at elevated temperatures. Assuming a lower bound J_c value of 96 kJ/m^2 [46 ft lb/in^2] at elevated temperature and a modulus of 193 GPa [28 × 10^3 ksi], a K_{Jc} of 136 MPa m$^{1/2}$ [124 ksi in$^{1/2}$] is calculated using Eq. (4-7). For low-yield strength materials such as austenitic stainless steels, a K_{Jc} in excess of 100 MPa m$^{1/2}$ [91 ksi in$^{1/2}$] may be sufficient to assure ductile failure.

Although the fracture toughness of wrought stainless steels in the annealed condition is generally high, the fracture toughness is dependent on the orientation of the fracture with respect to the rolling direction, the presence of inclusions, and cold work. The microstructure of wrought stainless steels tend to have inclusion stringers oriented along the longitudinal rolling

Table 4-5. Summary of Fracture Toughness for Wrought Types 304 and 316 SS*†

Parameter	Temperature Range	
	20–125 °C [68–257 °F]	**400–550 °C [752–1,022 °F]**
Mean J_c kJ/m^2 [ft lb/in^2]	672 [321]	421 [201]
Lower bound J_c kJ/m^2 [ft lb/in^2]	215 [103]	96 [46]
Upper bound J_c kJ/m^2 [ft lb/in^2]	1,700 [810]	1,300 [620]
Mean dJ/da MPa [ksi]	292 [42]	263 [38]
Lower bound dJ/da MPa [ksi]	59 [8.5]	79 [11.5]
Upper bound dJ/da MPa [ksi]	850 [123]	400 [58]
Mean tearing modulus	360 {at 93 °C [200 °F]}	525 {at 538 °C [1,000 °F]}
Lower bound tearing modulus	72 {at 93 °C [200 °F]}	158 {at 538 °C [1,000 °F]}
Upper bound tearing modulus	1,051 {at 93 °C [200 °F]	795 {at 538 °C [1,000 °F]}

*Mills, W.J. "Fracture Toughness of Austenitic Stainless Steels and Their Welds." *ASM Handbook. Vol. 19: Fatigue and Fracture*. Metals Park, Ohio: ASM International. pp. 733–756. 1995.
†Mills, W.J., "Fracture Toughness of Types 304 and 316 Stainless Steels and Their Welds." *International Materials Reviews*. Vol. 42. pp. 45–82. 1997.

direction. Measurement of the fracture toughness of Type 316 SS at 370 °C [698 °F] as a function of orientation has been reported by Garwood (1984). Table 4-6 lists the J value at the maximum load (J_{max}). The values of J_{max} are greater than the J_c and reflect both the fracture toughness and the tearing resistance (Mills, 1995). The fracture toughness is greatest for the longitudinal-short transverse (L-S) and longitudinal-long transverse (L-T) orientations. Cracks propagating perpendicular to the thickness of the material had lower fracture toughness. The lower fracture toughness observed in the short transverse-longitudinal (S-L) and the short transverse-long transverse (S-T) orientations can be attributed to the presence of stringers and inclusion clusters parallel to the crack plane that provide a low-energy path for crack propagation.

Table 4-6. Effect of Orientation on the Fracture Toughness (J_{max} Values Including Standard Deviation) of Type 316 SS at 370 °C [698 °F]*

Orientation†	L-S	L-T	T-S	T-L	S-T	S-L
J_{max} ±, kJ/m^2 [ft lb/in^2]	1900±79 [907±37]	1210±75 [578±36]	800±130 [380±62]	660±41 [315±20]	300±98 [140±47]	270±32 [130±15]

*Garwood, S.J. "Fracture Toughness of Stainless Steel Weldments at Elevated Temperatures." *Fracture Mechanics: Fifteenth Symposium.* ASTM STP 833. R.J. Sanford, ed. West Conshohocken, Pennsylvania: ASTM International. 1984.

†Notes: L-S — longitudinal-short transverse
L-T — longitudinal-long transverse
T-S — long transverse-short transverse
T-L — long transverse-longitudinal
S-T — short transverse-long transverse
S-L — short transverse-longitudinal

The effect of inclusions on fracture toughness is also reported by Balladon, et al. (1983) for Type 316L SS (Table 4-7). As a result of the high fracture toughness of Type 316L SS, most of the data reported by Balladon, et al. (1983) do not meet the criteria for valid J_{Ic} measurements. The J_{Ic} for a Type 316L SS with a low inclusion content is 1,560 kJ/m^2 [745 ft lb/in^2] for longitudinal-long transverse (L-T) and long transverse-longitudinal (T-L) orientations and 1,080 [516 ft lb/in^2] for the short transverse-longitudinal (S-L) orientation. Lower overall values of J_{Ic} are observed for the Type 316L SS heat with a high inclusion content. In the short transverse-longitudinal (S-L) orientation, the J_{Ic} is reduced to 260 kJ/m^2 [124 ft lb/in^2]. Similar reductions in the dJ/da and the tearing modulus are observed for the high inclusion content heat.

In addition to increasing the yield and tensile strength, cold work also decreases the fracture toughness of austenitic stainless steels. The fracture toughness and yield strength as a function of cold work for Type 316 SS annealed and aged at 650 °C [1,202 °F] for two hours are shown in Table 4-8 (Chipperfield, 1977). In the annealed condition, the J_c is 250 kJ/m^2 [120 ft lb/in^2] with 5-percent cold work, 110 kJ/m^2 [52 ft lb/in^2]; and with 30-percent cold work, 70 kJ/m^2 [33 ft lb/in^2]. The effect of cold work is also reported by Pawel, et al. (1994) and is shown in Table 4-9. The values of cold work for the materials tested by Pawel, et al. (1994) are not specified, but they may be estimated from the yield and tensile strength data. Alloys tested by Pawel, et al. (1994) are US316, containing 1.7-percent manganese and 0.67-percent silicon

Table 4-7. Fracture Toughness of Annealed Type 316L SS with Low and High Inclusion Contents*						
	Type 316L Heat A Inclusion Number: 41			Type 316L Heat B Inclusion Number: 85		
Orientation†	J_{Ic} kJ/m^2 [ft lb/in^2]	dJ/da MPa [ksi]	Tearing Modulus	J_{Ic} kJ/m^2 [ft lb/in^2]	dJ/da MPa [ksi]	Tearing Modulus
S-L	1,080 [516]	630 [91]	652	260 [124]	165 [24]	243
T-L	1,560 [745]	980 [142]	960	690 [330]	390 [57]	411
L-T	1,560 [745]	980 [142]	960	780 [373]	500 [73]	539

*Balladon, P., J. Heritier, and P. Rabbe. "Influence of Microstructure on the Ductile Rupture Mechanisms of a 316L Steel at Room and Elevated Temperatures." *Fracture Mechanics: Fourteenth Symposium–Volume II: Testing and Applications ASTM STP 791.* J.C. Lewis and G. Sines, eds. West Conshohocken, Pennsylvania: ASTM International. pp. II-496 through II-513. 1983.

†Notes: S-L — short transverse-longitudinal
T-L — long transverse-longitudinal
L-T — longitudinal-long transverse

Table 4-8. Effect of Cold Work on the Fracture Toughness of Type 316 SS at 20 °C [68 °F]*		
Cold Work Percent	Yield Strength MPa [ksi]	J_c kJ/m^2 [ft lb/in^2]
0	280 [40]	250 [120]
5	400 [58]	110 [52]
30	610 [88]	70 [33]

*Chipperfield, C.G. "A Method for Determining Dynamic J_Q and δ_i Values and its Application to Ductile Steels." Proceedings of the International Conference on Dynamic Fracture Toughness. London, England: The Welding Institute and American Society for Metals. pp.168–179. 1977.

Table 4-9. Effect of Cold Work on the Fracture Toughness and Mechanical Properties of Type 316 SS*					
Material	**Condition**	**Temperature °C [°F]**	**K_J MPa $m^{1/2}$ [ksi $in^{1/2}$]**	**Yield Strength MPa [ksi]**	**Tensile Strength MPa [ksi]**
J316	Annealed	22 [72]	393 [357]	275 [40]	575 [83]
		90 [194]	422 [384]	230 [33]	500 [73]
	Cold Worked	90 [94]	317 [288]	675 [98]	770 [112]
US316	Annealed	90 [194]	208 [189]	230 [33]	500 [73]
	Cold Worked	22 [72]	85 [77]	725 [105]	785 [114]
		90 [194]	85 [77]	715 [104]	770 [112]

*Pawel J.E., D.J. Alexander, M.L. Grossbeck, A.W. Longest, A.E. Rowclifffe, G.E. Lucas, S. Jitsukawa, A. Hishinuma, and K. Shiba. "Fracture Toughness of Candidate Materials of ITER First Wall Blanket and Shield Structures." *Journal of Nuclear Materials*. Vol. 212–215. pp. 442–447. 1994.

(high inclusion content), and J316, containing 0.23-percent manganese and 0.04-percent silicon (low inclusion content). Values of K_{Jc} are obtained using Eq. (4-7). The lower overall values for K_{Jc} for the US316 material can be attributed to the presence of inclusions. Cold work reduces the K_{Jc} measured at 90 °C [194 °F] from 208 MPa $m^{1/2}$ [189 ksi $in^{1/2}$] to 85 MPa $m^{1/2}$ [77 ksi $in^{1/2}$]. For J316, which has a lower inclusion content compared with US316, cold work reduces the K_{Jc} from 422 MPa $m^{1/2}$ [383 ksi $in^{1/2}$] to 299 MPa $m^{1/2}$ [272 ksi $in^{1/2}$].

4.2.2 Effects of Fabrication Processes on the Mechanical Properties of Type 316 SS

Fabrication processes such as welding can alter the mechanical properties of Type 316 SS. The effects of welding processes on the mechanical properties of austenitic stainless steels have been the subject of many reviews owing to the importance of these alloys for cryogenic storage, chemical processing, and nuclear power industries. Mechanical properties of stainless steel welds have been reported by Wood (1986) and Smith and Farrar (1993). Fracture toughness of austenitic stainless steel welds has been reported by Mills (1997, 1995, 1989, 1988a, 1987), Pawel, et al. (1994), and Gavenda, et al. (1995).

Welding processes typically increase the yield and tensile strength and decrease the ductility. Welded stainless steels typically *have* greater scatter in the mechanical properties compared to wrought materials (Smith and Farrar, 1993). The yield strength (σ_{YS}) of molybdenum-free austenitic weld metal as a function of temperature was empirically found to follow a polynomial expression shown as Eq. (4-9) (Wood, 1986).

$$\sigma_{YS}[\text{SS weld without Mo}](\text{MPa}) = 433.5 - 0.6584T + 0.13987 \times 10^{-2} T^2 - 0.14373 \times 10^{-5} T^3 \quad (4\text{-}9)$$

where T is temperature in degrees Celsius and limited to the range from 20 to 700 °C [68 to 1,292 °F]. Equation (4-10) is the best fit curve for the yield strength of molybdenum containing weld metal.

$$\sigma_{YS}[\text{SS weld with Mo}](\text{MPa}) = 460.4 - 0.6571T + 0.12974 \times 10^{-2}T^2 - 0.12307 \times 10^{-5}T^3 \quad (4\text{-}10)$$

Similarly, the tensile strengths of molybdenum-free and molybdenum-containing weld metals are provided in Eqs. (4-11) and (4-12).

$$\sigma_{TS}[\text{SS weld without Mo}](\text{MPa}) = 621.2 - 1.418T + 0.3355 \times 10^{-2}T^2 - 0.30888 \times 10^{-5}T^3 \quad (4\text{-}11)$$

$$\sigma_{TS}[\text{SS weld with Mo}](\text{MPa}) = 615.1 - 1.100T + 0.29638 \times 10^{-2}T^2 - 0.30254 \times 10^{-5}T^3 \quad (4\text{-}12)$$

The yield and tensile strength of Type 316 SS welds can be approximated using Eqs. (4-10) and (4-12). Figure 4-6 shows the yield strength of Type 316L SS plate in the annealed condition (Allegheny Ludlum, 1999) and the yield and tensile strengths of molybdenum-containing weld metal (Wood, 1986). The yield strength of weld metal is greater than that of the wrought plate; however, the difference in yield strength decreases with temperature. The tensile strength of the welded material is similar to that of the wrought plate. Ductility of the weld metal is typically 30 percent less than the wrought material (Smith and Farrar, 1993).

The yield and tensile strengths as a function of temperature and welding method for Type 308 SS filler metal are shown in Figure 4-7 (Mills, 1988a). Yield and tensile strengths are comparable for shielded metal-arc weld and submerged-arc weld materials. The yield strength of the gas tungsten-arc weld material is slightly lower than that for the other methods at elevated temperatures (no data reported for gas tungsten-arc welds at room temperature). Yield and tensile strengths for 16-8-2 (16Cr-8Ni-2Mo) filler metal are shown in Figure 4-8. Although the yield and tensile strength values in Figure 4-8 are not for manual metal-arc welds, the data are very similar to the values from the empirical correlations developed by Wood (1986) [Eqs. (4-9) and (4-11)] shown in Figure 4-6. The ductility of Types 308 and 16-8-2 SS filler metals as a function of temperature and welding method is shown in Figure 4-9. The ductility of stainless steel welds is typically less than the base alloy and is characterized by a large scatter band (Wood, 1986). For all welding methods and fillers shown in Figure 4-9, the ductility decreases 40–55 percent at 25 °C [77 °F] and 22–30 percent at 427 °C [800 °F]. Similar reductions in ductility are reported by Wood (1986) for manual metal-arc welds. At even higher temperatures, however, the ductility increases, and the ductility at 700 °C [1,292 °F] is similar to the ductility at 25 °C [77 °F]. For manual metal-arc welds at 25 °C [77 °F], the ductility ranges from 30–42 percent, whereas, at 300 °C [572 °F], the ductility decreases and ranges from 17–34 percent.

Welds in 300 series stainless steels typically contain a small amount of δ-ferrite, which is added to inhibit the formation of detrimental phases such as sulfides and phosphides. Inhibition of these low-melting point phases is important to reduce the solidification cracking. Although it has benefits for controlling solidification cracking, the presence of δ-ferrite can affect the mechanical properties of stainless steel welds. The yield and tensile strengths of welds are slightly dependent on the concentration of δ-ferrite. Increasing δ-ferrite from 5.2 to 15.7 percent

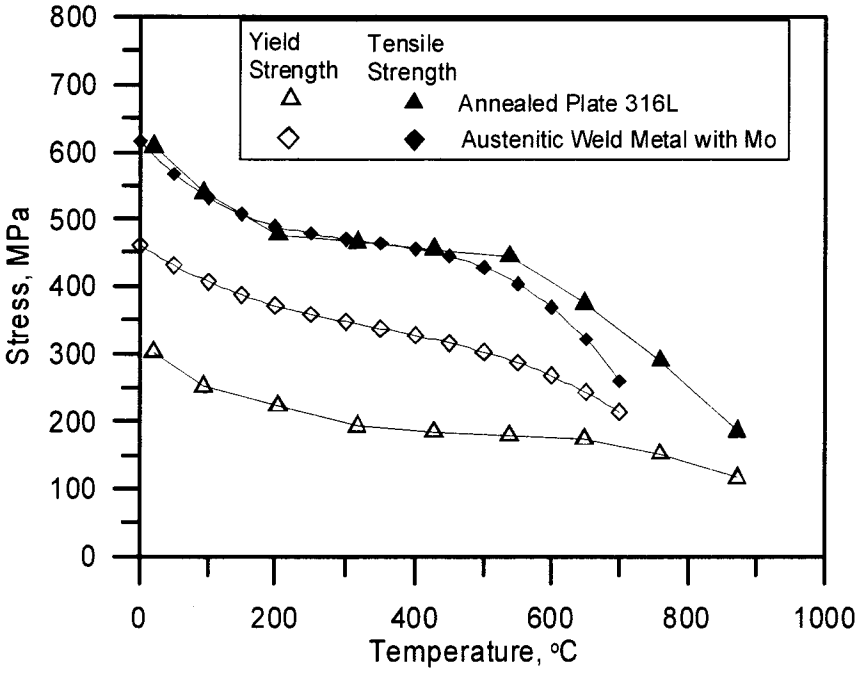

Figure 4-6. Yield and Tensile Strengths of Annealed Type 316L SS Plate (Allegheny Ludlum, 1999) and Austenitic Weld Metal with Molybdenum (Wood, 1986)

NOTE: Temperature provided in °C; for conversion to °F, use °F = 9/5 °C + 32. Stress provided in MPa; for conversion to ksi, use ksi = MPa/6.895.

increases the yields and tensile strengths by 8 to 10 percent (Hawthorne and Menke,1975). Because δ-ferrite is body-centered cubic, this phase has a ductile-to-brittle transition temperature that can decrease substantially the fracture toughness at low temperatures.

As discussed in Chapter 3, aging of the welded microstructure can result in phase transformations and element segregation, which can lead to a reduction in fracture toughness. Most aging studies have been conducted at temperatures in excess of 400 °C [752 °F]. At temperatures in the range of 600 to 800 °C [1,112 to 1,472 °F], the formation of χ and σ phases can reduce the ductility by 30 percent. The reduction in impact energy can be estimated using a Larson-Miller type parametric model (Smith and Farrar 1993). Long-term, low-temperature aging studies have been conducted by Alexander, et al. (1990) and Alexander and Nanstad (1995) on Type 308 SS shielded metal arc welds. The results of Charpy V-notch tests as a function of aging time and δ-ferrite content (ranging from 4 to 12 percent) are shown in Figure 4-10. In the unaged condition, the concentration of δ-ferrite is insignificant, and the impact energy of all welds is in the range 104–114 J [77–84 ft lb]. Aging at 343 °C [650 °F] has no significant effect on welds with 4-percent δ-ferrite; however, aging decreases the Charpy impact strength of welds with 8- and 12-percent δ-ferrite. The reduction in impact strength is attributed to phase separation in the δ-ferrite phase. Aging results in the formation of an iron-rich α-phase and a chromium-rich α′-phase. Aging at 343 °C [650 °F] also increases the ductile to brittle transition temperature. Figure 4-11 shows the transition temperature for an

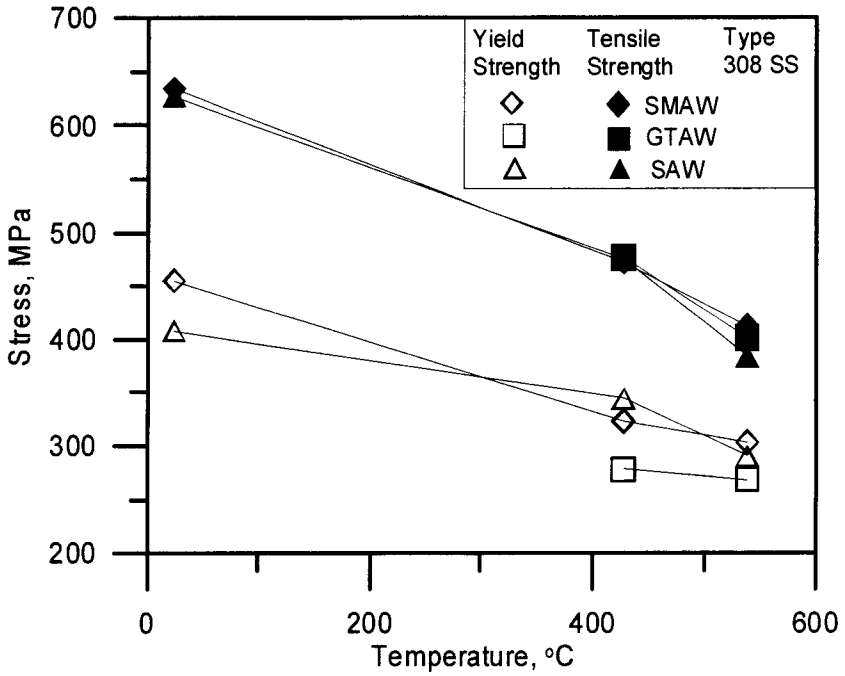

Figure 4-7. Yield and Tensile Strengths of Welded Stainless Steel Using Type 308 Filler (Mills, 1988a)

NOTE: Temperature provided in °C; for conversion to °F, use °F = 9/5 °C + 32. Stress provided in MPa; for conversion to ksi, use ksi = MPa/6.895.

SMAW—shielded metal-arc weld; GTAW—gas tungsten-arc weld; SAW—submerged-arc weld.

impact energy of 67.8 J [50.2 ft lb] for the Type 308 SS shielded metal-arc welds. In the unaged condition, the transition temperature for all welds is less than -20 °C [-4 °F]. The transition temperature welds containing 4-percent δ-ferrite increases by only a few degrees after aging for 20,000 hours. In contrast, the transition temperature for welds containing 12-percent δ-ferrite increases from -25 °C [-13 °F] in the unaged condition to 60 °C [140 °F] after aging for 20,000 hours.

Compared with the results of Alexander, et al. (1990), lower Charpy V-notch impact energies were reported by Hawthorne and Menke (1975) for Type 308 SS shielded metal-arc welds. With 5.2-percent δ-ferrite, the average Charpy V-notch impact energy is 86 J [64 ft lb]. The average impact energy decreases to 66 J [49 ft lb] for welds with 15.7-percent δ-ferrite (Hawthorne and Menke,1975). The impact energy is found to increase with test temperature as shown in Figure 4-12, presumably as a result of the increased ductility although this is not reflected in the elongation (Figure 4-9).

A summary of the Charpy impact energy for Type 308 and 316/16-8-2 welds is shown in Figure 4-13 (Gavenda, et al., 1996). For both materials, the submerged arc weld has the lowest

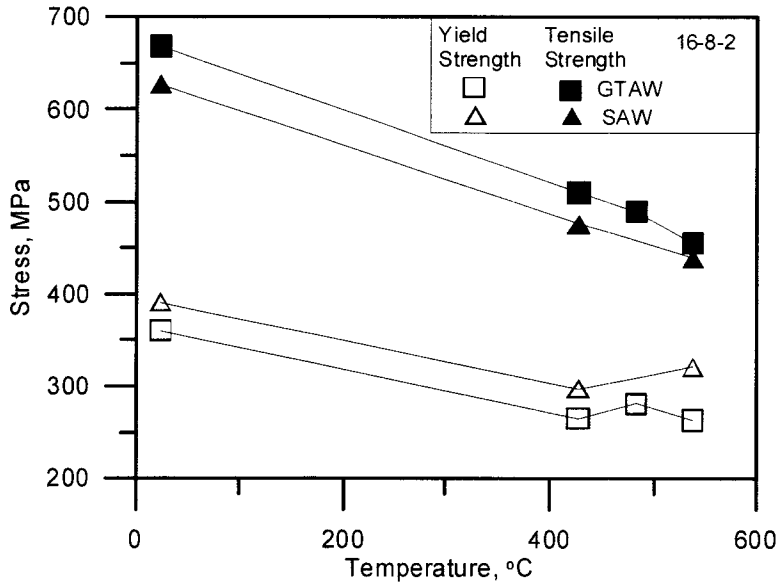

Figure 4-8. Yield and Tensile Strengths of Welded Stainless Steel Using 16Cr-8Ni-2Mo Filler (Mills, 1988a)

NOTE: Temperature provided in °C; for conversion to °F, use °F = 9/5 °C + 32. Stress provided in MPa; for conversion to ksi, use ksi = MPa/6.895.

GTAW—gas tungsten-arc weld; SAW—submerged-arc weld.

impact energy. The highest impact energy was observed for the gas tungsten arc welds and the gas metal arc welds. Type 308 SS appears to have a slightly higher impact strength compared with Type 316 SS welds. Impact energy of submerged-arc welded Type 316 SS/16Cr-8Ni-2Mo is in the range 50–80 J [37–59 ft lb] at 25 °C [77°F]. In contrast to the results reported by Hawthorne and Menke (1975), the impact strength does not appear to increase with temperature. The impact strength of gas tungsten-arc welds is in the range 110–160 J [80–120 ft lb] for the temperature range of 25–288 °C [77–550°F] and is not a function of temperature. Similar trends are observed for Type 308 SS welds. The impact strength of Type 308 SS shielded metal-arc welds is between that for the submerged-arc welds and the gas tungsten-arc welds and independent of temperature in the range 25–480 °C [77–900 °F].

The fracture toughness of stainless steel welds as a function of temperature and welding method is shown in Figure 4-14 (Mills, 1997; Gavenda, et al., 1996). The effect of welding methods on fracture toughness is similar to the effect of impact energy shown in Figure 4-13. The fracture toughness of submerged-arc welds is lower than either shielded metal-arc welds or gas tungsten-arc welds. For Type 316 SS submerged-arc welds, the J_{Ic} is in the range 110–200 kJ/m^2 [53–96 ft lb/in^2] at 25 °C [77 °F] and 288 °C [550 °F]. At 370 °C [698 °F], the J_{Ic} for submerged-arc welds is in the range 40–75 kJ/m^2. The low values of J_{Ic} are a result of the increased inclusion content of submerged-arc welds and the loss of ductility at elevated temperatures. Large variations in fracture toughness are observed for gas tungsten-arc welds, however, the J_{Ic} values are above 210 kJ/m^2 [100 ft lb/in^2]. The J_{Ic} values for shielded metal arc

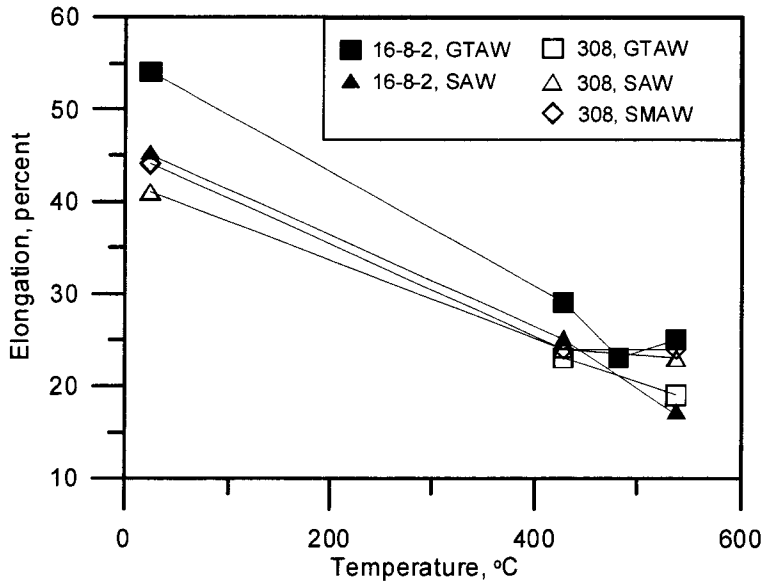

Figure 4-9. Ductility of Austenitic Weld Metal As a Function of Temperature (Mills, 1988a)

NOTE: Temperature provided in °C; for conversion to °F, use °F = 9/5 °C + 32.

SMAW—shielded metal-arc weld; GTAW—gas tungsten-arc weld; SAW—submerged-arc weld.

welds are in the range 60–260 kJ/m^2 [29–124 ft lb/in^2]. Table 4-10 provides a summary of the fracture toughness data for welded Types 304 and 316 SS. In addition to the lower J_{Ic}, the crack-growth resistance is also substantially lower for submerged-arc welds compared with gas tungsten-arc welds. The fracture toughness and crack growth resistance of heat-affected zones are not reduced by shielded metal-arc, submerged-arc, or gas tungsten-arc welding (Mills, 1997).

Because of their use in nuclear reactors, the effects of thermal aging and neutron fluence on the fracture toughness of austenitic stainless steels have been investigated (Mills, 1997). The fracture toughness of both Types 304 and 316 SS base alloys and welds is slightly reduced by thermal aging at temperatures between 450 and 566 °C [842 and 1,050 °F]. At 300 °C [572 °F], the significant reduction in fracture toughness is not observed for gas tungsten-arc welds even after aging for 34,000 hours. The fracture toughness of the base alloys, welds, and weld heat-affected zones can be reduced by high-energy neutron fluence. The welds and weld heat affected zones are more sensitive than the base alloys. The greatest reduction in fracture toughness occurs for neutron exposures between 3 and 10 dpa. The J_{Ic} of 316 shielded metal arc welds is reduced from 195 kJ/m^2 [93 ft lb/in^2] in the unexposed condition to 40 kJ/m^2 [19 ft lb/in^2] for an exposure of 11 dpa. The crack growth resistance is also reduced from 180 MPa [26 ksi] to 8 MPa [1 ksi] after such exposure.

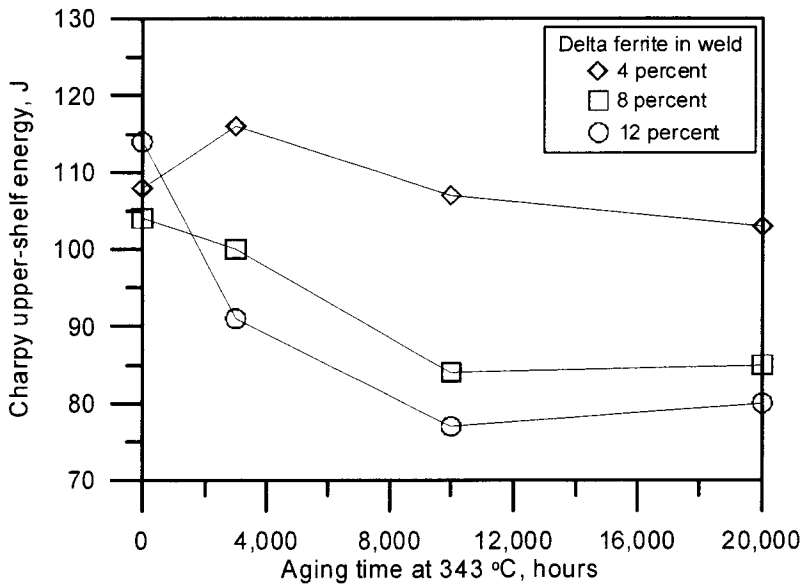

Figure 4-10. Charpy Upper-Shelf Energy for Type 308 SS Weld Metal As a Function of Aging Time at 343 °C [650 °F] and δ-ferrite Content (Alexander, et al., 1990)

NOTE: Impact energy provided in J; for conversion to ft lb, use ft lb = J/1.35.

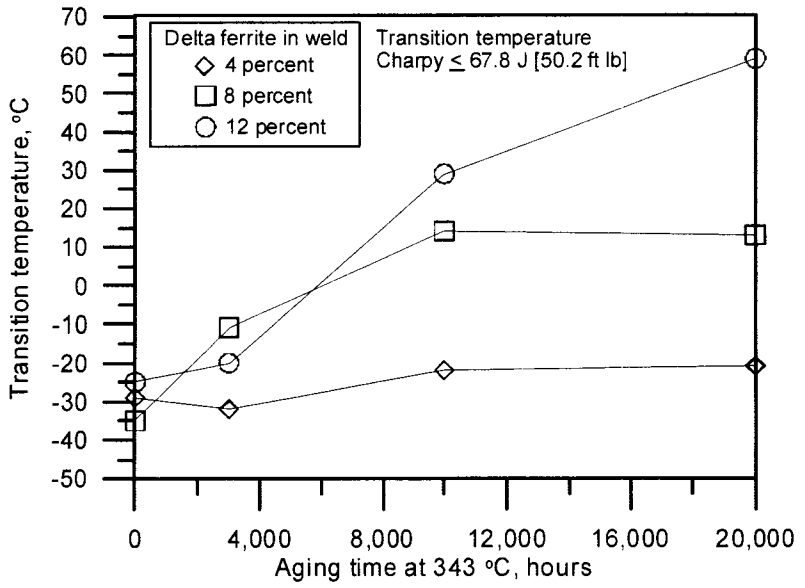

Figure 4-11. Effect of δ-ferrite Content in Type 308 SS Weld Metal on the Transition Temperature After Aging at 343 °C [650 °F] (Alexander, et al., 1990)

NOTE: Temperature provided in °C; for conversion to °F, use °F = 9/5 °C + 32.

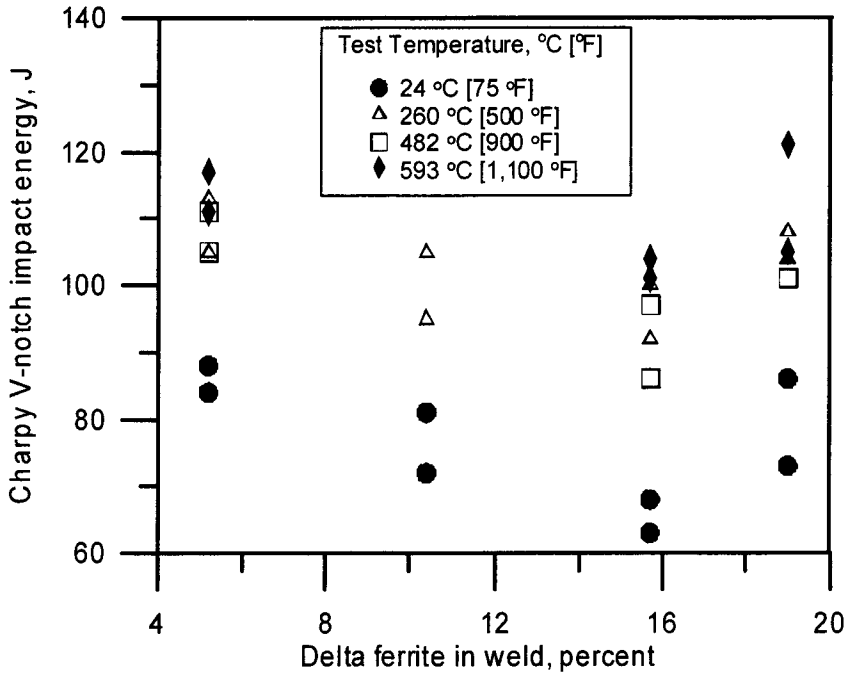

Figure 4-12. Effect of δ-ferrite Content in Type 308 SS Welds on the Charpy V-Notch Impact Energy (Hawthorne and Menke, 1975)

NOTE: Impact energy provided in J; for conversion to ft lb, use ft lb = J/1.35.

4.3 Effect of Fabrication Processes on the Mechanical Properties of Alloy 22

The mechanical properties of wrought Alloy 22 in the mill-annealed condition are similar to those for wrought Type 316 SS. In the wrought condition, the yield and tensile strengths of Alloy 22 are typically 20 percent higher than for Type 316 SS. Fabrication processes required to construct the waste packages may result in microstructural changes described in Chapter 3. Consequently, the mechanical properties of the Alloy 22 outer container can be affected. The information included in this section is compiled from data on Alloy 22 in several conditions including wrought, cold worked, thermally aged, as-welded and welded, and thermally aged. Matching filler metal was used for the welded material.

4.3.1 Mechanical Properties of Wrought Alloy 22

Alloy 22 is similar to Type 316 SS, and both alloys are low-strength, high-ductility materials that undergo strain hardening. The minimum yield and tensile strengths for Alloy 22 are shown in Figure 4-15 as a function of temperature (ASME International, 1995b). Both the yield and tensile strengths decrease with temperature. Correspondingly, the allowable stress also decreases with temperature. At temperatures above 560 °C [1,040 °F], the allowable stress decreases significantly and falls below 100 MPa [14.5 ksi] at 625 °C [1,157 °F]. Typical values

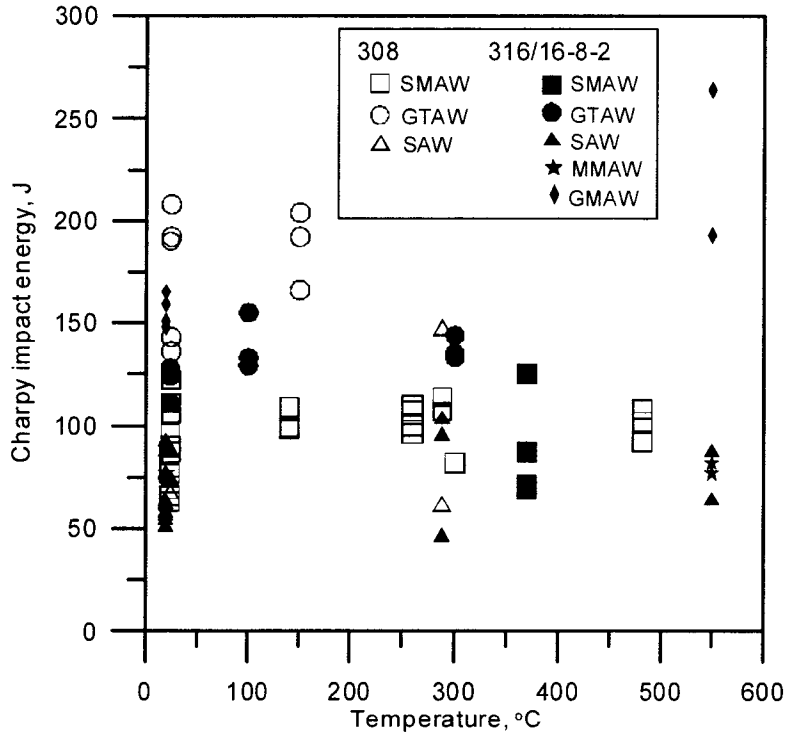

Figure 4-13. Charpy Impact Energy for Austenitic Stainless Steel Welds (Gavenda, et al., 1996)

NOTE: Temperature provided in °C; for conversion to °F, use °F = 9/5 °C + 32.

Impact energy provided in J; for conversion to ft lb, use ft lb = J/1.35.

SMAW—shielded metal-arc weld; GTAW—gas tungsten-arc weld; SAW—submerged-arc weld; GMAW—gas metal-arc weld; MMAW—manual metal-arc weld

of the yield strength, tensile strength, and ductility for Alloy 22 as a function of temperature are shown in Figure 4-16 (Haynes International, 2002). At 25 °C [77 °F], the yield strength of Alloy 22 is approximately 370 MPa [54 ksi] and the tensile strength is 790 MPa [115 ksi]. At 315 °C [600 °F], the yield strength of Alloy 22 decreases to approximately 260 MPa [38 ksi] and the tensile strength is 660 MPa [96 ksi]. In contrast to Type 316 SS, the ductility of Alloy 22 increases with temperature. The high ductility of Alloy 22 in the mill-annealed condition is apparent from the percent elongation measured on a 51-mm [2-in] gage length tensile specimen, which is typically greater than 60 percent over the temperature range 25–760 °C [77–1,400 °F]. Figure 4-17 shows the yield and tensile strengths of Alloy 22 increase with cold work at room temperature (Haynes International, 2002). The response of Alloy 22 is similar to Type 316 SS. The yield strength of Alloy 22 doubles from approximately 400 MPa [58 ksi] to more than 800 MPa [116 ksi] with 20-percent cold work. Ductility of the alloy is reduced from near 60 percent with no cold work to less than 30 percent with 20-percent cold work.

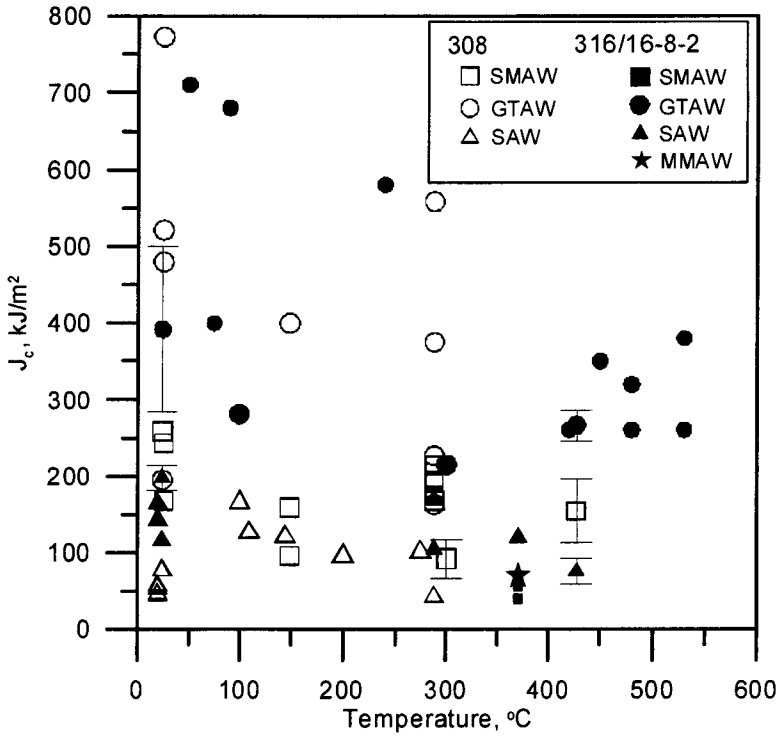

Figure 4-14. Fracture Toughness for Austenitic Stainless Steel Welds (Mills, 1997; Gavenda, et al., 1996)

NOTE: Temperature provided in °C; for conversion to °F, use °F = 9/5 °C + 32. Fracture toughness provided in kJ/m^2; for conversion to ft lb/in^2, use ft lb/in^2 = kJ/m^2/2.093.

SMAW—shielded metal-arc weld; GTAW—gas tungsten-arc weld; SAW—submerged-arc weld; MMAW—manual metal-arc weld

As discussed in Chapter 3, exposures to temperatures in the range 600–1000 °C [1,112–1,832 °F] can result in the precipitation of topologically close-packed phases (Cieslak, et al., 1986; Heubner, et al., 1989) The presence of these phases can increase the localized corrosion susceptibility of Alloy 22 (Heubner, et al., 1989; Pan, et al., 2003). Because these secondary phases are intermetallic and tend to form at grain boundary regions, the mechanical properties of Alloy 22 can be altered when a sufficient concentration of secondary phases is present. Figure 4-18 shows the yield strength of Alloy 22 measured at room temperature after isothermal aging at temperatures ranging 593–760 °C [1,100–1,400 °F] (Summers, et al., 1999). When sufficient concentrations of secondary phases are formed, the yield strength of Alloy 22 increases. At 760 °C [1,400 °F], aging for more than 100 hours is necessary to observe a measurable increase in yield strength. In comparing the results in Figure 4-18 with the time-temperature-precipitation diagram for Alloy 22 developed by Heubner, et al. (1989) (Figure 3-6), it is apparent that complete grain boundary coverage and precipitation of topologically close-packed phases within the grains are necessary to increase the yield strength of Alloy 22. Similarly, Figure 4-19 shows the ductility of Alloy 22, measured as reduction in area

Table 4-10. Summary of Fracture Toughness for Wrought Types 304 and 316 SS Welds*†			
Welding Method	**Gas Tungsten-Arc Weld**	**Submerged-Arc Weld**	**Gas Tungsten-Arc Weld**
Test Temperature	20–125 °C [68–257 °F]	20–125 °C [68–257 °F]	400–550 °C [752–1,022 °F]
Mean J_c kJ/m^2 [ft lb/in^2]	495 [237]	160 [76]	293 [140]
Lower bound J_c kJ/m^2 [ft lb/in^2]	300 [143]	100 [48]	180 [86]
Upper bound J_c kJ/m^2 [ft lb/in^2]	800 [382]	270 [129]	Not reported
Mean dJ/da MPa [ksi]	390 [57]	160 [23]	307 [45]
Lower bound dJ/da MPa [ksi]	260 [38]	110 [16]	107 [16]
Upper bound dJ/da MPa [ksi]	600 [87]	190 [28]	Not reported
Mean Tearing Modulus	340	130	350

*Mills, W.J. "Fracture Toughness of Austenitic Stainless Steels and their Welds." *ASM Handbook Volume 19: Fatigue and Fracture.* Metals Park, Ohio: ASM International. pp. 733–756. 1995.
†Mills W.J. "Fracture Toughness of Types 304 and 316 Stainless Steels and Their Welds." *International Materials Reviews.* Vol. 42. pp. 45–82. 1997.

at room temperature, is affected by the presence of topologically close-packed phases only when a large volume of these secondary phases is present (Rebak, et al., 2000). Aging at 760 °C [1,400 °F] for 70 hours results in a measurable decrease in the reduction in area. The alloy remains ductile, however. Extended aging for a period of several hundred hours at 760 °C [1,400 °F] is required to decrease significantly the ductility of Alloy 22. At lower temperatures, even longer aging times are necessary to reduce the ductility.

The impact toughness of Alloy 22 as a function of thermal aging time and temperature in the range 593–760 °C [1,100–1,400 °F] measured using Charpy V-notch test specimens at room temperature is shown in Figure 4-20 (Summers, et al., 2002). In contrast to the results for yield strength and ductility measurements as a function of thermal aging time and temperature, the impact strength of Alloy 22 is quite sensitive to the precipitation of topologically close-packed phases. For the unaged specimens, the impact strength is measured to be 352 J [260 ft lb]. Although the values of the high-impact strength for the unaged specimens are not valid because the specimens did not break, it is apparent that Alloy 22 in the mill-annealed condition is very ductile and resistant to fracture. Decreases in impact toughness are observed after thermal aging for 10 hours at 760 °C [1,400 °F]. After 70 hours at 760 °C [1,400 °F], the impact

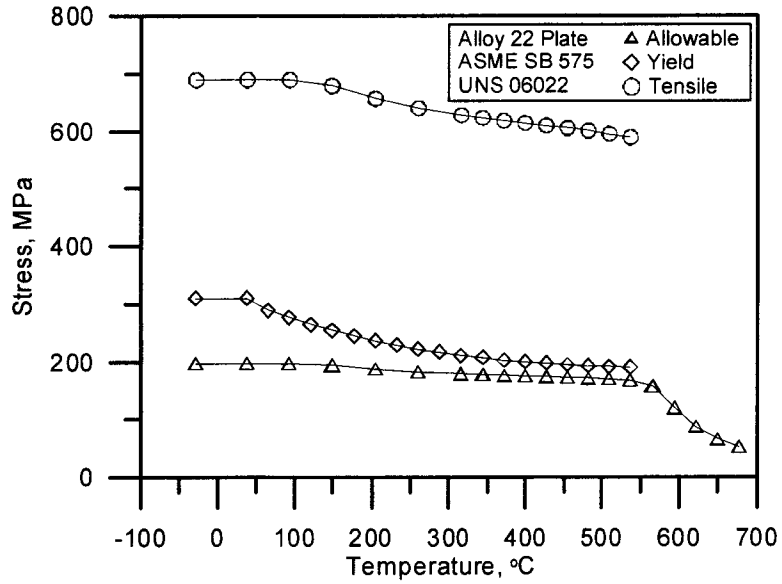

Figure 4-15. Yield Strength, Tensile Strength, and Allowable Stress for Alloy 22 (ASME International, 1995b)

NOTE: Temperature provided in °C; for conversion to °F, use °F = 9/5 °C + 32. Stress provided in MPa; for conversion to ksi, use ksi = MPa/6.895.

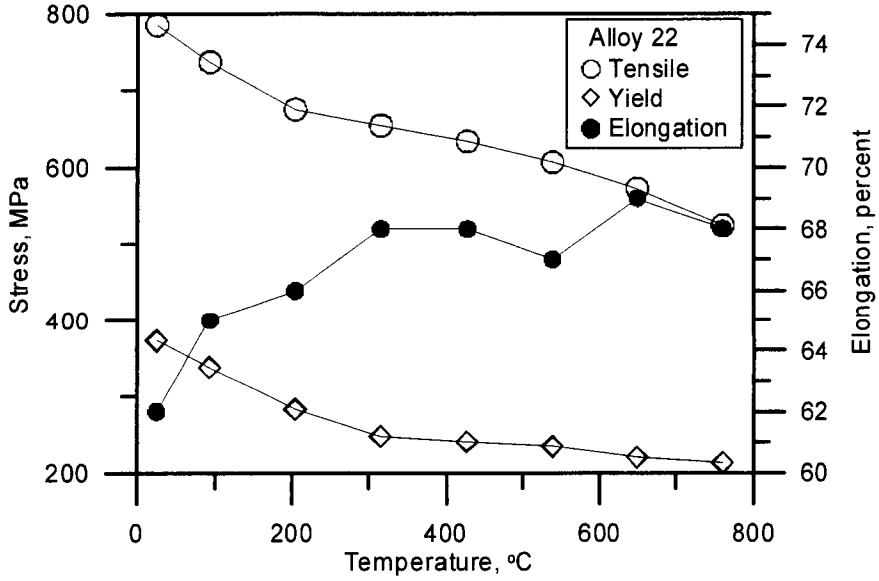

Figure 4-16. Yield Strength, Tensile Strength, and Ductility for Alloy 22 (Haynes International, 2002)

NOTE: Temperature provided in °C; for conversion to °F, use °F = 9/5 °C + 32. Stress provided in MPa; for conversion to ksi, use ksi = MPa/6.895.

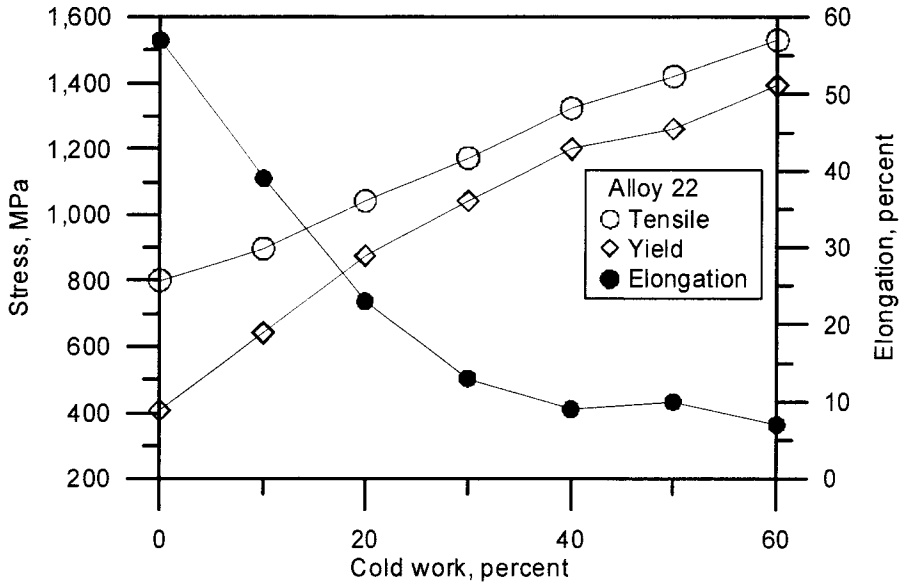

Figure 4-17. Effect of Cold Work on Yield Strength, Tensile Strength, and Ductility for Alloy 22 (ASME International, 2002)

NOTE: Stress provided in MPa; for conversion to ksi, use ksi = MPa/6.895.

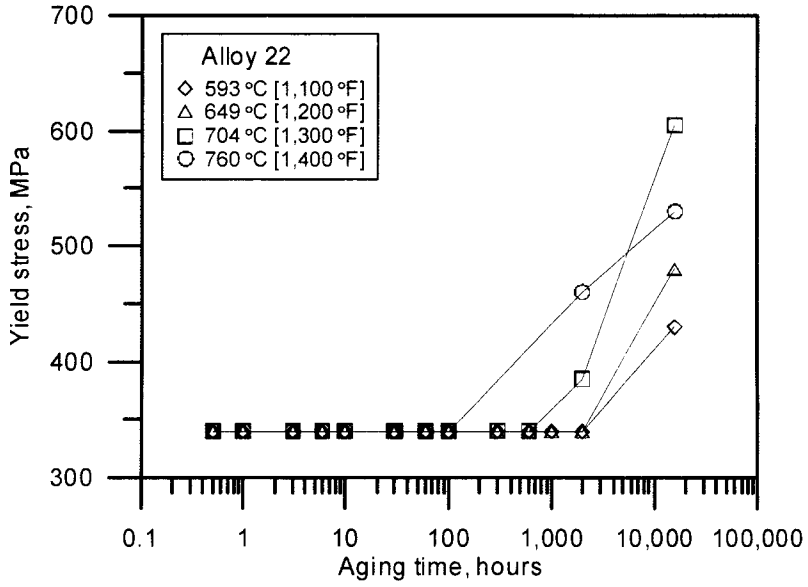

Figure 4-18. Effect of Thermal Aging Time and Temperature on Yield Strength of Alloy 22 (Summers, et al., 1999)

NOTE: Stress provided in MPa; for conversion to ksi, use ksi = MPa/6.895.

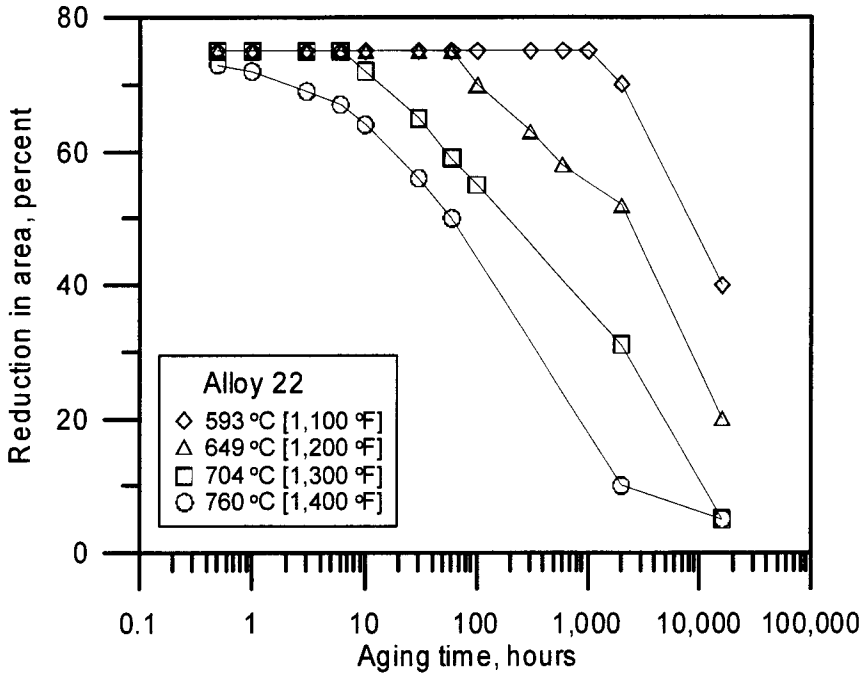

Figure 4-19. Effect of Thermal Aging Time and Temperature on Ductility of Alloy 22 (Rebak, et al., 2000)

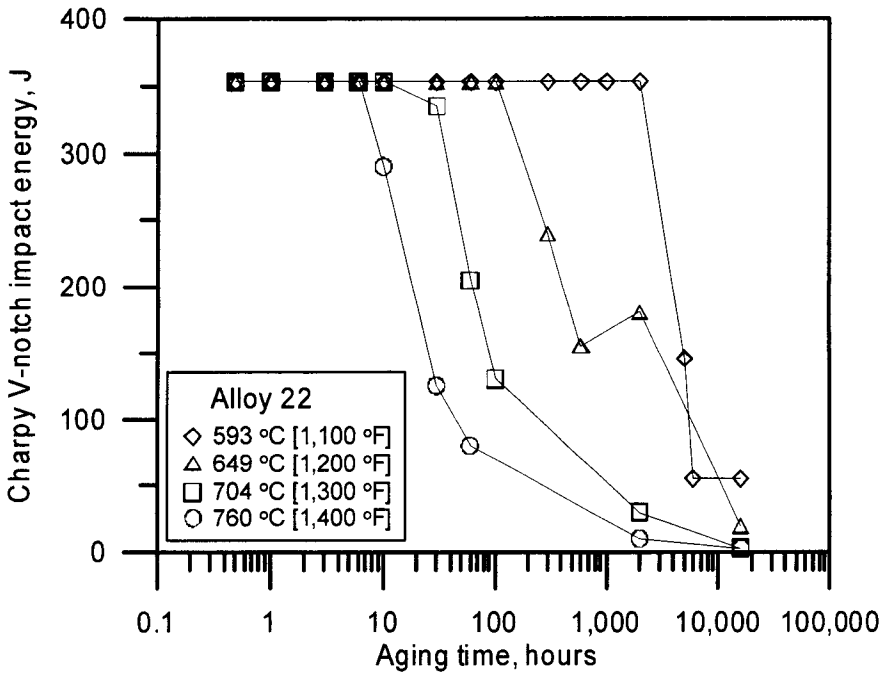

Figure 4-20. Charpy V-Notch Impact Energy of Alloy 22 As a Function of Thermal Aging Time and Temperature (Summers, et al., 2002)

toughness is reduced to below 100 J [74 ft lb]. The time-temperature-precipitation diagram for Alloy 22 reported by Heubner, et al. (1989) shown in Figure 3-6 indicates that after 10 hours at 750 °C [1,382 °F], the grain boundaries still are not completely covered, with topologically close-packed phase precipitates. At 750 °C [1,382 °F], the grain boundaries are completely covered and precipitation within the grains has occurred after 100 hours. Considering the results of Heubner, et al. (1989), it is apparent that significant reduction of the impact toughness occurs when topologically close-packed phase precipitates cover the grain boundaries of Alloy 22.

Fracture toughness data of Alloy 22 have not been reported. Based on the low yield strength, ductility, impact toughness, and strain-hardening characteristics, the fracture toughness of mill-annealed Alloy 22 is high and likely greater than the fracture toughness of annealed Type 316 SS. While data for Alloy 22 are not available, the fracture toughness of ductile nickel-chromium-iron alloys has been investigated. The minimum fracture toughness of Alloy 800 (42Fe-33Ni-21Cr) is reported to be 513 ± 12 kJ/m^2 [245 ± 6 ft lb/in^2] (Krompholtz, et al., 1988). Mills and Brown (1999) report the fracture toughness of Alloy 690 (58Ni-29Cr-9Fe) to be 440 kJ/m^2 [210 ft lb/in^2] in air. Similarly, the fracture toughness of Alloy 600 (72Ni-16Cr-8Fe) is reported to be 415 kJ/m^2 [198 ft lb/in^2] (Mills and Brown, 2001). Similar values are expected for Alloy 22 in the mill-annealed condition. Thermal aging and cold work are likely to reduce the fracture toughness of Alloy 22 based on the reduced ductility in tensile tests and the reduced impact toughness of the thermally aged material.

4.3.2 Effect of Welding and Thermal Exposure on Mechanical Properties of Alloy 22

Welded Alloy 22 has a heterogeneous microstructure with secondary phase precipitates. In the as-welded condition, the yield strength of Alloy 22 is 15 to 20 percent higher than the yield strength of the mill-annealed plate. The yield strength, tensile strength, and elongation of as welded Alloy 22 as a function of temperature are shown in Figure 4-21 (Haynes International, 2002). Although the yield strength is higher for the as-welded material compared with the mill-annealed material, the tensile strength is similar for both welded and mill-annealed Alloy 22. Elongation of the as-welded material is reduced; however, the welded material exhibits good ductility.

The yield strength of welded and aged Alloy 22 is shown in Figure 4-22 (Summers, et al., 2002). As previously indicated, the yield strength of the as-welded material is higher than that of the mill-annealed alloy. Figure 4-22 shows the yield strength of the as-welded alloy does not change with aging time up to 100 hours at temperatures in the range 593–760 °C [1,100–1,400 °F]. Although the data above 100 hours is limited to mostly material aged at 593 °C [1,100 °F], it appears that precipitation of topologically close-packed phases increases the yield strength. The effect of aging time on the ductility of welded Alloy 22 was not reported.

The effect of welding method on the Charpy V-notch impact energy of Alloy 22 is shown in Table 4-11 (Haynes International, 2002). The results are similar to the effect of welding method on the fracture toughness of stainless steels. Gas tungsten-arc welds and gas metal-arc welds have the highest impact toughness, which can be attributed to the low concentrations of inclusions. The impact toughness of the shielded metal-arc welds is much lower compared to the other welding methods. Shielded metal-arc welds typically have a higher inclusion content which can reduce the toughness and the ductility of the weld.

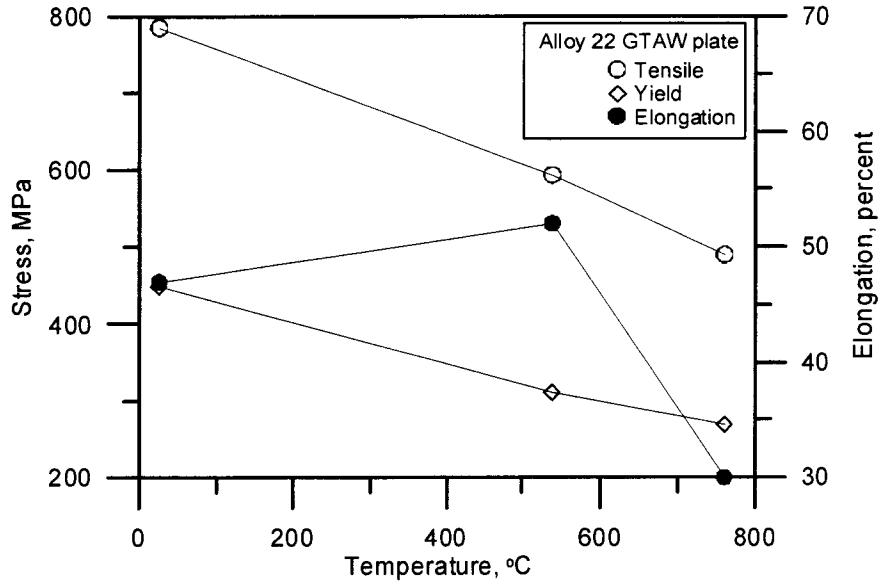

Figure 4-21. Yield Strength, Tensile Strength, and Ductility of Welded Alloy 22 (Haynes International, 2002)

NOTE: Temperature provided in °C; for conversion to °F, use °F = 9/5 °C + 32. Stress provided in MPa; for conversion to ksi, use ksi = MPa/6.895.

GTAW—gas tungsten-arc weld

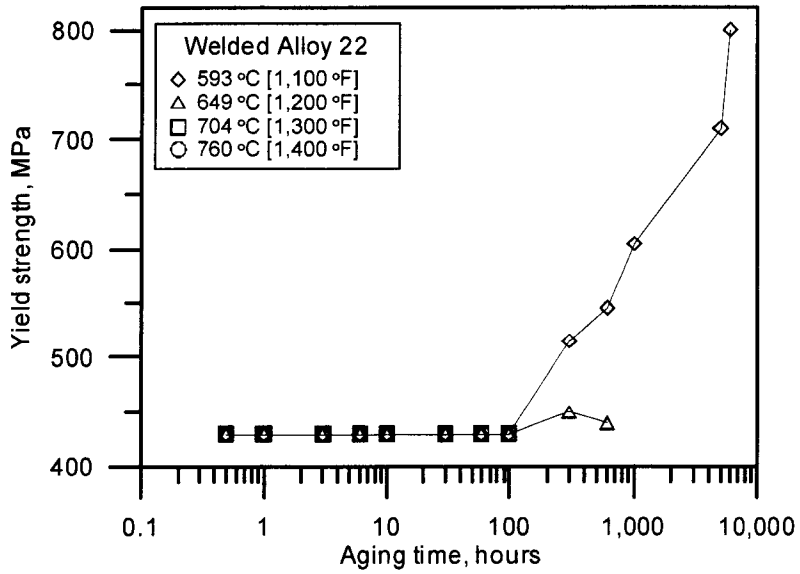

Figure 4-22. Yield Strength, Tensile Strength, and Ductility of Welded Alloy 22 (Summers, et al., 2002)

NOTE: Stress provided in MPa; for conversion to ksi, use ksi = MPa/6.895.

GTAW—gas tungsten-arc weld

Table 4-11. Charpy V-Notch Impact Energy for Various Welding Methods*		
Welding Method	**Charpy V-Notch Impact Energy at 25 °C [77 °F] J [ft lb]**	**Specimen Condition After Test Bend or Break**
Gas tungsten-arc weld	201 [148]	Break
Gas metal-arc weld short arc	164 [121]	Break
Gas metal-arc weld spray	202 [149]	Break
Shielded metal-arc weld	103 [76]	Break
*Haynes International. "Hastelloy C–22 Alloy." H–2019F. Kokomo, Indiana: Haynes International. 2002.		

The impact energy of gas tungsten-arc welded and aged Alloy 22 is strongly dependent on aging time and temperature. The impact energy and volume fraction of precipitates as a function of aging time at 649 °C [1,200 °F] and 760 °C [1,400 °F] are shown in Figures 4-23 and 4-24. For both aging temperatures, the impact energy of the welded and aged material decreases below 100 J [74 ft lb] when the volume fraction of the topologically close-packed precipitates increases above 0.05 to 0.08. For welded Alloy 22 aged at 649 °C [1,200 °F], this does not occur until after 300 hours. This transition occurs after 10 hours at 760 °C [1,400 °F]. The relationship between the Charpy V-notch impact energy of welded Alloy 22 and the volume fraction of topologically close-packed precipitates after isothermal aging is summarized in Figure 4-25. It is apparent that the effect of aging is similar for all temperatures in the range 593–760 °C [1,100–1,400 °F]. The greatest reduction in impact energy for the welded condition occurs when the volume fraction of precipitates increases to values in the range 0.6–0.8.

The Charpy V-notch impact energy (CVN) of welded Alloy 22 as a function of aging time is shown in Figure 4-26. Best-fit regression lines are also shown in Figure 4-26. The Charpy V-notch impact energy data are fit to equations of the form [Eq. (4-13)]

$$\text{CVN}\ (J) = (A_1 + A_2 T) + (B_1 + B_2 T)\text{Log}(t,\ \text{hours}) \qquad (4\text{-}13)$$

where

A_1 and A_2 — intercept and temperature dependance of the intercept
B_1 and B_2 — slope and temperature dependance of the slope

T — aging temperature (°C)
t — aging time (hours)

Actual values of the parameters obtained analyzing the data reported by Summers, et al. (2002) are shown in Eq. (4-14)

$$J = 1{,}402.8 - 1.60T + (0.16T - 213.0)\text{Log}(t) \qquad (4\text{-}14)$$

In addition to the actual Charpy V-notch impact energy data and best-fit regression lines, the estimated Charpy impact values are also shown in Figure 4-26. The maximum impact energy is

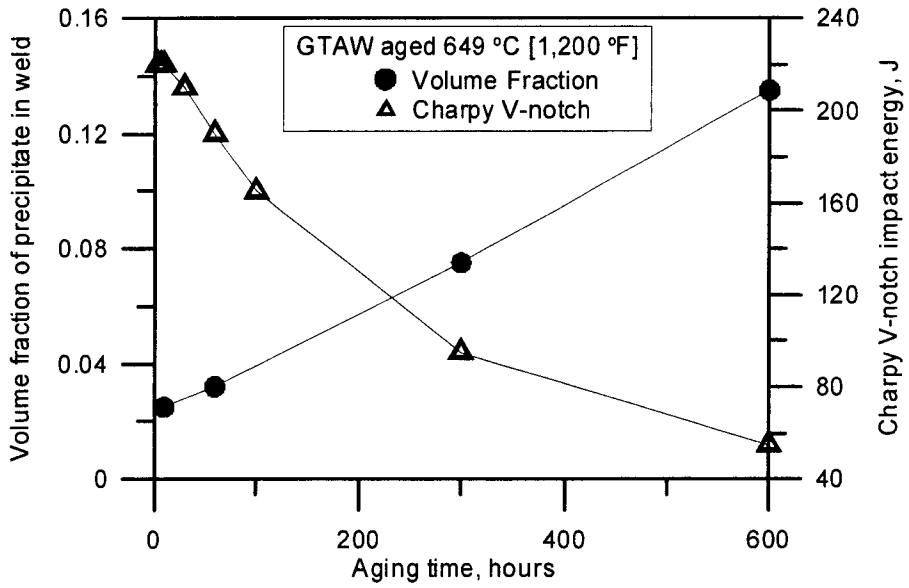

Figure 4-23. Charpy V-Notch Impact Energy and Volume Fraction of Precipitate for Welded Alloy 22 As a Function of Aging Time at 649 °C [1,200 °F] (Summers, et al., 2002)

NOTE: Impact energy provided in J; for conversion to ft lb, use ft lb = J/1.35.

GTAW—gas tungsten-arc weld

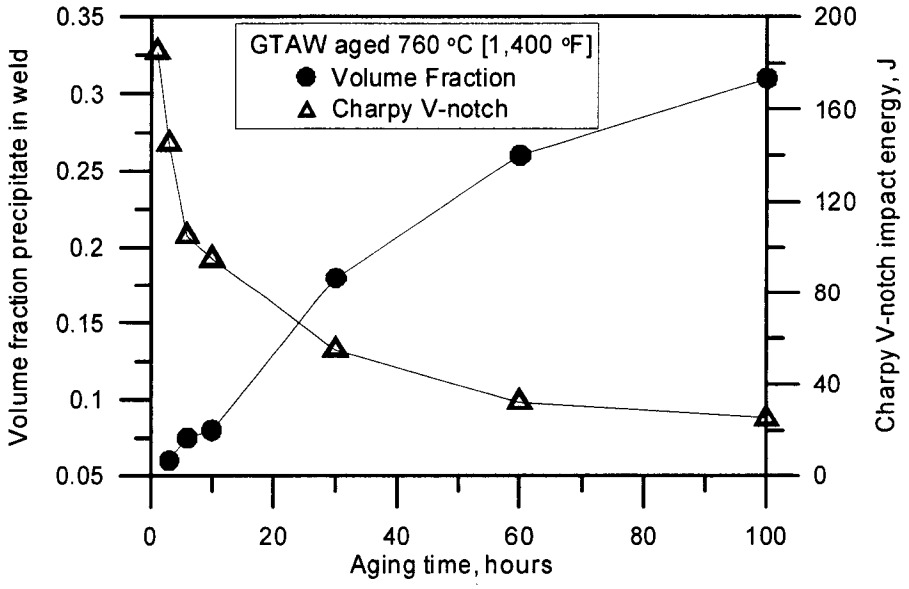

Figure 4-24. Charpy V-Notch Impact Energy and Volume Fraction of Precipitate for Welded Alloy 22 As a Function of Aging Time at 760 °C [1,400 °F] (Summers, et al., 2002)

NOTE: Impact energy provided in J; for conversion to ft lb, use ft lb = J/1.35.

GTAW—gas tungsten-arc weld

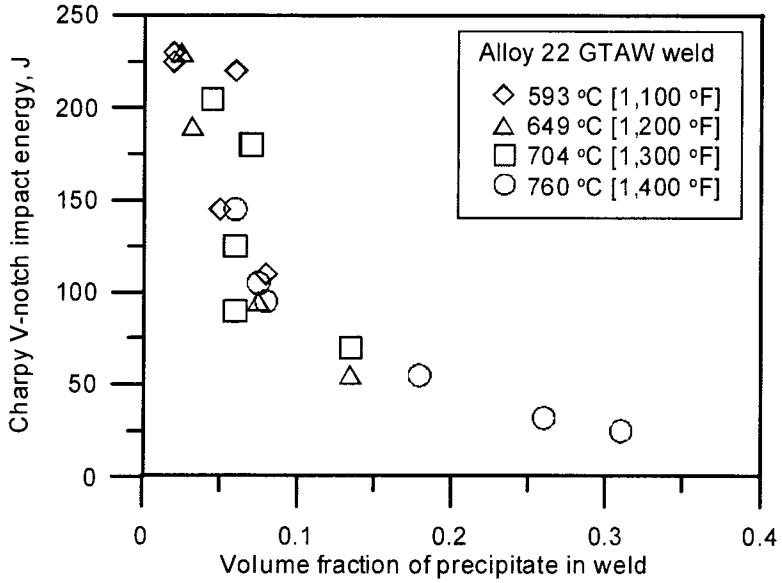

Figure 4-25. Charpy V-Notch Impact Energy As a Function of Volume Fraction of Precipitate for Welded Alloy 22 After Thermal Aging at 593 to 760 °C [1,100 to 1,400 °F] (Summers, et al., 2002)

NOTE: Impact energy provided in J; for conversion to ft lb, use ft lb = J/1.35.

GTAW—gas tungsten-arc weld

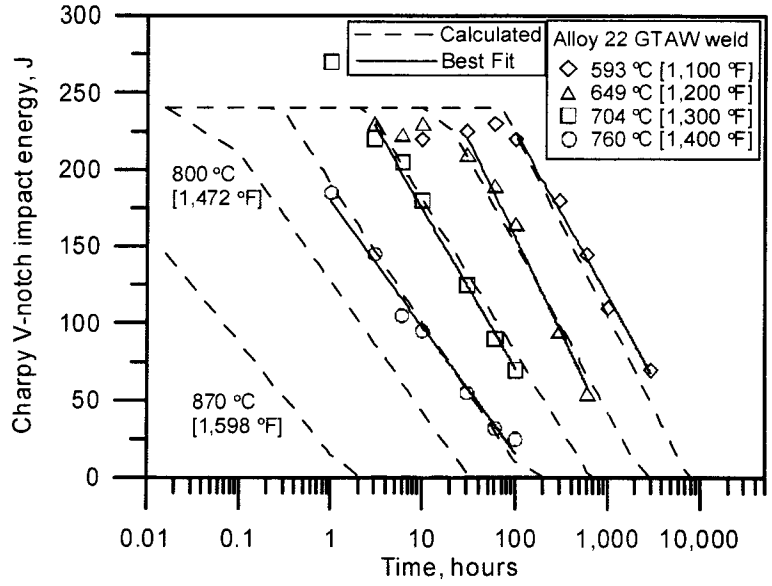

Figure 4-26. Charpy V-Notch Impact Energy As a Function of Thermal Aging at 593 to 760 °C [1,100 to 1,400 °F] (Summers, et al., 2002)

NOTE: Impact energy provided in J; for conversion to ft lb, use ft lb = J/1.35.

GTAW—gas tungsten-arc weld

fixed at 240 J [178 ft lb], and the minimum was fixed at 1 J [0.7 ft lb]. Calculated Charpy V-notch impact energies are similar to the actual measured values for all temperatures in the range 593–760 °C [1,100–1,400 °F]. Figure 4-26 also shows the calculated values for aging temperatures of 800 and 870 °C [1,472 and 1,598 °F] using Eq. (4-14). Extrapolation outside the range of 593 to 760 °C [1,100 to 1,400 °F] assumes that the parameters in Eq. (4-14) remain valid outside this temperature range. Below 593 °C [1,100 °F], precipitation of topologically close-packed phases may not occur even after extended aging. Long-range ordering may occur, however, the effect of this phase transformation on the impact strength of Alloy 22 has not been reported. Above 760 °C [1,400 °F], precipitation of topologically close-packed phases does occur, however, the validity of extrapolating Eq. (4-14) to higher temperatures is not established. The impact energies for Alloy 22 after aging at 800 and 870 °C [1,472 and 1,598 °F], calculated using Eq. (4-14), while likely conservative, have not been verified.

Fracture toughness data for welded Alloy 22 are not available; however, it is anticipated that the fracture toughness of Alloy 22 in the as-welded condition would be high based on the ductility of the weld metal and high impact strength in the welded condition. The fracture toughness of the welded material may be dependent on the welding method, based on the data shown in Table 4-9. In addition, the fracture toughness may be influenced by base and weld metal composition and specific parameters of the welding process, such as heat input and the number of weld repairs. Postweld solution annealing is beneficial for stainless steels; however, recent investigations conduced at CNWRA have shown that solution annealing of Alloy 22 welds is detrimental to the weld microstructure and the localized corrosion resistance. It is not clear if postweld heat treatments such as those proposed for the Alloy 22 outer disposal container welds and discussed in Chapter 2 is beneficial or detrimental to the fracture toughness.

4.4 Assessment of the Effects of Fabrication Processes on Mechanical Properties of Waste Package Materials

As previously discussed, both Type 316 SS and Alloy 22 are ductile alloys with high toughness, resulting in resistance to fracture. The failure mode for such materials is typically mechanical overload, leading to ductile failure by coalescence of microvoids rather than brittle fracture. Mills (1997) has binned the fracture toughness of materials into three categories:

- Low fracture toughness materials with J_{Ic} less than 30 kJ/m^2 [14 ft lb/in^2] or K_{Ic} less than 75 MPa m$^{1/2}$ [68 ksi in$^{1/2}$] and a tearing modulus less than 10. Fractures of these materials can occur at or below the yield strength with small flaw sizes.

- Intermediate fracture toughness materials with J_{Ic} of 30 to 150 kJ/m^2 [14 to 71 ft lb/in^2] or K_{Ic} in the range 75–100 MPa m$^{1/2}$ [68–91 ksi in$^{1/2}$] and a tearing modulus in the range 10–100. Fractures of these materials can occur at the yield strength with small to medium crack sizes.

- High fracture toughness materials with J_{Ic} greater than 150 kJ/m^2 [71 ft lb/in^2] or K_{Ic} greater than 100 MPa m$^{1/2}$ [91 ksi in$^{1/2}$] and a tearing modulus greater than 100. Fracture of these materials usually involves stable tearing at stresses above the yield strength.

For the low fracture toughness materials, a linear elastic fracture mechanics assessment is sufficient. For the intermediate fracture toughness materials, a fracture mechanics assessment may be required for materials in high-stress intensity applications. A fracture mechanics evaluation is generally not required for the high fracture toughness materials (Mills and Brown, 1999).

4.4.1 Failure Assessment of Type 316 SS

The approach proposed by U.S. Department of Energy to assess failure of the titanium drip shields and the waste packages is based on the failure assessment diagram using plain strain fracture toughness, K_{Ic}. Because of the low strength and high ductility of austenitic stainless steels, K_{Ic} values are usually not available. Values of J_{Ic} are available, however, and using Eq. (4-7), the fracture toughness, K_{Jc}, can be calculated and substituted for K_{Ic} to construct a failure assessment diagram.

A failure assessment diagram for Type 316 SS is shown in Figure 4-27. Values for K_{Jc} are obtained from J_{Ic} values in Tables 4-3 and 4-8 and a modulus of 170 GPa [25 × 10^6 ksi] for all materials. Minor variations in fracture toughness have little effect on the failure of the wrought stainless steel plate. Because the fracture toughness of the gas tungsten-arc welded stainless steel is similar to the wrought material, ductile failure is predicted for the welded material. Submerged-arc welds are also predicted to undergo ductile failure rather than fracture. The lower fracture toughness of the submerged arc welded material, however, pushes the material near the boundary between high to intermediate fracture toughness materials. The stainless steel failure assessment diagram also includes calculations for Type 316 plate with 30-percent cold work. It is apparent that with sufficient cold work, the failure mode can shift from ductile collapse to brittle fracture. The effect of 5-percent cold work is similar to the as-welded submerged arc weld. With 30-percent cold work, failure becomes a mixture of ductile failure and fracture.

The failure assessment diagram shown in Figure 4-27 addresses only the effects of single processes such as cold work or welding. The calculations shown in Figure 4-27 do not consider the possibility of synergistic effects that may be expected in the fabrication and closure of the waste packages. The combination of cold work and welding may need to be examined based on the effects of these single processes.

4.4.2 Failure Assessment of Alloy 22

Because of the limited data for the fracture toughness of corrosion resistant, nickel-chromium-molybdenum alloys, assessment of the failure of Alloy 22 is not straightforward. As previously indicated, values of K_{Ic} can be estimated from the Charpy V-notch impact energy for some materials. The empirical correlation shown in Eq. (4-8) was developed for pressure vessel steels. Because no such correlations exist for nickel-chromium-molybdenum alloys, the fracture toughness of austenitic nickel-chromium-iron alloys, measured with a J-integral method is converted to a K_{Jc} value using Eq. (4-7) and compared to the K_{Ic} value calculated from the Charpy V-notch impact energy using Eq. (4-8). The mechanical properties of Alloys 600 and 690 are shown in Table 4-12 (Mills and Brown, 2001) and Table 4-13 (Mills and Brown, 1999). Included are calculations of fracture toughness using Eqs. (4-7) and (4-8). For Alloy 600, a fracture toughness of 207 MPa $m^{1/2}$ [189 ksi $in^{1/2}$] is estimated from the Charpy V-notch impact energy of 244 J [180 ft lb]. This value is below the fracture toughness calculated from the J_{Ic}.

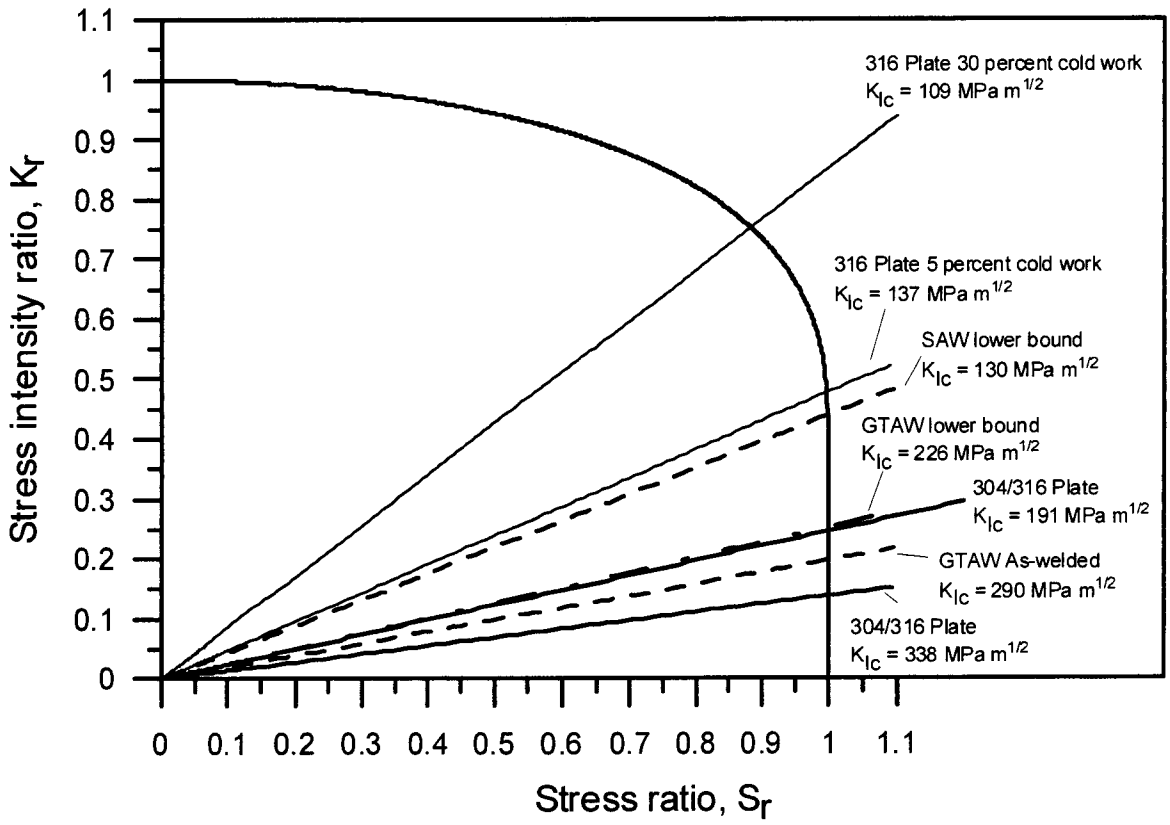

Figure 4-27. Failure Assessment Diagram for Type 304/316 SS

NOTE: Stress intensity provided in MPa $m^{1/2}$; for conversion to ksi $in^{1/2}$, use ksi $in^{1/2}$ = MPa $m^{1/2}$/1.1.

GTAW—gas tungsten-arc weld

For the base alloy at 24 °C [77 °F] in air, the J_{Ic} is determined to be 415 kJ/m^2 [198 ft lb/in^2]. Using Eq. (4-7), this value corresponds to a K_{Jc} of 298 MPa $m^{1/2}$ [270 ksi $in^{1/2}$]. This relationship implies the calculation of K_{Ic} from Charpy V-notch data will result in conservative values of fracture toughness. Similar results were obtained for Alloy 690 as shown in Table 4-13.

Additional data for welded Alloys 600 and 690 are included in Tables 4-12 and 4-13. The fracture toughness of the welded materials similar to the base metals when tests are performed in air. The fracture toughness decreases considerably when tests are performed in water. Mills and Brown (1999, 2001) attribute the decreased fracture toughness of welded Alloys 600 and 690 in water to hydrogen embrittlement. The data in Tables 4-12 and 4-13 indicate the minimum ductility and minimum fracture toughness of welded Alloy 600 occur at 54 °C [129 °F]. Increasing the temperature to 149 °C [129 °F] and 338°C [640 °F] results in an increase in the fracture toughness of the welded material. The temperature dependence of the fracture toughness in water is consistent with the expected behavior for a material susceptible to hydrogen embrittlement (Sridhar and Cragnolino, 1992).

Table 4-12. Mechanical Properties and Fracture Toughness of Alloy 600*							
Material, Test Condition, and Temperature °C [°F]	**Yield Strength MPa [ksi]**	**Ultimate Tensile Strength MPa [ksi]**	**Strain, Percent**	**Elastic Modulus GPa [ksi]**	**J_{Ic}, kJ/m^2 [ft lb/in^2]**	**Charpy V-Notch J [ft lb]**	**K_{Ic} from J_{Ic} or Charpy V-Notch MPa m$^{1/2}$ [ksi in$^{1/2}$]**
Base alloy, air, 24 °C [77 °F]	337 [49]	709 [103]	50	214 [31 × 10^5]	—	244 [180]	207 [189]
Base alloy, air, 24 °C [77 °F]	337 [49]	709 [103]	50	214 [31 × 10^5]	415 [198]	—	298 [270]
Base alloy, air, 54 °C [129 °F]	319 [46]	654 [95]	37	214 [31 × 10^5]	415 [198]	—	298 [270]
Base alloy, air, 338 °C [640 °F]	288 [42]	655 [95]	39	199 [29 × 10^5]	415 [198]	—	287 [261]
Base alloy, water 54 to 149 °C [129 to 300 °F]	267 [39]	594 [86]	35	210 [30 × 10^5]	284 [136]	—	244 [222]
GTAW† Transverse, air, 24 °C [77 °F]	430 [62]	689 [100]	40	214 [31 × 10^5]	553 [264]	—	341 [310]
GTAW Transverse, air, 54 °C [129 °F]	436 [63]	689 [100]	34	214 [31 × 10^5]	350 [167]	—	274 [249]
GTAW Transverse, air, 338 °C [640 °F]	423 [61]	643 [93]	42	199 [29 × 10^5]	350 [167]	—	264 [240]
GTAW Transverse, water 54 °C [129 °F] sample A2	474 [69]	601 [87]	18	214 [31 × 10^5]	33 [16]	—	83 [75]
GTAW Transverse, water 54 °C [129 °F] sample C2-C4	474 [69]	601 [87]	18	214 [31 × 10^5]	13 [6]	—	53 [48]

Table 4-12. Mechanical Properties and Fracture Toughness of Alloy 600* (continued)							
Material, Test Condition, and Temperature, °C [°F]	**Yield Strength MPa [ksi]**	**Ultimate Tensile Strength MPa [ksi]**	**Strain Percent**	**Elastic Modulus GPa [ksi]**	**J_{Ic}, kJ/m^2 [ft lb/in^2]**	**Charpy V-Notch J [ft lb]**	**K_{Ic} from J_{Ic} or Charpy V Notch MPa m$^{1/2}$ [ksi in$^{1/2}$]**
GTAW Transverse, water 149 °C [300 °F] sample A2	Not reported	Not reported	Not reported	210 [30 × 10^5]	200 [96]	—	203 [185]
GTAW Transverse, water 338 °C [640 °F] sample A2	397 [58]	571 [83]	32	199 [29 × 10^5]	459 [219]	—	302 [275]

*Mills, W.J. and C.M. Brown. "Fracture Toughness of Alloy 600 and an EN82H Weld in Air and Water." *Metallurgical Transactions.* Vol. 32A. pp. 1,161–1,174. 2001.
†GTAW—gas tungsten-arc weld

A failure assessment diagram for Alloy 600 (Figure 4-28) was constructed using the data in Table 4-12. Figure 4-28 again shows the calculation of fracture toughness using Charpy V-notch impact data is conservative for the base alloy. Unfortunately, no Charpy V-notch impact data due available for the welded Alloy 600. The effects of hydrogen embrittlement are apparent. In the worst case, welded Alloy 600 could be susceptible to a mixed mode failure. Similar results and conclusions are obtained after the construction of the failure assessment diagram for Alloy 690 shown in Figure 4-29.

Figure 4-30 shows the failure assessment diagram constructed for Alloy 22. Because fracture toughness data for Alloy 22 are not available, the failure assessment diagram is constructed using the Charpy V-notch impact data. The high Charpy V-notch impact energy reported for Alloy 22 in both the mill-annealed and the as-welded conditions is reflected in the high fracture toughness. Failure is controlled by continuum mechanics and specifically ductile collapse. Values of the Charpy V-notch impact energy for the gas tungsten-arc welded Alloy 22 aged at 870 °C [1,598 °F] are taken from the calculations shown in Figure 4-26 and used to estimate the fracture toughness with Eq. (4-8). The calculations suggest that thermal aging of welded Alloy 22 decreases the fracture toughness. After 30 minutes at 870 °C [1,598 °F], failure of the welded and aged material is no longer purely ductile.

The calculations used in Figure 4-30 contain several critical assumptions including the calculation of Charpy V-notch impact energy at 870 °C [1,598 °F] (Figure 4-26) and the subsequent calculation of fracture toughness. Because the validity of these assumptions cannot be verified with the data presently available, the calculations in Figure 4-30 must be used with caution. In addition to the assumptions necessary to construct the failure assessment diagram for Alloy 22, several important issues are not addressed because of the lack of

Table 4-13. Mechanical Properties and Fracture Toughness of Alloy 690*							
Material, Test Condition, and Temperature °C [°F]	**Yield Strength MPa [ksi]**	**Ultimate Tensile Strength MPa [ksi]**	**Strain Percent**	**Elastic Modulus GPa [ksi]**	**J_{Ic}, kJ/m^2 [ft lb/in^2]**	**Charpy V-Notch J [ft lb]**	**K_{Ic} from J_{Ic} or Charpy V-Notch, MPa m$^{1/2}$ [ksi in$^{1/2}$]**
Base alloy, air, 24 °C [77 °F]	352 [51]	703 [102]	46	211 [31 × 10^5]	—	190 [140]	206 [187]
Base alloy, air, 54 °C [129 °F]	352 [51]	703 [102]	46	211 [31 × 10^5]	440 [210]	—	298 [270]
Base alloy, air, 338 °C [640 °F]	352 [51]	703 [102]	46	201 [29 × 10^5]	440 [210]	—	298 [270]
Base alloy, water, 54 °C [129 °F]	352 [51]	703 [102]	46	211 [31 × 10^5]	103 [49]	—	146 [133]
Base alloy, water, 149 °C [300 °F]	352 [51]	703 [102]	46	206 [29 × 10^5]	485 [232]	—	316 [288]
GTAW† Transverse, air, 54 °C [129 °F]	352 [51]	703 [102]	46	211 [31 × 10^5]	810 [387]	—	413 [376]
GTAW Transverse, air, 338 °C [640 °F]	352 [51]	703 [102]	46	201 [29 × 10^5]	810 [387]	—	403 [367]
GTAW Transverse, water, 54 °C [129 °F] Minimum value	352 [51]	703 [102]	46	211 [31 × 10^5]	20 [10]	—	65 [59]
GTAW Transverse, water 54 °C [129 °F] Average of three values	352 [51]	703 [102]	46	211 [31 × 10^5]	65 [31]	—	112 [102]
GTAW Transverse, water 93 °C [200 °F] Average of two values	352 [51]	703 [102]	46	206 [29 × 10^5]	365 [175]	—	268 [243]

*Mills, W.J. and C.M. Brown. "Fracture Behavior of Nickel-Based Alloys in Water." B–T–3240. West Mifflin, Pennsylvania: Bettis Atomic Power Laboratory. 1999.
†GTAW—gas tungsten-arc weld

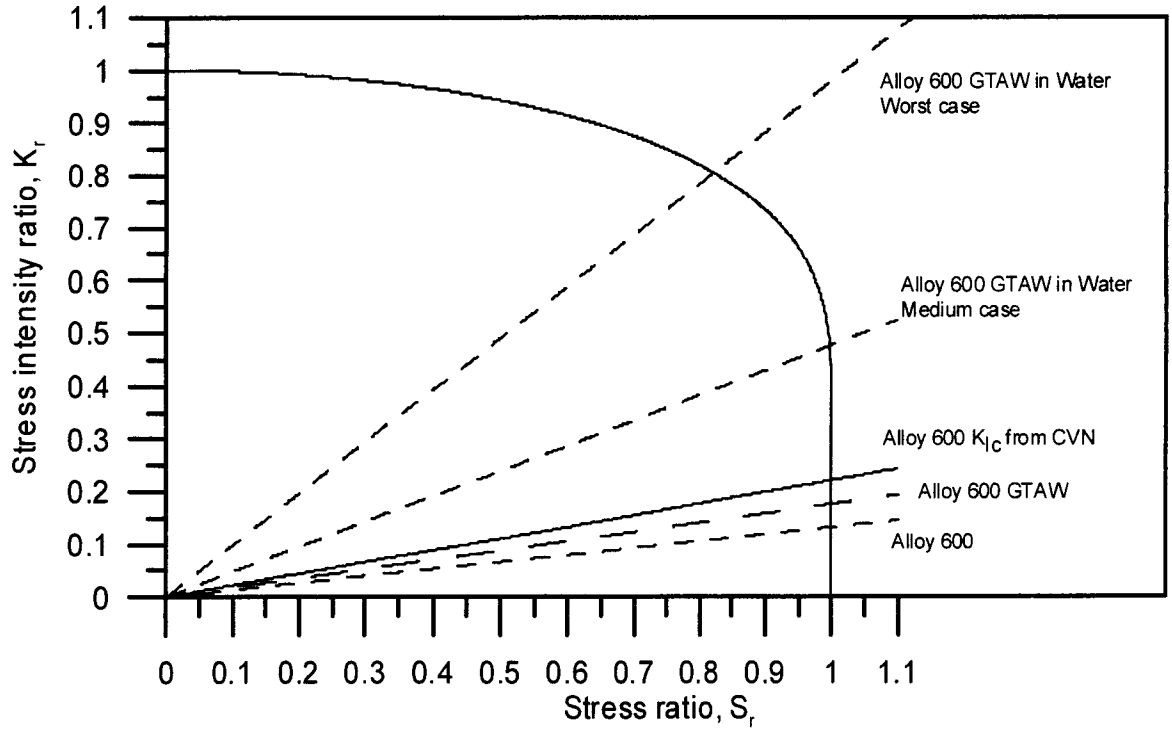

Figure 4-28. Failure Assessment Diagram for Alloy 600

NOTE: Stress intensity provided in MPa $m^{1/2}$; for conversion to ksi $in^{1/2}$, use ksi $in^{1/2}$ = MPa $m^{1/2}$/1.1.

GTAW—gas tungsten-arc weld; CVN—Charpy V-notch

necessary information. The fracture toughness of Alloy 22 is likely to be dependent on the welding method based on the data shown in Table 4-11. Variations in base metal and filler metal composition may also alter the fracture toughness of Alloy 22. Recent studies conducted at CNWRA indicate that postweld solution annealing at 1,125 °C [2,057 °F] can reduce the localized corrosion resistance of the welded material. Possible detrimental effects of solution annealing on the fracture toughness of welded Alloy 22 have not been assessed.

The fracture toughness of Alloy 22 is likely to be high in the mill-annealed condition. Fabrication processes are known to reduce the ductility and impact strength of Alloy 22. Cold work, welding, solution annealing, and stress mitigation methods used in the fabrication and closure of the waste packages may decrease the fracture toughness of the alloy. The effect of fabrication processes on the fracture toughness of Alloy 22 should be evaluated including the complete range of fabrication processes, welding methods, and weld repairs. The results of the fracture mechanics assessment and strain rate effects that may increase the yield and tensile strengths and reduce ductility and fracture toughness should be considered in the waste package design evaluations.

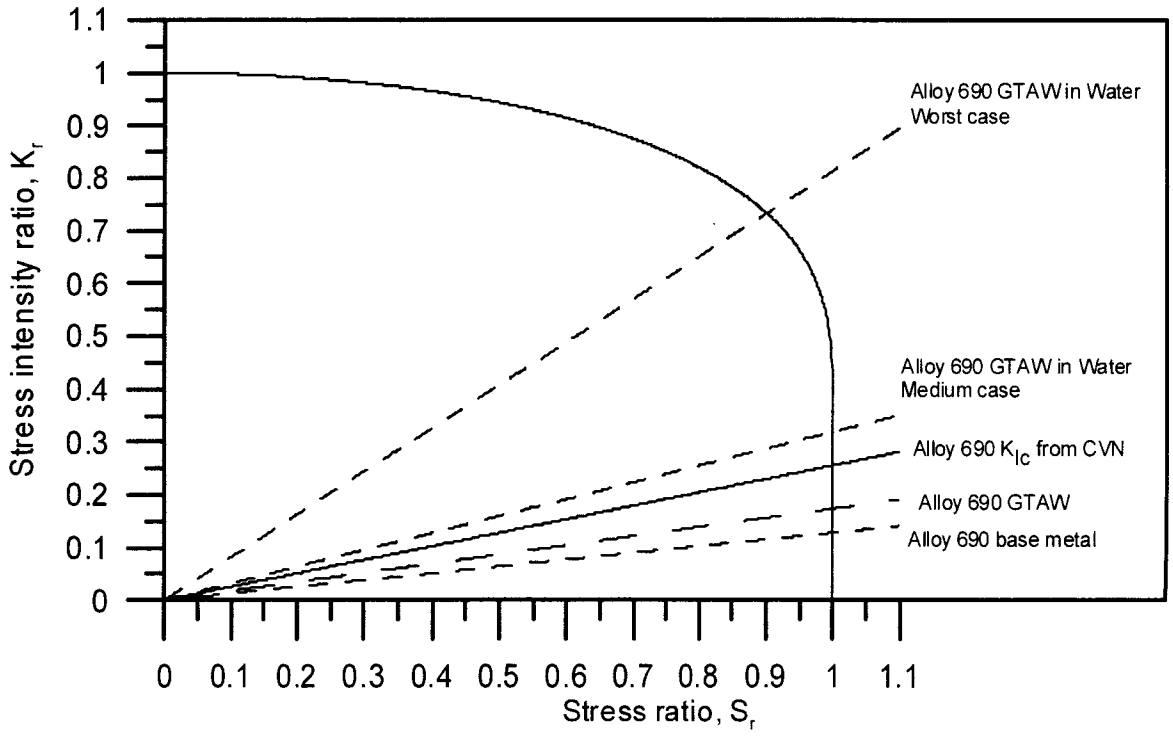

Figure 4-29. Failure Assessment Diagram for Alloy 690

NOTE: Stress intensity provided in MPa $m^{1/2}$; for conversion to ksi $in^{1/2}$, use ksi $in^{1/2}$ = MPa $m^{1/2}$/1.1.

GTAW—gas tungsten-arc weld; CVN—Charpy V-notch

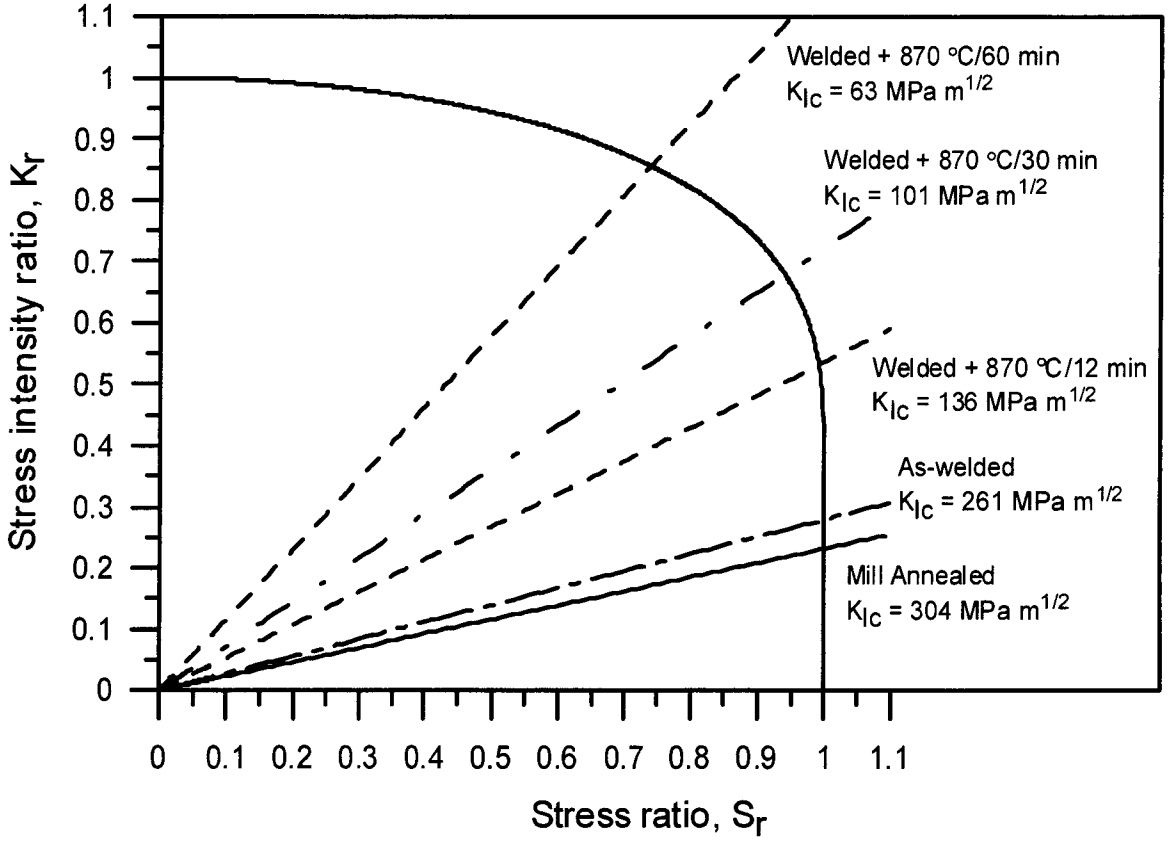

Figure 4-30. Failure Assessment Diagram for Alloy 22

NOTE: Stress intensity provided in MPa $m^{1/2}$; for conversion to ksi $in^{1/2}$, use ksi $in^{1/2}$ = MPa $m^{1/2}$/1.1.

5 SUMMARY, CONCLUSIONS, AND RECOMMENDATIONS

Sudden or sustained mechanical loading of the waste package may occur as a result of handling, emplacement operations, waste package drops, seismic events, rockfall, and drift degradation. The mechanical properties of the waste package materials are considered important factors that may influence the mechanical disruption of the waste packages and, hence, their lifetimes. Fabrication processes that lead to microstructural alteration may reduce the ductility and fracture toughness of the waste package materials. Limited work preformed by the U.S. Department of Energy (DOE) indicates that fabrication processes such as welding decrease the ductility and the impact toughness, impairing the mechanical resistance of Alloy 22. An assessment of the significance of these findings has not been provided, and additional characterization of the effects of the fabrication processes is planned. Investigations conducted to date do not address important factors such as the effects of compositional variations of the materials or the combined effects of multiple fabrication processes, including the possibilities of repairs, that will be used to construct and close the waste packages.

5.1 Waste Package Fabrication, Closure, and Stress Mitigation

The current DOE waste package design has a corrosion resistant Alloy 22 outer container with a Type 316 nuclear grade stainless steel inner container to provide structural support. Fabrication processes used in the production of the waste packages include forming and machining, welding, postweld heat treatments, and postweld stress mitigation operations. The rolled cylinders will be welded to construct the cylindrical body of the disposal containers. Welding also will be used to attach the bottom lid to the body of the disposal containers. The Alloy 22 outer container will have trunnion sleeves on the outside of the container body that are attached by welding. Internal structures, necessary to support in place the waste package contents, will be welded to the interior of the Type 316 nuclear grade stainless steel inner disposal container. After the welding operations are completed, the Alloy 22 disposal containers will be solution annealed and water quenched to mitigate residual stresses arising from welding. No postweld heat treatment is planned for the Type 316 nuclear grade stainless steel inner container. A single lid secured with a spread ring and seal welds will be used to close the inner container after waste loading, whereas dual closure lids will be installed and welded to the outer disposal container. Following a nondestructive examination, the residual stresses in the closure lid welds may be mitigated using several possible methods being developed. The combination of cold work, welding, postweld heat treatment, and postweld stress mitigation methods may alter the microstructure and mechanical properties of the waste package container materials. Characterization of the effects of the entire fabrication sequence on the microstructure and mechanical properties of the container materials is necessary to assess the performance of the waste packages.

5.2 Effects of Fabrication Processes on Microstructure

The microstructure and material properties of Type 316 nuclear grade stainless steel are strongly dependent on its chemical composition and thermomechanical history. The microstructure of wrought material is completely austenitic, whereas, welded material has a duplex structure consisting of austenite and ferrite phases. Further thermal aging results in the precipitation of carbides and intermetallic phases. Based on the evaluation of available time-temperature-precipitation diagrams established for similar stainless steels, Type 316 nuclear

grade stainless steel with a low carbon content is anticipated to hinder the formation of carbide precipitates and thus improve resistance to sensitization caused by chromium depletion at grain boundaries. On the other hand, cold working prior to aging may accelerate the precipitation of both carbides and intermetallic phases. For welded material, although approximately 3–8 wt% ferrite is needed for preventing hot cracking, control of the ferrite content is critical for performance of the welds, primarily because of the transformation of ferrite to embrittled phases. The ferrite content in the welds with heat-to-heat variations can be predicted based on chromium and nickel equivalents in the DeLong diagram. Welding processes have been shown to alter weld microstructures by changing the solidification behavior. Alloy chemistry and segregation of alloying elements also have profound effects on the kinetics of solid-state transformations. Altogether, the resultant weld microstructures, as influenced by the compositional variations and thermomechanical treatments, have a significant impact on the mechanical properties of the welds.

Changes in material microstructure resulting from fabrication processes are considered possible degradation mechanisms that may strongly influence the performance of the Alloy 22 waste package outer container. The microstructure of Alloy 22 is a single-phase, face-centered cubic solid solution in wrought condition. This alloy undergoes phase transformations after thermal aging, including precipitation of secondary topologically close-packed phases and carbides as well as long-range ordering. Thermal exposure of the mill-annealed Alloy 22 at 870 °C [1,598 °F] for only 5 minutes results in the formation of topologically close-packed phases at grain boundaries. No significant depletion of precipitate-forming elements has been detected in the grain-boundary regions in investigations conducted at the Center for Nuclear Waste Regulatory Analyses (CNWRA). The time-temperature-precipitation diagrams for precipitation of topologically close-packed phases and long-range ordering in wrought Alloy 22 have been established by DOE based on microstructural examinations and theoretical calculations. Microstructural characterization of the welded Alloy 22 in the as-welded condition shows formation of a dendritic structure and the presence of topologically close-packed phases in the interdendritic regions. Further aging and solution-annealing treatments of the welded material promotes precipitation of the secondary phases. The kinetics of phase transformations are determined based on the aging data measured from samples treated for accelerated, high-temperature conditions. Extrapolation of the shot-term data shows that both bulk precipitation of topologically close-packed phases and long-range ordering in the Alloy 22 base metal are not expected in 10,000 years at 300 °C [572 °F]. For Alloy 22 welds, extrapolation to 10,000 years for formation of 5 and 10 vol% topologically close-packed phases indicates the estimated temperatures are above 300 °C [572 °F]. Solution annealing of the welded materials is unable to redissolve these precipitates into a solid solution because of segregation of molybdenum in the interdendritic regions. Results from both experiments and theoretical calculations conducted at CNWRA indicate that heat-to-heat variations in the base metal and element segregation in the welds may significantly affect the stability of topologically close-packed phases as a consequence of the proposed fabrication and closure processes.

5.3 Effects of Fabrication Processes on Mechanical Properties

The effects of fabrication processes on the mechanical properties of austenitic stainless steels are receiving considerable attention as a result of the use of these materials in nuclear power plants. Multiple studies have investigated the yield strength, tensile strength, and ductility of austenitic stainless steel base metals and welds. Although a marginal loss of ductility is observed for welded materials, welded austenitic stainless steels remain quite ductile. Fracture

toughness measurements have been conducted to investigate the effects of crack orientation, cold work, inclusion content, temperature, weld metal composition, and welding method. Although heat-to-heat variations are large, the fracture toughness of austenitic stainless steel base metals and welds is generally high owing to their relatively low strength, strain hardening, and high ductility. Nevertheless, the fracture toughness of wrought austenitic stainless steel is dependent on inclusion content, cold work, and crack orientation. A minor amount of cold work can result in a substantial decrease in fracture toughness. Inclusions have the greatest impact on cracks oriented along the rolling direction and parallel to the surfaces of wrought plate. Welds in austenitic stainless steels also have high fracture toughness, but the toughness value is dependent on the welding processes. Welds produced with methods that result in a minimal increase in the inclusion content, such as gas tungsten-arc welding and gas metal-arc welding retain fracture toughness similar to that of the wrought base material. Welding methods that result in a substantial increase in inclusion content such as submerged-arc welding, reduce the fracture toughness of the weld. Nevertheless, the fracture toughness of welded stainless steels is generally sufficiently high to preclude fracture-dominated failure.

Limited information is available on the effects of fabrication processes on the mechanical properties of Alloy 22. The mechanical properties of Alloy 22 are similar to those for austenitic stainless steels, and the material can be characterized as a low-strength, high-ductility alloy that undergoes strain hardening. DOE evaluated the effects of welding and thermal aging on the ductility, yield strength, and impact fracture resistance of Alloy 22. Welded Alloy 22 has a slightly higher yield strength and lower ductility than the wrought material. Thermal aging at temperatures where the formation of topologically close-packed phases is known to occur reduces the ductility and adversely affects the fracture resistance of both wrought and welded Alloy 22.

The lack of fracture toughness measurements for Alloy 22 and related alloys increases the difficulty of evaluating the effects of fabrication processes on the response of the Alloy 22 waste package to mechanical loading that may occur during waste emplacement or for disposal conditions. Based on the similarity to austenitic stainless steels, the fracture toughness of Alloy 22 may be high but dependent on defect or crack orientation, cold work, welding method, and weld and filler metal composition. In addition to identifying and evaluating the individual effects of these parameters, possible additive and synergistic effects need to be considered.

5.4 Future Work

Evaluation of the effects of fabrication processes on the mechanical properties of Alloy 22 is necessary to assess the lifetimes of the waste packages. The DOE assessment of fabrication effects is based on limited experimental work with materials that do not accurately represent the expected condition of the fabricated and sealed waste packages. The effects of the complete range of fabrication processes on the ductility and fracture toughness need to be properly considered in the DOE and the U.S. Nuclear Regulatory Commission agreements. Additional experimental work and modeling that consider the range of expected repository environments, the complete fabrication sequence including postweld heat treatments and proposed stress mitigation methods, and variations in the alloy and filler metal composition are necessary. Future work CNWRA will independently evaluate the effects of fabrication processes on the mechanical properties of Alloy 22. Changes in mechanical properties will be related to the microstructure after welding, thermal aging, and postweld solution annealing. The design of the waste packages has not been finalized, and significant revisions to the designs and the

proposed fabrication processes have occurred recently. Some processes, such as laser peening and low-plasticity burnishing, are still being evaluated. Changes to the waste package design and the fabrication processes used in the construction of the disposal container and the closure and stress mitigation operations need to be evaluated to assess the performance in the proposed repository. Significant changes to the waste package design or the proposed fabrication processes will require a reevaluation of the effects of fabrication processes on the microstructure, ductility, and fracture toughness of the waste package container materials.

6 REFERENCES

Advani, A.H., L.E. Murr, D.G. Atteridge, and R. Chelakara. "Mechanisms of Deformation-Induced Grain Boundary Chromium Depletion (Sensitization) Development in Type 316 Stainless Steels." *Metallurgical Transactions A.* Vol. 22A. pp. 2,917–2,934. 1991.

Alexander, D.J. and R.K. Nanstad. "The Effect of Aging for 50,000 Hours at 343 °C on the Mechanical Properties of Type 308 Stainless Steel Weldments." Seventh International Symposium on Environmental Degradation of Materials in Nuclear Power Systems—Water Reactors. Vol. 2. Houston, Texas: NACE International. pp. 747–758. 1995.

Alexander, D.J., K.B. Alexander, M.K. Miller, and R.K. Nanstad. "The Effect of Aging at 343 °C on Type 308 Stainless Steel Weldments." *Fatigue, Degradation and Fracture MPC.* Vol. 30. PVP Vol. 195. W.H. Bamford, C. Bect, S. Bhandari, J.D. Gilman, L.A. James, and M. Prager, eds. New York City, New York: ASME International. pp. 187–192. 1990.

Allegheny Ludlum. *Technical Data Blue Sheet Stainless Steels Chromium Nickel Molybdenum Types 316 (S31600), 316L (S31603), 317 (S31700), 317L (S31703).* Brackenridge, Pennsylvania: Allegheny Ludlum. 1999.

Anderson, T.L. *Fracture Mechanics Fundamentals and Applications.* 2nd Edition. Boca Raton, Florida: CRC Press. 1995.

Anderson, M.J., N.R. Brown, J.D. Cloud, P.R.Z. Russell, and L.J. Trautner. "Waste Package Design for License Application." Proceedings of 10th International High-Level Radioactive Waste Management Conference, Las Vegas, Nevada, March 30–April 3, 2003. La Grange Park, Illinois: American Nuclear Society. pp. 714–719. 2003.

ASM international. *Metals Reference Book.* M. Bauccio, ed. 3rd Edition. Materials Park Ohio: ASM International. 1992.

ASME International. "Rules for Construction of Nuclear Power Plant Components, Division 1, Subsection NC, Class 2 Components." *Section III, 2001 ASME Boiler and Pressure Vessel Code.* New York City, New York: ASME International. 2001a.

———. "SA–240 Specification for Heat Resisting Chromium and Chromium Nickel Stainless Steel Plate, Sheet, and Strip for Pressure Vessels." New York City, New York: ASME International. 2001b.

———. "Rules for Construction of Nuclear Power Plant Components, Division 1, Subsection NB, Class 1 Components." *Section III, 1995 ASME Boiler and Pressure Vessel Code.* New York City, New York: ASME International. 1995a.

———. "Materials." *Section II, 1995 ASME Boiler and Pressure Vessel Code.* New York City, New York: ASME International. 1995b.

ASTM International. "Standard Test Methods and Definitions for Mechanical Testing of Steel Products." *A370–02: Annual Book of Standards. Vol. 3.01: Metals—Mechanical Testing; Elevated and Low-Temperature Tests; Metallography.* West Conshohocken, Pennsylvania: ASTM International. 2002a.

———. "Standard Test Methods for Tension Testing of Metallic Materials." *E8–01: Annual Book of Standards. Vol. 3.01: Metals—Mechanical Testing; Elevated and Low-Temperature Tests; Metallography.* West Conshohocken, Pennsylvania: ASTM International. 2002b.

———. "Standard Test Methods for Notched Bar Impact Testing of Metallic Material." *E23–02: Annual Book of Standards. Vol. 3.01: Metals—Mechanical Testing; Elevated and Low-Temperature Tests; Metallography.* West Conshohocken, Pennsylvania: ASTM International. 2002c.

———. "Standard Test Method for Plane-Strain Fracture Toughness of Metallic Materials." *E399–90: Annual Book of Standards. Vol. 3.01: Metals—Mechanical Testing; Elevated and Low-Temperature Tests; Metallography.* West Conshohocken, Pennsylvania: ASTM International. 2002d.

———. "Standard Test Method for Measurement of Fracture Toughness." *E1820–01: Annual Book of Standards. Vol. 3.01: Metals—Mechanical Testing; Elevated and Low-Temperature Tests; Metallography.* West Conshohocken, Pennsylvania: ASTM International. 2002e.

Balladon, P., J. Heritier, and P. Rabbe. "Influence of Microstructure on the Ductile Rupture Mechanisms of a 316L Steel at Room and Elevated Temperatures." Fracture Mechanics: Fourteenth Symposium. Vol. II: Testing and Applications. ASTM STP 791. J.C. Lewis and G. Sines, eds. West Conshohocken, Pennsylvania: ASTM International. pp. II-496 through II-513. 1983.

Barsom, J.M. and S.T. Rolfe. "Correlations Between K_{Ic} and Charpy V-Notch Test Results in the Transition-Temperature Range." *Impact Testing of Metals.* ASTM STP 466. West Conshohocken, Pennsylvania: ASTM International. pp. 281–302. 1970.

Begley, J.L. and J.D. Landes. "The J Integral As a Fracture Criterion." Fracture Toughness—Proceedings of the 1971 National Symposium on Fracture Mechanics: Part II. ASTM STP 514. West Conshohocken, Pennsylvania: ASTM International. pp. 1–20. 1971.

Brooks, J.A. and A.W. Thompson. "Microstructural Development and Solidification Cracking Susceptibility of Austenite Stainless Steel Welds." *International Materials Reviews.* Vol. 36. pp. 16–44. 1991.

Bruemmer, S.M. "Quantitative Modeling of Sensitization Development in Austenitic Stainless Steel." *Corrosion.* Vol. 46. pp. 698–709. 1990.

Chipperfield, C.G. "A Method for Determining Dynamic J_q and δ_i Values and its Application to Ductile Steels." Proceedings of the International Conference on Dynamic Fracture Toughness. London, England: The Welding Institute and American Society for Metals. pp. 168–179. 1977.

Cieslak, M.J., T.J. Headley, and A.D. Romig, Jr. "The Welding Metallurgy of Hastelloy Alloys C-4, C-22, and C-276." *Metallurgical Transactions.* Vol. 17A. pp. 2,035–2,047. 1986.

CRWMS M&O. "Waste Package Operations Fabrication Process Report." TDR–EBS–ND–000003. Rev. 02. Las Vegas, Nevada: CRWMS M&O. 2001a.

———. "Waste Package Project FY–01 Closure Methods Report." TDR–EBS–ND–000006. Rev. 00. Las Vegas, Nevada: CRWMS M&O. 2001b.

———. "Supplemental Science and Performance Analysis—Report Volume 1 of 2." TDR–MGR–MD–000007. Rev. 00. Las Vegas, Nevada: CRWMS M&O. 2001c.

———. "Repository Safety Strategy: Plan to Prepare the Safety Case to Support Yucca Mountain Site Recommendation and Licensing Considerations." TDR–WIS–RL–000001. Rev. 04 ICN 01. Las Vegas, Nevada: CRWMS M&O. 2000a.

———. "Total System Performance Assessment for Site Recommendation." TDR–WIS–PA–000001. Rev. 00 ICN 01. Las Vegas, Nevada: CRWMS M&O. 2000b.

———. "Update to the EIS Engineering File for the Waste Package in Support of the Final EIS." TDR–EBS–MD–000010. Rev. 00 ICN 01. Las Vegas, Nevada: CRWMS M&O. 2000c.

———. "Waste Package Operations Fabrication Process Report." TDR–EBS–ND–000003. Rev. 01. Las Vegas, Nevada: CRWMS M&O. 2000d.

———. "Aging and Phase Stability of Waste Package Outer Barrier." ANL–EBS–MD–000002. Rev. 00. Las Vegas, Nevada: CRWMS M&O. 2000e.

DOE. "Yucca Mountain Science and Engineering Report—Technical Information Supporting Site Recommendation Consideration." DOE/RW–0539–1. Rev. 1. Las Vegas, Nevada: DOE, Office of Civilian Radioactive Waste Management. 2002.

Dunn, D.S., D. Daruwalla, and Y.-M. Pan. "Effect of Fabrication Processes on Materials Stability—Characterization and Corrosion." San Antonio, Texas: CNWRA. 2003.

Garwood, S.J. "Fracture Toughness of Stainless Steel Weldments at Elevated Temperatures." Fracture Mechanics: Fifteenth Symposium. ASTM STP 833. R.J. Sanford, ed. West Conshohocken, Pennsylvania: ASTM International. 1984.

Gavenda, D.J., W.F. Michaud, T.M. Galvin, W.F. Burke, and O.K. Chopra. NUREG/CR–6428, "Effects of Thermal Aging on Fracture Toughness and Charpy-Impact Strength of Stainless Steel Pipe Welds." Argonne, Illinois: Argonne National Laboratory. pp. 333–359. 1996.

Gill, T.P.S., M. Vijayalakshmi, P. Rodriguez, and K.A. Padmanabham. "On Microstructure—Property Correlation of Thermally Aged Type 316L Stainless Steel Weld Metal." *Metallurgical Transactions A.* Vol. 20A. pp. 1,115–1,124. 1989.

Hall, E.L. and C.L. Briant. "Chromium Depletion in the Vicinity of Carbides in Sensitized Austenitic Stainless Steels." *Metallurgical Transactions A.* Vol. 15A. pp. 793–811. 1984.

Hawthorne, J.R. and B.H. Menke. "Influence of Delta Ferrite Content and Welding Variables on Notch Toughness of Austenitic Stainless Steel Weldments." Symposium on Structural Materials for Service at Elevated Temperatures in Nuclear Power Generation MPC–1. New York City, New York: ASME International. 1975.

Haynes International. *Hastelloy C-22 Alloy.* H–2019F. Kokomo, Indiana: Haynes International. 2002.

Heubner, U.L., E. Alepeter, M.B. Rockel, and E. Wallis. "Electrochemical Behavior and Its Relation to Composition and Sensitization of NiCrMo Alloys in ASTM G–28 Solution." *Corrosion.* Vol. 45. pp. 249–259. 1989.

Iwadate, T., T. Karaushi, and J. Watanabe. "Prediction of Fracture Toughness K_{Ic} of $2^1/_4$Cr-1Mo Pressure Vessel Steels from Charpy V-Notch Test Results. Flaw Growth and Fracture." ASTM STP 631. West Conshohocken, Pennsylvania: ASTM International. pp. 493–506. 1977.

Kanninen, M.F. and C.H. Popelar. *Advanced Fracture Mechanics.* New York City, New York: Oxford University Press. 1985.

Karmazin, L. "Lattice Parameter Studies of Structure Changes of Ni-Cr Alloys in the Region of Ni_2Cr." *Materials Science and Engineering.* Vol. 54. pp. 247–256. 1982.

Krompholtz, K., G. Ullrich, H.P. Alder, G. Gnirss, H. Huthmann, M. Rodig, and F. Schubert. "Fracture Toughness of Alloy 800 at Room Temperature." Proceedings of a Specialists Meeting: High Temperature Metallic Materials for Gas-Cooled Reactors, Cracow, Austria, June 20–23, 1988. Vienna Austria: International Atomic Energy Agency, International Working Group on Gas-Cooled Reactors IWGGCR–18. pp. 153–162. 1988.

Lai, J.K.L. "A Review of Precipitation Behaviour in AISI Type 316 Stainless Steel." *Materials Science and Engineering.* Vol. 61. pp. 101–109. 1983.

Migala, T.S. and T.L. Jacobs. "Low Plasticity Burnishing: An Affordable, Effective Means of Surface Enhancement." Proceedings of the 13th International Federation for Heat Treatment and Surface Engineering Congress, Columbus, Ohio, October 7–10, 2002. Columbus, Ohio: 2002.

Mills, W.J. "Fracture Toughness of Types 304 and 316 Stainless Steels and Their Welds." *International Materials Reviews.* Vol. 42. pp. 45–82. 1997.

———. "Fracture Toughness of Austenitic Stainless Steels and Their Welds." *ASM Handbook Vol. 19: Fatigue and Fracture.* New York City, New York: ASM International. pp. 733–756. 1995.

———. "Effect of Loading Rate and Thermal Aging on the Fracture Toughness of Stainless-Steel Alloys." Fracture Mechanics: Perspectives and Directions Twentieth Symposium. ASTM STP 1020. R.P. Wei and R.P. Gangloff, eds. West Conshohocken, Pennsylvania: ASTM International. pp. 459–475. 1989.

———. "Fracture Toughness of Stainless Steel Welds." Fracture Mechanics: Nineteenth Symposium. ASTM STP 969. T.A. Crane, ed. West Conshohocken, Pennsylvania: ASTM International. pp. 330–355. 1988a.

———. "Heat-to-Heat Variations in the Fracture Toughness of Austenitic Stainless Steels." *Engineering Fracture Mechanics*. Vol 30. pp. 469–492. 1988b.

———. "Fracture Toughness of Aged Stainless Steel Primary Piping and Reactor Vessel Materials." *Transactions of the American Society of Mechanical Engineers*. Vol. 109. pp. 440–448. 1987.

Mills, W.J. and C.M. Brown. Fracture Toughness of Alloy 600 and an EN82H Weld in Air and Water. *Metallurgical Transactions*. Vol. 32A. pp. 1,161–1,174. 2001.

———. "Fracture Behavior of Nickel-Based Alloys in Water." B–T–3240. West Mifflin, Pennsylvania: Bettis Atomic Power Laboratory. 1999.

NRC. NUREG–1762, "Integrated Issue Resolution Status Report." Rev. 0. Washington, DC: NRC. August 2002.

———. "Issue Resolution Status Report, Key Technical Issue: Container Life and Source Term." Rev. 3b. Washington, DC: NRC. 2001.

Olson, D.L. "Prediction of Austenitic Weld Metal Microstructure and Properties." *Welding Journal*. Vol. 64. pp. 281–294. 1985.

Pan, Y.-M, D.S. Dunn, and G.A. Cragnolino. "Phase Stability and Corrosion of Alloy 22 As a High-Level Nuclear Waste Container Material." Proceedings of the Mike Meshii Symposium: Electron Microscopy—Its Role in Materials Science. J.R. Weertman, M. Fine, K. Faber, W. King, and P. Liaw, eds. Warrendale, Pennsylvania: The Minerals, Metals, and Materials Society. pp. 201–208. 2003.

Pawel J.E., D.J. Alexander, M.L. Grossbeck, A.W. Longest, A.E. Rowclifffe, G.E. Lucas, S. Jitsukawa, A. Hishinuma, and K. Shiba. "Fracture Toughness of Candidate Materials of ITER First Wall Blanket and Shield Structures." *Journal of Nuclear Materials*. Vol. 212-215. pp. 442–447. 1994.

Payer, J.H., J.A. Beavers, T.M. Devine, G.S. Frankel, R.H. Jones, R.G. Kelly, and R.M. Latanision. "Peer Review of the Waste Package Materials Performance Final Report." Las Vegas, Nevada: DOE. 2002.

Prevey, P.S., J. Telesman, T. Gabb, and P. Kantzos. "FOD Resistance and Fatigue Crack Arrest in Low-Plasticity Burnished IN718." Proceedings of the 5th National Turbine Engine High Cycle Fatigue Conference, Chandler, Arizona, March 7–9, 2000. Chandler, Arizona. 2000.

Rebak, R.B., T.S.E. Summers, and R.M. Carranza. "Mechanical Properties Microstructure and Corrosion Performance of C-2 Alloy Aged at 260 °C to 800 °C." Scientific Basis for Nuclear Waste Management XXIII. Symposium Proceeding 608. R.W. Smith and D.W. Shoesmith, eds. Warrendale, Pennsylvania: Materials Research Society. pp. 109–114. 2000.

Rolfe, S.T. and S.R. Novak. "Slow-Bend K_{Ic} Testing of Medium-Strength High-Toughness Steels." *Review of Developments in Plane Strain Fracture-Toughness Testing.* ASTM STP 463. West Conshohocken, Pennsylvania: ASTM International. pp. 124–159. 1970.

Smith, J.J. and R.A Farrar. "Influence of Microstructure and Composition on Mechanical Properties of Some AISI 300 Series Weld Metals." *International Materials Reviews.* Vol. 38. pp. 25–51. 1993.

Sridhar, N. and G. Cragnolino. "Stress-Corrosion Cracking of Ni-Base Alloys." *Stress-Corrosion Cracking.* R.H. Jones, ed. Materials Park, Ohio: ASM International. 1992.

Summers, T.S.E., R.B. Rebak, T.A. Palmer, and P. Crook. "Influence of Thermal Aging on the Mechanical and Corrosion Properties of GTAW Welds on Alloy N06022." Scientific Basis for Nuclear Waste Management XXV. Symposium Proceedings 713. B.P. McGrail and G.A. Cragnolino, eds. Warrendale, Pennsylvania: Materials Research Society. pp. 45–52. 2002.

Summers, T.S.E., M.A. Wall, M. Kumar, S.J. Matthews, and R.B. Rebak. "Phase Stability and Mechanical Properties of C-22 Alloy Aged in the Temperature Range 590 to 760 °C for 16,000 Hours." Scientific Basis for Nuclear Waste Management XXII. Symposium Proceedings 556. D.J. Wronkiewicz and J.H. Lee, eds. Warrendale, Pennsylvania: Materials Research Society. pp. 919–926. 1999.

Weiss, B. and R. Stickler. "Phase Instabilities During High Temperature Exposure of 316 Austenitic Stainless Steel." *Metallurgical Transactions A.* Vol. 3A. pp. 851–866. 1972.

Wood, D.S. *The Tensile Properties of Austenitic Steel Weld Metals.* EUR 10125 EN. Brussels, Belgium: Commission of the European Communities. 1986.